Structural characterisation of the p53 binding domain of RBBP6 and its mechanism of interaction with p53

By

Bonnie Leigh Russell

Submitted in accordance with requirements

for the degree

Doctor of Philosophy

in the

COLLEGE OF AGRICULTURE AND ENVIRONMENTAL SCIENCES

DEPARTMENT OF LIFE AND CONSUMER SCIENCES

at the

UNIVERSITY OF SOUTH AFRICA
FLORIDA CAMPUS

SUPERVISOR

PROF. M. NTWASA

June 2022

Declaration

I, **Bonnie Leigh Russell,** hereby declare that the thesis titled "**Structural characterisation of the p53 binding domain of RBBP6 and its mechanism of interaction with p53"**. , which I hereby submit for the degree of **Doctor of Philosophy in Life Sciences** at the University of South Africa, is my own work and has not previously been submitted by me for a degree at this or any other institution.

I declare that the thesis does not contain any written work presented by other persons whether written, pictures, graphs or data or any other information without acknowledging the source.

I declare that where words from a written source have been used, the words have been paraphrased and referenced and where exact words from a source have been used, the words have been placed inside quotation marks and referenced.

I declare that I have not copied and pasted any information from the Internet, without specifically acknowledging the source and have inserted appropriate references to these sources in the reference section of the dissertation or thesis.

I declare that during my study I adhered to the Research Ethics Policy of the University of South Africa, received ethics approval for the duration of my study prior to the commencement of data gathering, and have not acted outside the approval conditions.

I declare that the content of my dissertation/thesis has been submitted through an electronic plagiarism detection program before the final submission for examination.

Student signature: 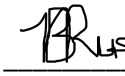 Date: 06/06/2022

Dedication

I dedicate this thesis to my husband, Jason, who after all this time, has always been by my side.

Acknowledgements

To the late Helmut Bente, an amazing gentleman, taken too soon, and my motivation as well as an example of why we need to keep fighting against cancer.

To my mom, Lindsay, for the immense support she has given me over the years and for teaching me to be a hard worker, but also the importance of being kind to oneself.

To my dad, Anthony, and to Nola, for always supporting me and being willing to listen to me. Especially our long conversations on genetics, vaccinations and evolution.

To my sister Amy, and brother-in-law Warren, for your endless support, 'scary game' distractions and constant reminders to "take it one day at a time".

To my brother Nicholas, and sister-in-law Tracy, for supporting me, always looking out for me and reminding me to look after myself.

To the Evans's and Dominick's for being my second family. Double the support and double the love. Thanks particularly to Lisa and Stewart for Wednesday night dinners, peppermint crisps and all the other spoils and support along the way.

To Tom Budge, for all the support, care and guidance since my undergraduate days.

To Zara, Kenny, Ogden, and Faith for, as always, making even the bad days better.

To my fellow students and colleagues for the competition, encouragement and support. Particularly to Sibusiso and Selisha for being such good friends. Laughing so much with you guys was key to me making it through.

To the late Tonny Mathebula, my first lab companion. You will never be forgotten.

To Dr Aurelie Deroubaix for the training and support on the confocal LSM780 /Airyscan of the Life Sciences Imaging Facility of Wits Medical School which is funded by the NRF.

To Dr Nishal Parbhoo for his patience, insight, and always making me feel so welcome in the labs. As well as Prof Samantha Gildenhuys for her belief in me and my abilities.

To Mr Sibusiso Malindisa and Dr Elize Symington for the assistance with abstract translations. And to Jonathan Lembelani Daka for his persistence in helping me with funding.

To my supervisor, Prof Monde Ntwasa, for the support, knowledge and positive energy. As well as the opportunity to work in his lab and under his mentorship. I am grateful for his patience, enthusiasm, and valuable insights during every stage of this work.

To Buboo Bioinovations and the University of South Africa for the financial support.

And last, but certainly not least, to Jason, who was there each and every day, and who has helped in ways that words could not do justice to.

"Im Leben ist nichts so schlecht das da auch nicht etwas Gutes darin ist, man muss es nur suchen"

– Nothing in life is so bad, that there is nothing good in it–you just have to look for it.

Abstract

Worldwide, cancer is a major health issue, causing millions of deaths every year. Retinoblastoma binding protein 6 (RBBP6) is thought to facilitate the interaction between p53 and its prototypical negative regulator, MDM2. RBBP6 has been found to be overexpressed in several cancers and its ability to interact with p53 and cause its degradation, makes it a prospective biomarker and drug target in cancer therapy. In order to target this interaction, a better understating of the p53 binding domain of RBBP6 is needed. In this thesis, expression trials were undertaken for the recombinant p53 binding domain of RBBP6 (namely RBBP6 p53BD) under several conditions. These included different bacterial cell lines, inducer concentrations and post-induction growth time, as well as the domain with and without a polyhistidine tag. The best expression conditions found were NiCo21 (DE3) cells, 37 °C, 0.1 M IPTG and 16 hours post-induction growth. A three-step purification protocol is presented for the polyhistidine-tagged RBBP6 p53BD, utilising hydrophobic interaction and nickel IMAC chromatography. RBBP6 p53BD was purified to approximately 95 % homogeneity. The purified recombinant domain was shown to have structure and be functional as it could bind endogenous p53. The domain was characterised using clear native PAGE and far-UV CD and was found to exist in a single monomer form. Its secondary structure was predicted to be largely intrinsically disordered with 59 % random coil, 19 % alpha-helices, 9 % beta-strands, and 13 % turns. The stability of the domain was also investigated using far-UV CD when the protein was exposed to increasing temperature or known denaturants. The spectrum produced by RBBP6 p53BD with increasing temperature showed a gain in secondary structure and high percentage recovery of its native state after returning to starting temperature. Greater structural changes were seen in the presence of denaturants, with the greatest structural change and lowest percentage recovery seen in the presence of guanidinium chloride. High purity and stability are important for future investigations into the structure of RBBP6 p53BD and drug interaction studies. Localisation images produced from immunocytochemistry experiments are presented here that show different subcellular localisation of RBBP6 and p53 in the cancer cell lines A549, MCF7 and MDA-MB-231 and compared to the normal cell line, HEK293 T. With normal cells having the highest localisation of RBBP6 in the nucleus and negligible localisation in the cytoplasm. Cancer cells still showed the high localisation in the nucleus but higher localisation in the cytoplasm than normal cells. Colocalisation images of p53 and RBBP6 in cancer cell lines are also presented, indicating that p53 and RBBP6 localise in similar cell regions. Using the plugin JACoP from ImageJ, the Manders coefficient of p53 to RBBP6 was predicted to be 0.761 in MCF7 cells and 0.784 in A549 cells. The Manders coefficient of RBBP6 to p53 was found to be 0.904 for MCF7 and 0.834 for A549 cells. The Pearson's coefficient was found to be 0.759 for MCF7 and 0.630 for A549 cells. This Indicates positive colocalisation of

p53 and RBBP6 in both MCF7 and A549 cells, suggesting that these proteins could interact *in vivo*. Co-immunoprecipitation assays were performed and showed the ability of endogenous p53, RBBP6 and MDM2 to interact and form a complex *in vitro* in cancer and normal cell lines. Thus supporting RBBP6 as a facilitator to p53 and MDM2's interaction in human cells as well as supporting RBBP6 as a potential cancer therapy drug target.

Abstract (Zulu)

Emhlabeni wonke, umdlavuza uyinkinga enkulu yezempilo, ebulala izigidi zabantu minyaka yonke. I-Retinoblastoma ebopha amaprotheni 6 (RBBP6) kutholakale ukuthi iningi kakhulu kumangqamuzana omdlavuza. I-RBBP6 kucatshangwa ukuthi yenza kube lula ukusebenzisana phakathi kwe-p53 nesilawuli sayo esikhulu i-MDM2. Ikhono le-RBBP6 lokusebenzelana ne-p53 futhi libangele ukuwohloka kwayo liyenza iRBBP6 ibe i-biomarker kanye nokusetshenziswa yemithi ekwelapheni umdlavuza eqondiswe kuyo. Okokuqala, kule thesis, ngiqale ngezivivinyo zokukhiqiza esibophezelayo se-p53 se-RBBP6 (okungukuthi i-RBBP6 p53BD) ngaphansi kwezimo ezimbalwa. Izimo ezinhle kakhulu zokukhiqhiza iRBBP6 p53BD ezitholiwe kwakuyisizinda esinomaka we-polyhistidine kumangqamuzana e-NiCo21 (DE3), ezingeni lokushisa i-37 °C, kanye ne 0.1 M IPTG kumahora angu-16 okukhula kumangqamuzana. Iphrothokholi yokukhishwa kwe-RBBP6 p53BD okulandela ukukhiqhizwa kwayo enezinyathelo ezintathu, kusetshenziswa ukusebenzisana kwe-hydrophobic kanye ne-nickel IMAC chromatography. I-RBBP6 p53BD ekhiqhiziwe ibonakale inesakhiwo futhi siyasebenza njengoba singahlanganisa ne-p53 etholakala kumangqamuzana. Ukuzinza kwe-RBBP6 p53BD ekhiqhiziwe kuphenyisiswe nge-PAGE kanye ne-CD ye-UV ekude futhi kwatholakala ukuthi ikhona kufomu elilodwa le-monomer futhi iqukethe inani elikhulu lokuphazamiseka kwangaphakathi. Ukuzinza kwesizinda (i-RBBP6 p53 BD) kuphinde kwaphenywa kusetshenziswa i-CD ye-UV ekude kwatholakala ukuthi kunoshintsho oluncane kwisakhiwo se-RBBP6 p53BD ezingeni lokushisa elikhulayo noma ama-denaturants aziwayo ahloliwe. Ukuhlanzeka okuphezulu nokuzinza kubalulekile ophenyweni oluzayo mayelana nesakhiwo se-RBBP6 p53BD kanye nezifundo zokusebenzisana nemithi. Okwesibili, izithombe ezibonisa amazinga ahlukene we-RBBP6 kanye ne-p53 kumdlavuza kanye kumangqamuzana avamile zikhiqizwe ekuhlolweni kwe-immunocytochemistry. Lapho utadisha izithombe ze-colocalisation ama-coefficients ka-Manders kanye ne-Pearson akhiqizwa abonisa ukuhlangana okuhle phakathi kwe-p53 ne-RBBP6 kuwo womabili amangqamuzana omdlavuza e-MCF7 kanye ne-A549, okuphakamisa ukuthi lawa maprotheni angasebenzisana emzimbeni. Ukuhlolwa kwe-Co-immunoprecipitation kwenziwa futhi babonisa ikhono le-endogenous p53, i-RBBP6 ne-MDM2 ukusebenzisana nokwenza i-complex kumangqamuzana omdlavuza kanye navamile. Ngakho-ke imiphumela isekela i-RBBP6

njengomgqugquzeli ekusebenzisaneni kwe-p53 ne-MDM2 kumangqamuzana omuntu kanye nokusekela i-RBBP6 njengethagethi yemithi esingaba khona yokwelapha umdlavuza.

Abstract (Afrikaans)

Kanker is wêreldwyd 'n groot gesondheidskwessie, wat jaarliks miljoene sterftes veroorsaak. Daar is gevind dat retinoblastoombindende proteïen 6 (RBBP6) ooruitgedruk word in verskeie kankers. Daar word vermoed dat RBBP6 die interaksie tussen p53 en sy belangrikste negatiewe reguleerder, MDM2, fasiliteer. RBBP6 se vermoë om met p53 te reageer en die agteruitgang daarvan te veroorsaak, maak dit 'n voornemende biomerker en geneesmiddelteiken in kankerterapie. Eerstens, in hierdie tesis, is uitdrukkingsproewe onderneem vir die rekombinante p53-bindingsdomein van RBBP6 (naamlik RBBP6 p53BD) onder verskeie toestande. Bevindinge toon dat die beste uitdrukkingstoestande was die domein met 'n polihistidienmerker in NiCo21 (DE3) selle, 37 °C, 0.1 M IPTG en 16 uur na-induksie groei. 'n Drie-stap suiweringsprotokol word aangebied vir die polihistidien-gemerkte RBBP6 p53BD, deur gebruik te maak van hidrofobiese interaksie en nikkel IMAC chromatografie. Daar is getoon dat die gesuiwerde rekombinante domein struktuur het en funksioneel is aangesien dit endogene p53 kon bind. Die domein is gekarakteriseer deur gebruik te maak van clear native-PAGE en ver-UV circular dichroism daar is gevind dat dit in 'n enkele monomeervorm bestaan en 'n groot hoeveelheid intrinsieke versteuring bevat. Die stabiliteit van die domein is ook ondersoek deur gebruik te maak van ver-UV CD wanneer die proteïen aan toenemende temperatuur of bekende denaturante blootgestel is, en daar is gevind dat dit relatief min verandering in struktuur en 'n goeie hoeveelheid herstel onder alle toestande het. Hoë suiwerheid en stabiliteit is belangrik vir toekomstige ondersoeke rondom die struktuur van RBBP6 p53BD en geneesmiddelinteraksiestudies. Tweedens word lokaliseringsbeelde wat uit immunositochemie-eksperimente geproduseer word hier aangebied wat verskillende uitdrukkingsvlakke van RBBP6 en p53 in die kanker- en normale sellyne toon. Wanneer die kolokaliseringsbeelde bestudeer word, het die gegenereerde Manders en Pearson se koëffisiënte gedui op positiewe kolokalisering tussen p53 en RBBP6 in beide MCF7 en A549 selle, wat daarop dui dat hierdie proteïene in vivo interaksie kan hê. Ko-immunopresipitasietoetse is uitgevoer en dit het die vermoë van interaksie tussen endogene p53, RBBP6 en MDM2 getoon en om 'n kompleks in vitro te vorm in kanker en normale sellyne. Dit ondersteun dus RBBP6 as 'n fasiliteerder in p53 en MDM2 se interaksie in menslike selle, asook RBBP6 as 'n potensiële kankerterapie-teiken.

Keywords

Cancer, RBBP6, p53, MDM2, RBBP6 p53BD, far-UV circular dichroism, *Escherichia coli* expression, protein stability, co-immunoprecipitation assay, colocalisation.

Research outputs

1. Oral presentation:
   SASBMB 2022 conference
   Investigating the interaction of RBBP6, p53 and MDM2 in normal and cancerous cell lines.
   Russell, BL and Ntwasa, M.
2. Peer-reviewed article submitted for review, original research:
   Russell, BL and Ntwasa, M.
   Expression, purification, and characterisation of the p53 binding domain of Retinoblastoma binding protein 6 (RBBP6).
   Plos one. 11 March 2022. Article under review
3. Peer-reviewed published article, not related to work produced in PhD:
   Chamoné Munnik, Malungi P Xaba, Sibusiso T Malindisa and Bonnie L Russell and Selisha A Sooklal.
   Drosophila melanogaster: A platform for anticancer drug discovery and personalized therapies.
   2022
   Frontiers in Genetics: Pharmacogenetics and Pharmacogenomics. Volume 13: 949241
   DOI: 10.3389/fgene.2022.949241
4. Peer-reviewed published article, not related to work produced in PhD:
   Russell, BL, Sooklal, SA, Malindisa, ST, Daka, LJ and Ntwasa, M.
   The Tumor Microenvironment Factors That Promote Resistance to Immune Checkpoint Blockade Therapy.
   2021
   Frontiers in Oncology. Volume 11: 641428.
   DOI: 10.3389/fonc.2021.641428.
5. Peer-reviewed published article, not related to work produced in PhD:
   Russell, BL, Gildenhuys, S.
   Bluetongue virus viral protein 7 stability in the presence of glycerol and sodium chloride.
   2020
   Clinical and Experimental Vaccine Research. Volume 9(2). Pages 108-118.
   DOI: 10.7774/cevr.2020.9.2.108.
6. Peer-reviewed published article, produced in MSc:
   Russell, BL and Gildenhuys, S.
   Solubilisation and purification of recombinant bluetongue virus VP7 expressed in a bacterial system.
   2018. Protein Expression and Purification. Volume 147. Pages 85-93.
   DOI: 10.1016/j.pep.2018.03.006
7. Peer-reviewed published article, produced in MSc:
   Russell, BL, Gildenhuys, S and Parbhoo, N.
   Analysis of Conserved, Computationally Predicted Epitope Regions for VP5 and VP7 across 3 Orbiviruses.
   2018. Bioinformatics and Biology Insights. Volume 12. Pages 1-12.
   DOI: 10.1177/1177932218755348.

Table of Contents

List of Figures

List of Tables

Abbreviations

A_{280}	absorbance at 280 nm
A340	absorbance at 340 nm
Å	Ångström
bp	base pairs
CD	circular dichroism
cDNA	complimentary deoxyribonucleic acid
cm	centimetre
CO2	carbon dioxide
Co-IP	co-immunoprecipitation
Da	Dalton
DAPI	4',6-diamidino-2-phenylindole
DCM	DWNN catalytic module
DMEM	Dulbecco's modified eagle medium
DNA	deoxyribonucleic acid
DWNN	domain with no name
ε	molar extinction coefficient
E.coli	*Escherichia coli*
ExPASy	Expert Protein Analysis System
far-UV CD	far-ultraviolet circular dichroism
HEK	human embryonic kidney
IDP	intrinsically unfolded protein
IDR	intrinsically unfolded region
IMAC	immobilized metal affinity chromatography
IPTG	isopropyl β-D galactoside
kb	kilobase
kDa	kilodalton
LB	Luria-Bertani broth
M	molar
MDM2	Mouse Double Minute 2
MDMX	Murine double minute X
µl	microlitre
µM	micromolar
µm	micrometre
ml	millilitre
Mpe1	mutant PCFII extrogenic suppressor 1

MW	molecular weight
MWCO	molecular weight cut-off
mRNA	messenger ribonucleic acid
NADH	nicotinamide adenine dinucleotide
NES	nuclear export signal
ng	nanogram
Ni	nickel
NLS	nuclear localisation signal
nm	nanometre
NRSMD	normalized root mean square deviation
OD_{600}	optical density at 600 nm
p21	cyclin-dependent kinase inhibitor 1
P2P-R	proliferation potential-related protein
p53	protein 53
PACT	p53-associated cellular protein testes derived
PAGE	polyacrylamide gel electrophoresis
PBS	Phosphate buffered saline
PDB	Protein Data Bank
pI	isoelectric point
pRb	retinoblastoma protein
PVDF	polyvinylidene fluoride
RBBP6	retinoblastoma binding protein 6
RBBP6 p53BD	retinoblastoma binding protein 6 binding domain
RBQ-1	retinoblastoma binding Q protein 1
RING	really interesting new gene
ROI	region of interest
rpm	revolutions per minute
SDS	sodium dodecyl sulphate
TAE	Tris-acetate-EDTA
TBST	Tris-buffered saline with tween 20
[Θ]	mean residual ellipticity
UV	ultra violet
V	volts
w/v	weight per volume

1. Introduction

1.1 Cancer: A global health problem

Worldwide, cancer is a major health issue, having resulted in over 19 million new cases and 10 million deaths in 2020 (Ferlay *et al*., 2021). It is now estimated that 1 in every 5 individuals will get cancer in their lifetime, and 1 in every 10 will lose their lives (Ferlay *et al*., 2021). For South Africa, in 2020, the highest incidences were prostate, lung and skin cancer, with the three leading mortality cancer types being lung, prostate and oesophagus (Ferlay *et al*., 2021). Cancer affects people of all ages, sex and race; however, there are drastic variations seen between individuals for many of the characteristics of cancer, including growth rate, invasiveness, and age of onset (World Health Organization, 2015). The economic impact of cancer is substantial and is continuing to increase. The overall global annual expenditure on cancer in 2010 was found to be approximately 1.16 trillion USA dollars, resulting from several factors, including loss of workforce and therapy costs (Stewart and Wild, 2014). This only emphasises the desperate need for efficient and economical diagnostic and therapeutic options for cancer patients.

Currently, there are several cancer therapy options available, including surgery, chemotherapy, radiotherapy, immunotherapy, hormone therapy, targeted therapy and stem cell or bone marrow transplants. However, many anti-cancer drugs and therapies cause severe side effects, including nausea, diarrhoea, hair loss, and pain (Tanaka *et al*., 2008). Along with surgery, chemotherapy and radiotherapy are still the most commonly used treatments. Chemotherapy is known to not be limited to explicitly targeting cancer cells and instead targets normal cells as well, and therefore, causes many problems with the destruction of healthy tissue (Bruce *et al*., 1966). Although potentially more targeted than chemotherapy, radiotherapy has been found to increase the risk of developing subsequent cancer after treatment and complications in reproductive, cardiovascular and central nervous systems (Newhauser *et al*., 2016). This emphasises that finding new strategies and therapies that can selectively target cancer cells without harming normal cells is imperative to improving cancer therapy. One of the most promising emerging therapies is the targeted therapy of proteins in cancer cells, as less side effects have been seen for this therapy when compared to traditional therapies (Hahn *et al*., 2021).

All cancers are caused by a cascade of events that result in abnormal cell proliferation due to a defective cell cycle progression, which leads to irregular cell division because the cancer cells' genetic mutations cause the cells to bypass the cell cycle checkpoints (Boveri, 1914; Pardee, 1989; Hartwell and Weinert, 1989). Apoptosis, also known as programmed cell death or 'suicide', was first defined by Kerr and colleagues (Kerr *et al*., 1972). Apoptosis occurs when normal cells become

damaged or diseased and results in the cell undergoing predefined morphological changes, ultimately resulting in the cell's death and thus prevention of further proliferation. Cancer cells cannot carry out routine apoptosis and, therefore, continuously proliferate, resulting in the formation of tumours (Vaux *et al*., 1988; Hanahan and Weinberg, 2011). *P53* is a key tumour suppressor gene that encodes the protein p53 that is in charge of initiating cell cycle arrest for DNA repair or apoptosis when DNA is unrepairable.

1.2 Structure, function and regulation of p53

Over 50 percent of documented human cancer tumours have been found to contain p53 mutations. In addition to this, the majority of other cancers that retain the native p53 protein have defects in other components in the p53 pathway (Crawford *et al*., 1981; Nigro *et al*., 1989; Hollstein *et al*., 1991; Vogelstein *et al*., 2000). This emphasises the significance of the tight regulation of p53 to ensure healthy cell growth and function as well as in the prevention of tumourigenesis.

The p53 gene in *Homo sapiens* (humans) is located on the short arm of chromosome 17 (17p13.1) and encodes a protein of 393 residues. The molecular weight of p53 is 43 kDa, despite being called p53. It was named p53, as it migrated to an apparent weight of 53 kDa on an SDS-PAGE. p53 has been variously nicknamed "the guardian of the genome", "the policeman of the oncogenes", and "the dictator of life and death", as it is of great importance in the cell. p53 acts as a transcription factor that stimulates or represses at least 50 known genes (Lane, 1992; Levine, 1997). During cellular stress, p53 becomes activated, resulting in a cascade of cellular response mechanisms that inhibit tumour formation by initiating cell cycle arrest for DNA repair or apoptosis if DNA is unrepairable (Finlay *et al*., 1989; Hartwell and Weinert, 1989; Martinez *et al*., 1991; Vogelstein *et al*., 2000; Riley *et al*., 2008). p53 also significantly aids in retaining the native genome by playing a role in nucleotide excision repair systems (Wang *et al*., 1991; Wang *et al*., 1995). The majority of p53's known functions occur in the nucleus, most notably its action as a transcription factor. However, recent studies suggest that through its action in the cytoplasm, specifically in mitochondria, p53 can initiate apoptosis independently of its transcriptional activity. It does this by inhibiting anti-apoptotic proteins, BCL2 and BAX and promoting cytochrome C release and, therefore, apoptosis induction (Mancini *et al*., 2009; Kroemer *et al*., 2015).

p53 arranges as a tetramer protein *in vivo* (Jeffrey *et al*., 1995), with each subunit consisting of four main domains, namely the transactivation domain (N-terminus) (alternatively called the oligomerisation domain), the core DNA binding domain, the tetramerisation domain and regulatory domain (C-terminus) (Wang *et al*., 1994; Levine, 1997; Joerger and Fersht, 2008) as seen in Figure 1.1.

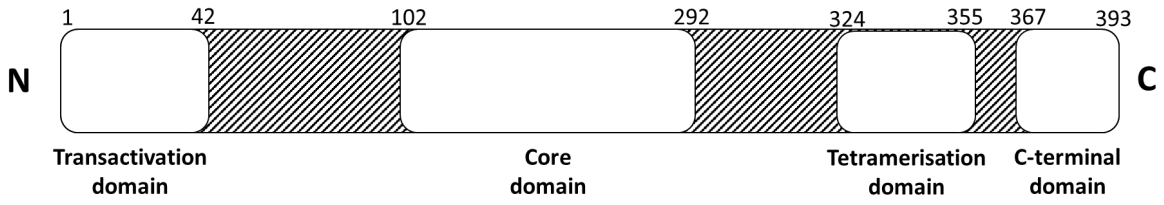

Figure 1.1. Organisation of the domains found in p53.

Arrangement of p53 molecule depicting the four functional domains, namely the transactivation domain, the core DNA binding domain, the tetramerisation domain, and the regulatory domain (C-terminal). Residue numbers are shown at the top, and each domain is labelled. The N and C terminals have been marked.

The N-terminal transactivation domain assists with the regulation of gene expression by acting as the binding site for several proteins, including parts of the transcription machinery and p53's major negative regulator, MDM2 (Poyurovsky *et al*., 2010). The core DNA binding domain is responsible for sequence-specific DNA binding and is the domain that has the highest occurrence of mutations. These mutations result in p53's inability to activate proteins in the apoptosis or cell cycle arrest pathways (el-Deiry *et al*., 1992). The tetramerisation domain causes the tetramer protein formation and contains the nuclear export signal (NES) (Stommel *et al*., 1999). Lastly, the C-terminal regulatory domain contains the nuclear localisation signal (NLS) and is involved in non-specific DNA binding (Shaulsky *et al*., 1990).

Since p53 has a major role in inhibiting cell growth, it must be very carefully regulated. Levels of p53 within the cell are generally relatively low, mainly due to its short half-life. However, this can be altered with cellular stress signals that influence p53's transcription, translation, stability, subcellular localisation and activity (Woods and Vousden, 2001). p53 is regulated through several post-translational modifications, including phosphorylation, methylation, acetylation, sumoylation, and ubiquitination. For example, four significant post-translational modifications that involve just the C terminal of p53 are (1) acetylation resulting in enhancement of sequence-specific binding of p53 to DNA (Gu and Roeder, 1997), (2) ubiquitination by MDM2, resulting in p53 being targeted for proteasomal degradation (Brooks and Gu, 2006), (3) Sumoylation which promotes the transcriptional activity of p53 (Moll and Petrenko, 2003) and (4) neddylation which inhibits the transcriptional activity of p53 (Xirodimas *et al*., 2004).

MDM2 is the prototypical negative regulator of p53. However, there are other cellular proteins that have been linked to p53 regulation (Ntwasa, 2015). Importantly, some proteins regulate p53 through influencing the interaction between MDM2 and p53. Firstly, a protein known as AFR

stabilises p53 by interacting with MDM2 and inhibiting it from ubiquitinating proteins (Stommel and Wahl, 2005). Secondly, MDMX is a protein that can bind p53 and has high homology to MDM2. However, instead of directly causing p53's ubiquitination, it appears to interact with MDM2 and enhance MDM2's ubiquitination of p53 (Stommel and Wahl, 2005; Ghosh *et al*., 2003). Lastly, Pirh2 and Cop1 are E3 ubiquitin ligases that, like MDM2, catalyse p53 ubiquitination, resulting in its degradation. Interestingly, like MDM2, p53 is involved in inducing their expression, creating more negative feedback loops in p53's pathway (Lee and Lozano, 2006; Leng *et al*., 2003).

1.3 MDM2 and its role in p53 regulation

Mouse double minute 2 (MDM2) is so named as it was first discovered on double chromosomes of spontaneously transformed mouse 3T3 fibroblasts and was later associated with p53 (Cahilly-Snyder *et al*., 1987; Momand *et al*., 1992). MDM2 exists in several vertebrate species and has homologs in certain invertebrates, such as the deer tick and tridroplax; however, no homolog has been found in *Drosophila melanogaster* (Momand *et al*., 1992; Finlay, 1993; Lane and Verma, 2012). The MDM2 gene is located on chromosome 12q14.3–q15 and encodes a 491 amino acid protein with a molecular weight of 55 kDa. Two transcriptional promoter elements control MDM2's expression, and one of these elements is reliant on p53 (Cahilly-Snyder *et al*., 1987; Mendoza *et al*., 2014).

MDM2 contains a p53 binding domain at its N-terminal and a RING finger domain at its C-terminal, which is involved in E3 ligase activity (Honda *et al*., 1997; Poyurovsky *et al*., 2010). In addition, MDM2 also contains a nuclear localisation signal (NLS) and a nuclear export signal (NES), which allows MDM2 to be present in both the nucleus and cytoplasm and its ability to move between them (Roth *et al*., 1998). MDM2 is a major negative regulator of p53, targeting it for ubiquitination, ultimately resulting in p53's degradation in the proteasome (Stommel and Wahl, 2005). The significance of MDM2's role in the regulation of p53 is seen in approximately 10 % of human cancers showing MDM2 overexpression, which in turn results in amplified p53 degradation and the resultant uncontrolled cell proliferation and prevention of the tumour suppressor function of p53 (Stommel and Wahl, 2005).

MDM2 regulates p53 activity in several ways, including: (1) by disrupting its transcriptional activity, (2) by catalysing its degradation through ubiquitination (Momand *et al*., 1992; Haupt *et al*., 1997) and (3) by facilitating its transportation out of the nucleus (Stewart *et al*., 2001). The cytoplasm is where the 26S proteasome degrades the ubiquitinated p53 (Brooks and Gu, 2006; Lim *et al*., 2004). MDM2 and p53 interact through the hydrophobic cleft of MDM2 and the N-terminal transactivation domain of p53, resulting in p53's alpha-helix being buried within the hydrophobic

cleft. This, in turn, prevents the transactivation domain of p53 from interacting with the transcription machinery. After MDM2 binds to and targets p53 for ubiquitination, it is believed to be at least partly responsible for transporting p53 from the nucleus to the cytoplasm, as MDM2 contains a nuclear export signal. Further studies have shown that p53 can independently export itself out of the nucleus using its own nuclear export signal in the C terminal domain (Stommel *et al*., 1999; Zhang and Xiong, 2001). In addition, it has been shown that p53 ubiquitination and degradation can occur in the cytoplasm and the nucleus (Yu *et al*., 2000), thus highlighting the complexity of the regulation of p53 and its major negative regulators.

As p53 transcriptionally activates the oncogene MDM2, higher levels of p53 result in increased expression of MDM2 and therefore increased degradation of p53 in an auto-regulatory feedback loop (Momand *et al*., 1992; Oliner *et al*., 1993; Barak *et al*., 1993). MDM2 can catalyse its own ubiquitination and resultant degradation, making MDM2 have a short life span in the cells, which is very important for the strict control over the quantity of p53 within the cell (Fang *et al*., 2000). To increase p53 levels within the cell, inhibition of the p53-MDM2 interaction is needed, which is often achieved using stress signals that can initiate several independent pathways (Vogelstein *et al*., 2000). These pathways include direct inhibition of MDM2 expression, post-translation modification of MDM2 and p53 and expression of proteins involved in the inhibition of MDM2's function and affect the localisation of MDM2 and p53 within the cell. An example of this is the kinases, Chk1 and Chk2, which are expressed due to DNA damage, and were found to phosphorylate p53. Phosphorylated p53 results in the inhibition of the interaction between p53 and MDM2 and, therefore, ultimately, the inhibition of p53's degradation (Chehab *et al*., 2000). Thus a potential cancer therapeutic strategy could involve interrupting this vital p53-MDM2 interaction (Nag *et al*., 2013).

It is estimated that there are approximately 72 possible mRNA splice variants of MDM2 from its gene transcript; however, apart from MDM2 and MDMX, only MDM2-A, MDM2-B and MDM2-C have been found expressed in various tumours (Rosso *et al*., 2014). Isoforms MDM2 A, B and C are all missing exons from their p53 binding domain, nuclear localisation signalling domain and nuclear export signalling domain. Therefore they can interact with full-length MDM2 through their RING finger domains but cannot cause the degradation of p53 (Sigalas *et al*., 1996; Saadatzadeh *et al*., 2017). The overexpression of MDM2 isoforms has been linked to poor prognosis (Zheng *et al*., 2013). MDMX is a well-known isoform of MDM2 and is a homologue to MDM2 but lacks nuclear localisation and export signals. This results in MDMX predominantly being localised in the

cytoplasm. Although MDMX does not directly cause degradation of p53, MDMX binding to MDM2 stabilises MDM2 and results in increased p53 degradation.

In $MDM2^{-/-}$, $P53^{+/+}$ and $MDMX^{-/-}$, $p53^{+/+}$ null mice, the presence of endogenous MDM2 or MDMX is not enough to compensate for the absence of one another, suggesting that they work together in the p53 degradation (Jones *et al*., 1995; Parant *et al*., 2001). MDM2's role in p53 degradation is amplified during cancer formation leading to low p53 levels in the cells. This, in turn, compromises p53-mediated apoptosis and therefore increases cell proliferation. MDM2 and MDMX have a complicated relationship in which they interact with p53, which is still not fully understood, particularly *in vivo* (Shadfan *et al*., 2012).

1.4 Retinoblastoma binding protein 6 (RBBP6)

RBBP6, a 200 kDa eukaryotic protein, has been linked to many biological processes, including transcription, embryonic development, mRNA processing and ubiquitination (Simons *et al*., 1997; Li *et al*., 2007; Kappo *et al*., 2012; Di Giammartino *et al*., 2014). Several studies propose that it plays a role in the tight control of the cell cycle (Gao *et al*., 2002; Gao and Scott, 2002; Gao and Scott, 2003; Scott *et al*., 2003). The RBBP6 gene in *Homo sapiens* (humans) is located on chromosome 16p22.2, and mammalian RBBP6 has been found to bind to two tumour suppressor proteins, namely p53 and pRB (Saijo *et al*., 1995; Simons *et al*., 1997). RBBP6 is also known as retinoblastoma binding Q protein 1 (RBQ-1) (Sakai *et al*., 1995), and the mouse homologues are p53-associated cellular protein testes-derived (PACT) (Simons *et al*., 1997) and proliferation potential-related protein (P2P-R) (Witte and Scott, 1997). The yeast homolog, Mpe1 (approximately 49.5 kDa) has been linked to pre-mRNA processing (Vo *et al*., 2001). The *Drosophila* homologue, namely SNAMA, is not associated with p53 but instead has been found to be important for apoptosis and crucial for the development of the embryo (Mather *et al*., 2005).

Three independent studies isolated and cloned RBBP6 between 1995 and 1997. Firstly Sakai and colleagues probed for pRb interacting partners in small lung cell carcinoma cells and discovered a 140 kDa protein and named it RBQ-1 (Sakai *et al*., 1995). RBQ-1 consists of residues 150-1146 of the now known full-length RBBP6. RBQ-1's binding to pRb was found to be biologically relevant as it was inhibited by adenovirus E1A protein. Next, Simons and colleagues used p53 as a probe in mouse testes cells and discovered the mouse homologue PACT (p53 associated cellular protein-testes) (Simons *et al*., 1997). PACT corresponds to the residues 207-1792 of full-length RBBP6. PACT was found to bind wild type p53, but not p53 that contained a mutation in the core DNA binding domain, suggesting that PACT interacts with the core DNA binding domain of p53. They also

determined that PACT could bind both p53 and pRB simultaneously. This makes RBBP6 one of very few proteins that bind both p53 and pRB, which are critical cell cycle proteins.

Lastly, Witte and Scott discovered the mouse protein P2P-R (Proliferation Potential Related protein) via its association with heterogeneous nuclear ribonucleoprotein particles by screening the 3T3 cDNA λgt11 expression library using antibodies that can identify heterogeneous nuclear ribonucleoproteins (hnRNPs) (Witte and Scott, 1997). P2P-R consists of residues 199-1792 of full-length RBBP6. They showed that P2P-R expression is very low in terminal differentiation, and overexpression of P2P-R restricts mitosis and stimulates apoptosis in Saos2 (Sarcoma osteogenic 2) cells. These cells lack p53; therefore, they suggested that P2P-R causes apoptosis through a caspase-3 dependent pathway (Witte and Scott, 1997). Caspase-3 is an effector caspase responsible for cleaving several proteins in response to apoptotic signalling, including pRb, MDM2 and topoisomerase I.

PACT and RBBP6 may be involved in pre-mRNA processing, as they are expressed in nuclear speckles and contain a serine/arginine (SR) domain. This is relevant as the main site for pre-mRNA processing is in the nuclear speckles, and a previously identified family of splicing factors contains SR-rich regions (Simons *et al*., 1997). Witte and Scott also demonstrated that RBBP6 interacts with heterogeneous nuclear ribonucleoprotein particles and can bind to single-stranded nucleic acids (Witte and Scott, 1997). The yeast homologue of RBBP6, Mpe1, was found to form part of the Saccharomyces cerevisiae cleavage and polyadenylation factor and be essential for mRNA 3'-end cleavage and polyadenylation (Vo *et al*., 2001). After this, Shi and colleagues used mass spectrometry to show that RBBP6 forms part of the complete human pre-mRNA 3' processing complex; however, RBBP6's exact role in mRNA processing still remains unclear (Shi *et al*., 2009). RBBP6 has been found to be overexpressed in several cancers and has been identified as a potential cancer biomarker (Chen *et al*., 2013; Moela and Motadi, 2016; Mbita *et al*., 2019; Xiao *et al*., 2019; Wang *et al.*, 2020).

1.5 Structure of RBBP6

RBBP6 consists of several highly conserved regions, as seen in Figure 1.2, including an N-terminal ubiquitin-like domain (Domain with no name (DWNN)), a CCHC zinc finger domain, a RING (Really Interesting New Gene) finger domain, a proline-rich domain, a serine/arginine (SR) domain as well as p53 and pRB interacting domains. All homologs of RBBP6 contain the DWNN, Zinc finger and RING finger domains collectively called a DWNN Catalytic Module (DCM). Only the RBBP6 homologs of higher eukaryotes contain some or all of the additional domains mentioned above.

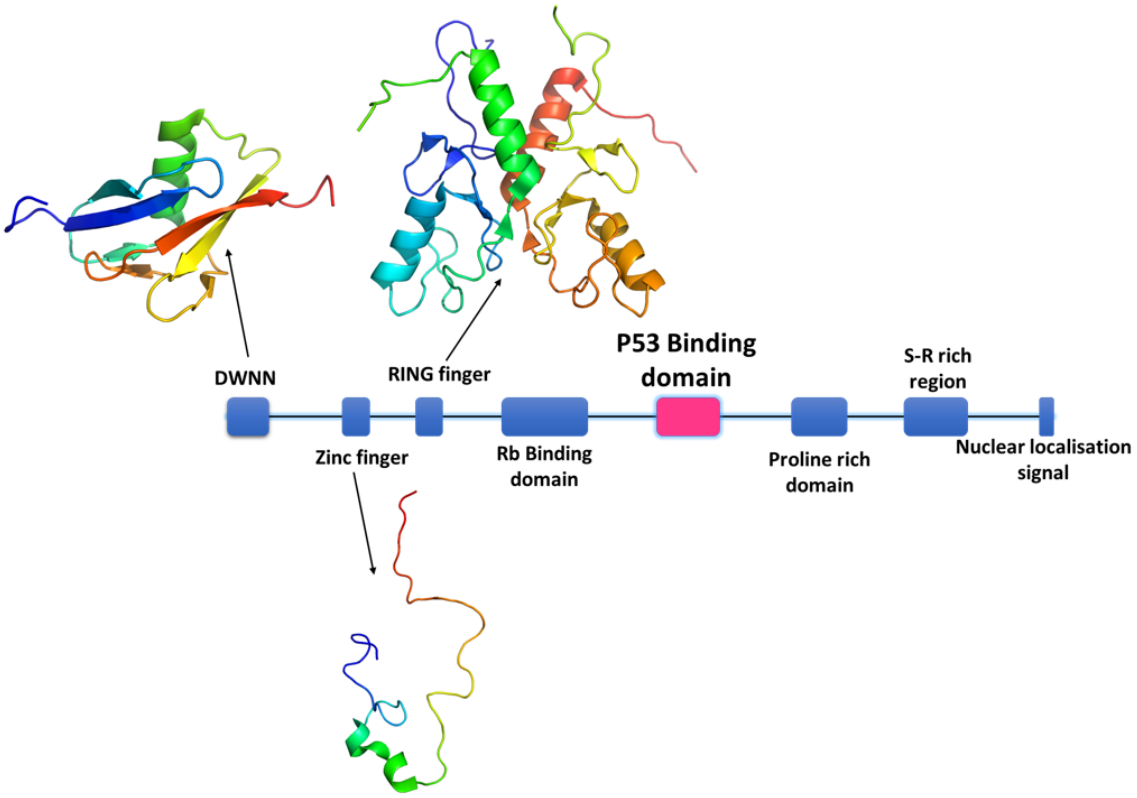

Figure 1.2. Organisation of the domains found in RBBP6.

Showing domain order starting with N-terminal DWNN followed by a CCHC zinc finger, a RING finger domain, pRB and p53 binding domains, a proline-rich domain, an SR domain, and the nuclear localisation signal domain found at the C terminal. The determined structure for the DWNN, CCHC zinc finger and RING finger domains are depicted and were acquired from the protein data bank using codes 2C7H, 3ZTG and 2YSA, respectively and viewed using a PyMOL Molecular Graphics System (2.5.2 Edu), Schrodinger, LLC.

Invertebrate RBBP6 is shorter than mammalian RBBP6 and does not contain the pRB or p53 binding site (Sakai *et al*., 1995; Simons *et al*., 1997). To date, the only determined and published three-dimensional structures of RBBP6 domains are that of the DWNN, the CCHC zinc finger and the RING finger, as shown in Figure 1.2 (Pugh *et al*., 2006; Kappo *et al*., 2012).

RBBP6 mRNA occurs in one of four transcripts namely 6.1 kb (isoform 1) (GenBank: AB112074, NP008841), 6.0 kb (isoform 2) (GenBank: AB112075, NP061173), 1.1 kb (isoform 3) (GenBank: BC029352, NP116015) (Pugh *et al*., 2006) and the *in silico* identified 3.2 kb (isoform 4). The expression patterns of isoforms 2 and 4 are not clear yet; however, studies found that the expression of isoform 1 is increased in cancers, whereas isoform 3 (containing only the DWNN) is down-regulated in several cancers (Gao and Scott, 2003; Pugh *et al*., 2006; Li *et al*., 2007; Mbita *et al*., 2012).

1.6 RBBP6's interaction with and role in p53 regulation

Li and colleagues suggested that RBBP6 promotes p53 degradation by facilitating p53's interaction with MDM2 and, ultimately, its ubiquitination (Li *et al*., 2007). In their study, they performed *in vivo* ubiquitination assays by co-transfecting HEK293 cells with plasmids encoding PACT (mouse homologue of RBBP6) and MDM2. Increased expression of PACT and MDM2 resulted in increased p53 ubiquitination. Increased p53 ubiquitination was not seen when cells were transfected with the PACT plasmid alone. Therefore, Li and colleagues suggested that despite RBBP6 having its own RING finger domain, it doesn't cause ubiquitination of p53 itself, but instead acts as a facilitator or scaffold in which p53 and MDM2 can interact (Li *et al.*, 2007). In addition to this, when a mutant PACT plasmid that did not contain the RING finger domain was used, the increased p53 degradation was not seen even in the presence of increased MDM2 expression, suggesting that MDM2 interacts with RBBP6's RING finger in the p53 degradation process.

Li and colleagues also suggested that the PACT-p53 interaction may be anti-apoptotic, especially in embryos. In $PACT^{-/-}$ mice, the disruption of PACT resulted in embryonic death before day 7.5, as well as overexpression of p53 and extensive apoptosis (Li *et al*., 2007). The embryos were also smaller and displayed delayed development. The knockdown of PACT decreased the p53-MDM2 interaction in mice, resulting in increased p53 levels and therefore increased apoptosis and cell cycle arrest. The introduction of $PACT^{-/-}$, $p53^{-/-}$ mutation was only able to partially delay embryonic death to 11.5 days. This suggests that PACT plays an important role in embryonic development, and this role may be linked to its interaction with p53, particularly in early embryonic development (Li *et al*., 2007). This was also seen in *Drosophila melanogaster,* where RBBP6 homologue, SNAMA was essential for embryonic development as early and ectopic apoptosis was seen when SNAMA was mutated (Mather *et al*., 2005). Studies with $MDM2^{-/-}$ mice, also found embryonic death occurred before day 7.5, but in $MDM2^{-/-}$, $p53^{-/-}$ mice the embryonic lethality was rescued. This shows MDM2's role in embryonic development is solely involved in the regulation of p53 as $MDM2^{-/-}$, $p53^{-/-}$ mice developed normally (Jones *et al*., 1995; Montes de Oca Luna *et al*., 1995). This also shows that RBBP6 has functions independent of p53 and MDM2, including in embryonic development. On the other hand, $p53^{-/-}$ mice were found to be viable; however, significantly more susceptible to tumour development (Donehower *et al*., 1992).

Xiao and colleagues further showed RBBP6's involvement in p53 degradation in the human colorectal cancer cell lines SW620 and HT29 (Xiao *et al*., 2018a). They showed that the silencing of RBBP6 in these cells decreased the interaction of p53 and MDM2 and increased p53 levels within the cells. The increased levels of p53 within the cells, in turn, resulted in increased apoptosis and cell cycle arrest. This was significant as they found that silencing RBBP6 before radiotherapy

resulted in a greater response to the radiotherapy in both cell lines. Similarly, in nude mice with HT29 xenograft tumours, a greater response to radiotherapy was seen when radiotherapy was combined with RBBP6-shRNA lentiviral vector treatment. Thus, suggesting that overexpression of RBBP6 was at least partially responsible for the resistance to radiotherapy in colorectal cancer cells.

The consequence of the increased p53 degradation in the cell is the evasion of apoptosis, uncontrolled cell proliferation and repression of p53-depended gene transcription. Overexpression of RBBP6 has been found in several cancer types and correlates with poor prognosis, especially in oesophageal and colon cancer (Yoshitake *et al*., 2004; Dlamini *et al*., 2005; Chen *et al*., 2013; Dlamini *et al*., 2019). This demonstrates the significance of the effect that overexpression of this protein can cause and, therefore, highlights RBBP6 as a candidate protein for cancer therapy for cancers where native p53 is maintained (Ntwasa *et al*., 2018).

1.7 p53 binding domain of RBBP6

Given RBBP6's part in the increased degradation of p53 within the cell, a need for understanding its mechanism of interaction with p53 has arisen. Research has been conducted to define the residues of RBBP6, which correspond to the p53 binding domain of RBBP6. Simon and colleagues used a recombinant C-terminal portion of PACT (residues 1220-1562) to conduct *in vitro* binding studies with wild type and mutated (codon 270 arg→cys) p53 (Simons *et al*., 1997). They found that wild type p53 bound with this region but not the mutated p53. This demonstrated that the p53 binding domain of RBBP6 was located within residues 1200-1562 of PACT, which corresponds to residues 1428-1792 in full-length human RBBP6, shown in Figure 1.3. Gao and Scott investigated a truncated form of RBBP6 from mice known as P2P-R (Gao and Scott, 2003). Three constructs of full-length P2R-R were investigated, namely residues 1204-1404, 1204-1314 and 1315-1404. They found that p53 could bind the 1204-1404 residue sequence and the 1204-1314 residues sequence but not the 1315-1404 residue sequence. The 1204-1314 residues sequence corresponded to residues 1380-1490 in full-length human RBBP6, shown in Figure 1.3. These two predicted sequences show minimal overlap, with only region 1428-1490 present in both.

Three postgraduate research studies independently investigated the p53 binding domain of RBBP6. Firstly, Ndabambi investigated two residue sequences from full-length RBBP6, specifically residues 1428-1792 and residues 1428-1753, as shown in Figure 1.3 (Ndabambi, 2004). These segments were expressed in BL21 (DE3) cells with a GST tag. Purification utilised GST fusion and cation exchange chromatography and was shown only for the construct with the polylysine tail (residues 1428-1792). After purification multiple truncations of the domain were found using SDS-PAGE analysis, possibly due to proteolysis of the lysine-rich region. Due to the recombinant domain's

instability no further analysis was performed, resulting in a need for further studies into the domain's structure and function.

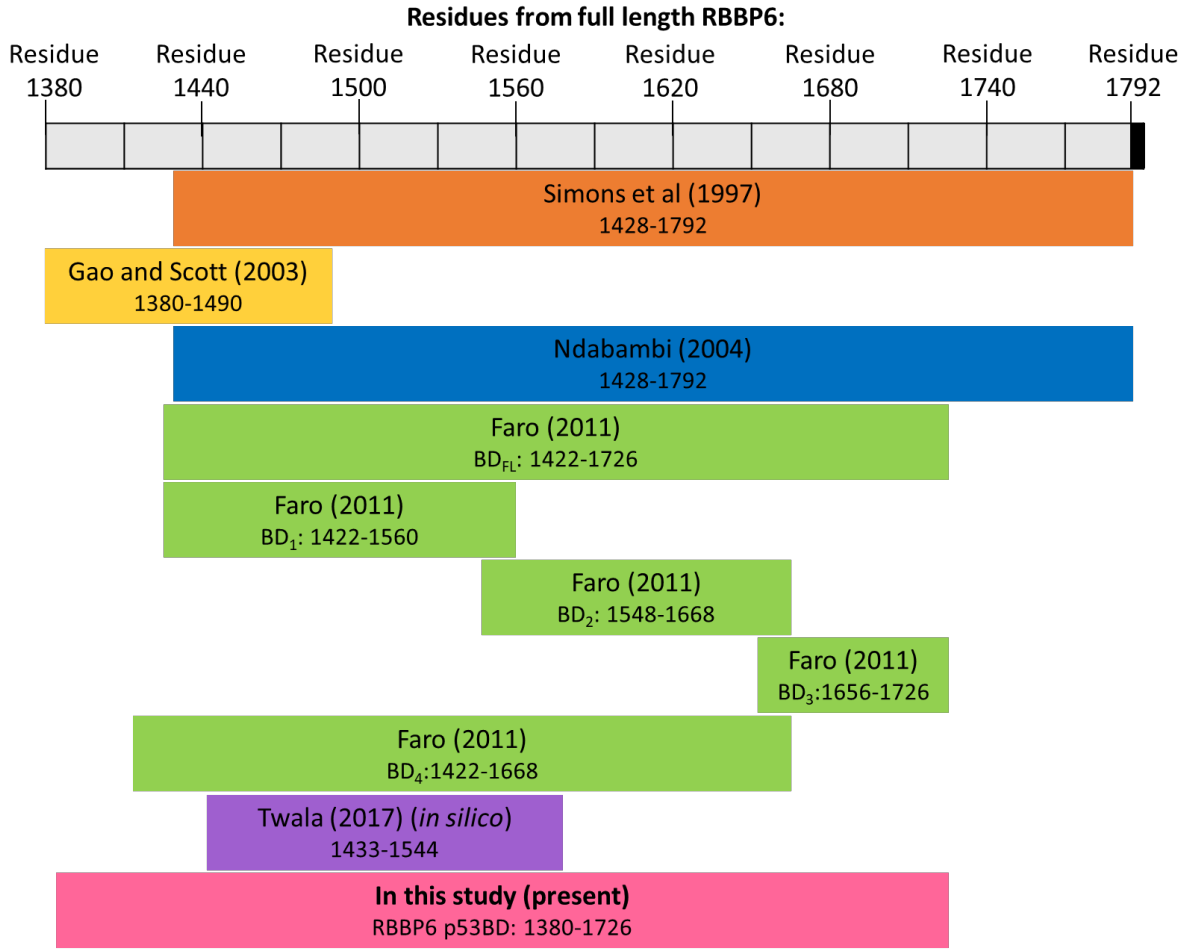

Figure 1.3. The p53 binding domain of RBBP6.

The corresponding RBBP6 residue sequences discovered by Simons et al. (1997) (orange) in PACT mouse homologue and Gao and Scott (2003) (yellow) in mouse, P2P-R, a truncated version of RBBP6 to correspond to the p53 binding domain of RBBP6. The residue sequences that were analysed by postgraduate students Ndabambi (2004) (blue) and Faro (2011) (green). The residues that were investigated for in silico structure by Twala (2017) (purple). Lastly, the residue sequence for the RBBP6 p53BD that was investigated in this study (pink).

Another study, by Faro expressed five constructs representing varying residue fragments to narrow down the p53 binding domain of RBBP6. The constructs investigated consisted of p53BD$_{FL}$ (1422-1726), p53BD$_1$ (1422-1560), p53BD$_2$ (1548-1668), p53BD$_3$ (1656-1726), p53BD$_4$ (1422-1668) (Figure 1.3) (Faro, 2011). All constructs were expressed with a GST-HA tag in bacterial cells. GST pull-down assays showed that p53BD$_{FL}$ and p53BD$_4$ bound p53's core DNA binding domain. p53BD$_4$ was purified using a glutathione agarose column followed by ion-exchange chromatography with a

heparin column. The purified $p53BD_4$ was then shown to bind endogenous p53 in co-immunoprecipitation assays. Through NMR studies, it was suggested that $p53BD_4$ was unfolded, even when bound to p53. The expressed transcripts were again found to be unstable as multiple degradation products were detected on SDS-PAGE, even after interaction with p53. Although this study helped to narrow down the amino acid residue sequence covering the p53 binding domain of RBBP6, the instability of the expressed transcripts prevented experimentation beyond NMR studies. Therefore there is still a need to further investigate the structure and function of the p53 binding domain of RBBP6.

In 2017, Twala sought to identify potential drugs that could target the p53 binding domain of RBBP6 (Twala, 2017). The structure of the p53 binding domain of RBBP6 has not been determined yet. Therefore, the amino acid sequence of the p53 binding domain of RBBP6 was used to perform *in silico* structural predictions. Residues 1433-1544 from full-length RBBP6 were used as identified by the UniprotKB database (RBBP6 unique entry identifier: Q7Z6E9) as the p53 binding domain of RBBP6 (shown in Figure 1.3). Using two programs, namely I-TASSER (Yang *et al*., 2015) and eThread-Modeller (Brylinski *et al*., 2012), multiple protein models were predicted and their quality accessed. The top predicted model had a predominantly alpha-helical structure with some random coil present for both programs.

In this present study, recombinant protein encompassing residues 1380-1726 of full-length RBBP6 was expressed and studied (shown in Figure 1.3). This was to remove the polylysine tail at the C-terminal end of RBBP6, suspected of causing increased proteolysis. Additional N and C-terminal residues compared to $p53BD_4$ in Faro (Faro, 2011) were included to improve the domain's stability. The p53 binding domain of RBBP6 investigated in this study will be referred to as "RBBP6 p53BD".

1.8 Nicotinamide adenine dinucleotide (NADH) binding to the p53BD of RBBP6

Nicotinamide adenine dinucleotide (NADH) is a co-enzyme and is present in every living cell (Xiao *et al*., 2018b). NAD+ is reduced to NADH by dehydrogenases. NADH can exhibit both oxidising and reducing properties as NAD+ accepts electrons donated from other molecules and becomes reduced to form NADH. NADH is also a reducing agent as it donates electrons to the electron transport chain. This occurs within the mitochondria. NADH is, in turn, oxidised by the electron transport chain, which is then involved in the generation of ATP through oxidative phosphorylation (OXPHOS). The NAD^+/NADH redox couple is an essential regulator in cellular energy metabolism. A NADH/NAD+ redox imbalance, at first, causes reductive stress, leading to oxidative stress and ultimately oxidative damage to the cellular macromolecules. Thus, various pathological conditions have been linked to the loss of redox homeostasis (Wu *et al*., 2016).

After predicting the structure of the p53 binding domain in RBBP6 using its amino acid sequence, Twala used the model produced for *in silico* binding site prediction studies using the FTSite Webserver server (Twala, 2017). This was followed by drug binding studies using Schrödinger-Maestro v10.7: Glide SP to screen the Zinc drug database (Zdd). The compound predicted to bind to the p53 binding domain of RBBP6 was NADH. NADH is a negatively charged dinucleotide, as its structure consists of nicotinamide and adenine combined by their phosphate groups. Twala suggested that NADH could be used as a good lead compound to act as a support molecule to another drug compound in order to effectively disrupt the RBBP6-p53 interaction (Twala, 2017). Therefore the veracity of the binding of NADH to RBBP6 needs to be experimental examined as NADH could be an important co-factor that could be utilised in future drug development.

1.9 Subcellular localisation and colocalisation studies

p53 and MDM2 have been reported to be present in the nucleus and the cytoplasm of normal and cancer cell lines and both proteins possess internal nuclear localisation and export signals (Shaulsky *et al*., 1990; Roth *et al*., 1998; Stommel *et al*., 1999). In fact, the ability of these two proteins to move between the nucleus and cytoplasm has been found to be significant for control over these protein's functions (Roth *et al*., 1998; Woods and Vousden, 2001). On the other hand the larger isoforms of RBBP6 have been found to be present predominantly in the nucleus, particularly in nuclear speckles in normal cells, supporting its involvement in pre-mRNA splicing (Simons *et al*., 1997). RBBP6 isoform 3, which is the shortest isoform, has been found to be highly expressed in the cytoplasm, and is down-regulated in cancer cells (Mbita *et al*., 2012). Several studies using immunohistochemistry have found higher localisation of the larger RBBP6 isoforms in the cytoplasm of cancer cells compared to normal cells showing differential expression levels of RBBP6 in normal and cancer cell lines (Dlamini *et al*., 2019; Motadi *et al*., 2011; Motadi *et al*., 2018).

To further investigate the ability of p53 and RBBP6 to interact it first needs to be determined if they localise in similar subcellular locations. Colocalisation observes the spatial overlap in two or more fluorescent signals produced within a defined area, imaged using microscopy (Smallcombe, 2001). Colocalisation can predict the possibility of interaction of two molecules based on their proximity to one another within a cell (Zinchuk *et al*., 2007). In this study the colocalisation of RBBP6 and p53 was investigated. It must be noted that colocalisation alone is not enough for the conformation of protein interactions, as a microscope's resolution is not enough to discern the exact location of two distinct molecules (Dunn *et al*., 2011). Instead, colocalisation can be used as a probe to investigate the localisation of proteins to similar cellular structures, thereby supplying supportive information that proteins naturally have close proximity within the cell. Further experiments such as co-

immunoprecipitation can be undertaken to support the interaction of proteins that have positive colocalisation.

In colocalisation, the background and auto-fluorescence of the cell need to be identified and rectified. This is usually achieved by setting thresholds that remove pixels with intensity values lower than those produced by the proteins or cellular structures of interest. Bleed-through, also known as cross-talk, is when the signal from one fluorophore leaks into the channel reserved for a different fluorophore and leads to false-positive results. Several conditions need to be met to prevent bleed-through, including (1) emission filters need to be optimised, (2) sequencing scanning needs to be conducted and (3) the excitation and emission spectra for chosen fluorophores need to be well separated. In addition to this, several controls need to be performed, including (1) slides that only contain one fluorophore, (2) secondary antibodies alone, (3) a primary antibody with the other protein's secondary antibody and (4) unstained slides to check for auto-fluorescence generated during the slide preparation process (Smallcombe, 2001).

There are several ways to depict colocalisation. Firstly, merging the green and red images to give yellow points where colocalisation occurs (Dunn *et al*., 2011). However, this method can be influenced by the individual signals having different intensities, as only if both signals have the same intensity will the yellow colouring be evident. This means that if concentrations of the molecules differ or if one signal is stronger, then a false negative will be given (Bolte and Cordelières, 2006). Next, a scatterplot can be used that plots green channel against red channel individual pixel intensities, with a straight line gradient showing positive colocalisation and separate axes plots depicting the lack of a relationship (Dunn *et al*., 2011).

Lastly, to quantify colocalisation analysis, a statistical approach can be taken. Several colocalisation coefficients can be calculated, each with advantages and limitations (Bolte and Cordelières, 2006; Dunn *et al*., 2011). Several algorithms have been designed to calculate numerous coefficients applicable to colocalisation analysis. Each of these coefficients evaluates colocalisation using a different approach, and the decision on which coefficient to use in each case depends on the application and outlook (Bolte and Cordelières, 2006). The best approach is to evaluate colocalisation by considering more than one statistical approach. The Pearson's correlation coefficient and the Manders overlap coefficient are two important colocalisation coefficients commonly calculated.

1.9.1 Pearson's correlation coefficient

In 1896 the Pearson's correlation coefficient was created to measure pattern recognition (Pearson, 1896), and later it was used in fluorescent microscopy colocalisation studies (Manders *et al*., 1992). Pearson's coefficient is defined as:

$$\mathrm{PCC} = \frac{\sum_i \left(R_i - \bar{R}\right) \times \left(G_i - \bar{G}\right)}{\sqrt{\sum_i \left(R_i - \bar{R}\right)^2 \times \sum_i \left(G_i - \bar{G}\right)^2}} \quad (1)$$

where Ri is the red channel and Gi is the green channel in pixel "i"and $\bar{R}$ is the mean intensity of the red channel, and $\bar{G}$ is the mean intensity of the green channel across the entire image.

The sum is taken over all pixels. Pearson's correlation coefficient can have a value from -1 and +1, with +1 signifying perfect correlation, 0 signifying no significant correlation and -1 signifying perfect inverse correlation. Its main advantage is its elegant simplicity, measuring individual pixel covariance between two images, independent of signal levels and background, making it relatively user bias-free.

The main downfall of Pearson's correlation coefficient is its assumption that each pixel is an independent data point (McDonald and Dunn, 2013). Pearson's correlation coefficient is not ideal in some biological instances as it only takes into consideration the variation of green and red pixel intensities and shows them in a simple linear relationship. This makes It vulnerable to the extent to which both distinct red and green pixel intensities vary from background threshold intensity and the different levels of signal found in each channel (Bolte and Cordelières, 2006; Dunn *et al*., 2011). This results in the coefficient produced being less accurate in cells where the proteins of interest are present in varying proportions in different locations in the cell (Dunn *et al*., 2011; McDonald and Dunn, 2013). To account for this, in these situations, for the Pearson's correlation coefficient, a region of interest (ROI) is defined.

1.9.2 Manders overlap coefficient

Manders adapted the Pearson's coefficient in 1993 to consider individual pixel intensity values (Manders *et al*., 1993), resulting in a more accurate indicator of colocalisation. The Manders overlap coefficient is such that:

$$\mathrm{MOC} = \frac{\sum_i \left(R_i \times G_i\right)}{\sqrt{\sum_i R_i^2 \times \sum_i G_i^2}} \quad (2)$$

where Ri is the intensity of the red channel and Gi is the intensity of the green channel in pixel "i".

The sum is taken over all pixels. The Manders coefficient can have a value of 0 and 1, with 0 signifying no significant colocalisation and 1 signifying perfect colocalisation. The Manders coefficient is advantageous as it directly assesses the portion of red pixels that overlaps with green pixels and vice versa (Manders *et al*., 1993). This results in two coefficients, such that:

$$M_1 = \frac{\sum_i R_{i,\text{colocal}}}{\sum_i R_i} \tag{3}$$

where $R_{i,\ colocal}$ = Ri if Gi > 0 and $R_{i,\ colocal}$ = 0 if Gi = 0, and

$$M_2 = \frac{\sum_i G_{i,\text{colocal}}}{\sum_i G_i} \tag{4}$$

where $G_{i\ ,colocal}$ = Gi if Ri > 0 and $G_{i,\ colocal}$ = 0 if Ri = 0.

Thus providing a measure of the population of the green pixels colocalising with the red pixels and vice versa, giving a measure of the true overlap of two signals. This is important, particularly in many biological studies (Bolte and Cordelières, 2006; Dunn *et al*., 2011).

The Manders coefficient is particularly vulnerable to background signals resulting from auto-fluorescence or non-specific antibody binding as the absolute value Ri of a signal is used. Therefore this background signal must be detected and removed before analysis; this is usually achieved by setting thresholds (Dunn *et al*., 2011). Costes and co-workers developed an automatic method to identify the threshold values that can determine the range of pixel values considered above the threshold, indicating positive colocalisation (Costes *et al*., 2004). In the Costes method, a coefficient is calculated for each pixel. Lower red and green intensity values are placed on a regression line until a negative Pearson's coefficient is obtained. This provides an easy and unbiased method for threshold determination. This is achieved by estimating the maximum threshold intensity for each channel colour below which the pixels do not display any statistical correlation.

1.10 Using spectroscopy to investigate protein characteristics

Spectroscopy utilises the principle that all molecules absorb, transmit or reflect light over a specific wavelength range. Absorbance spectroscopy investigates the relationship between particles and electromagnetic radiation. The absorption of light is measured as a function of its wavelength (Lakowicz, 1999). A spectrophotometer measures the quantity of photons absorbed as light passes through a sample. The maximum protein absorption is found at approximately 280 nm and is produced predominantly by tryptophan and tyrosine, with phenylalanine and cysteine disulphide

bonds contributing to a minor extent (Schmid, 2001). The absorbance spectrum can be utilised to calculate protein concentration.

A protein's secondary structure refers to the local arrangement in the space of adjacent ammo acid residues, which are maintained by hydrogen bonds and include alpha-helix and beta-strand conformations. Circular dichroism can compute the variance between absorption coefficients for left and right circulatory polarised light of molecules that contain one or more chiral chromophores (light-absorbing groups) (Ranjbar and Gill, 2009). Absorption by disulphide groups, aromatic side chains, and the peptide backbone causes a protein's spectrum (Woody, 1995).

The peptide backbone predominantly produces the signal in the far-UV region (180-250 nm). The far-UV circular dichroism (CD) spectrum produced by a protein can be used to determine its secondary structure as the peptide backbone adopting different secondary structures produces known spectrum characteristics. Proteins that contain alpha-helices have minima at 208 nm and 222 nm and a positive peak near 190 nm. Beta-strands have a minimum at 218 nm and a positive peak at 196 nm. Lastly, random coils display a positive peak at 212 nm and a minimum at 195 nm (Ranjbar and Gill, 2009). As far-UV CD can be used to determine the presence of secondary structure, it can also be used to investigate protein conformational changes due to environmental variables (Ranjbar and Gill, 2009). Absorption in the far-UV wavelength range (180-250 nm) is highly vulnerable to interference from buffer components and contaminants (Kelly and Price, 2000). Therefore, buffers need to be chosen carefully, and certain experiments can only be evaluated over a portion of the wavelength range.

Lastly, fluorescence can be used to investigate the tertiary structure of a protein. Fluorescence studies use the energy emitted from light in the electromagnetic spectrum to excite electrons from the ground state to an excited state and measure fluorescence released as they return to the ground state (Schmid, 2001). In proteins, the intrinsic fluorophores are the aromatic amino acids tryptophan, tyrosine and phenylalanine. The fluorescence studied for proteins is mainly the result of tryptophan, as tyrosine and phenylalanine emission is mainly transferred to tryptophan (Lakowicz, 1999). The recombinant RBBP6 p53BD used in this study does not contain any tryptophan residues, and therefore fluorescence studies of the tertiary structure were not undertaken.

1.11 Justification of Study

Worldwide, cancer is a major health concern, and there is a great need to develop new cancer therapies. RBBP6 is a 200 kDa eukaryotic protein that is able to bind to p53, a major tumour suppressor protein, and cause p53's degradation. This makes RBBP6 an excellent potential cancer

therapy drug target; however, understanding its ability to interact with p53 is critical in exploiting this interaction in cancer therapy.

1.12 Aim

This study aims to investigate the structure and stability of the p53 binding domain of RBBP6 after expression and purification from a bacterial expression system. It also aims to investigate the interaction between endogenous p53, RBBP6 and MDM2 in normal and cancer mammalian cell lines.

1.13 Objectives

1. To successfully express recombinant p53 binding domain of RBBP6 (RBBP6 p53BD) using a bacterial cell expression system.
2. To successfully purify recombinant RBBP6 p53BD, using necessary chromatographic techniques.
3. To characterise the structure and stability of RBBP6 p53BD using several probes, including clear native PAGE and far-UV CD.
4. To investigate the functionality of the recombinant RBBP6 p53BD using co-immunoprecipitation assays with endogenous p53.
5. To investigate the interaction between endogenous p53 and RBBP6 using immunocytochemistry and co-immunoprecipitation.

2 Methods and materials

2.1 Materials

2.1.1 General

Two pET28a plasmids were procured from GenScript® and were generated by inserting the codon-optimized cDNA sequence that encodes the p53 binding domain of RBBP6 into a pET28a plasmid. Firstly the Ndel and Notl restriction sites were used to include an N-terminal histag (Figure A1 in appendix). Secondly, Ncol and Notl restriction sites were used to exclude the histag (Figure A2 in appendix). The recombinant plasmids were then supplied to Prof. Monde Ntwasa. The p53 binding domain insert used residues 1380-1726 from full-length RBBP6 (NM_006910.4). These residues were chosen by combining the regions identified by Simons and colleagues and Gao and Scott as representing the p53 binding domain of RBBP6, with residues 1727-1792 removed due to a high lysine content that could have caused issues in downstream experiments (Simons *et al*., 1997; Gao and Scott, 2003). GenScript® performed confirmation of gene insert in the plasmid via sequencing alignment and restriction digests. SDS-PAGE and Western blot protein molecular mass markers

were obtained from Thermo Scientific (Massachusetts, United States). Phenol, CM sepharose and histidine affinity nickel cross-linked agarose resins were obtained from Cytiva (formally GE Healthcare Life Sciences) (Uppsala, Sweden). Ultra-pure urea and guanidinium chloride was obtained from Sigma-Aldrich (St. Louis, MO, USA), and any additional chemicals were of analytical grade.

2.1.2 Cell lines

Table 2.1: Mammalian cell lines used in this study.

Cell type	Species	Origin	Cultured in
HEK293	Human	Human embryonic kidney	DMEM
A549	Human	Epithelial lung adenocarcinoma	DMEM
MDA MB 231	Human	Breast adenocarcinoma	DMEM
MCF 7	Human	Breast adenocarcinoma	DMEM

2.1.3 Antibodies

Table 2.2: Primary antibodies used in this study.

Antigen	Antibody	Use	Species	Company	Product code
MDM2	Monoclonal IgG2a	WB, IP	Mouse	Abcam	ab16895
RBBP6	Polyclonal IgG	WB, IP, ICC	Rabbit	Novusbio	NBP1-49535
RBBP6	Polyclonal IgG	WB, IP, ICC	Rabbit	Santa Cruz	A304-975A
P53	Polyclonal IgG	WB, IP,ICC	Rabbit	Santa Cruz	Sc-25767
P53	Polyclonal IgG	WB	Goat	Santa Cruz	Sc-17577
P53	Monoclonal IgG2a	WB, IP, ICC	Mouse	Abcam	ab1101
Polyhistidine	Monoclonal IgG	IP,WB	Mouse	Sigma	H-1029
Polyhistidine	Monoclonal IgG	WB	Rabbit	Sigma	SAB5600227

Table 2.3: Secondary antibodies used in this study.

Antigen	Antibody	Use	Species	Company	Product code
Mouse	pAb	WB. IP	Goat	Abcam	ab205719
Rabbit	pAb	WB, IP	Goat	Abcam	ab6721
Goat	pAb	WB	Rabbit	Abcam	ab6697
Mouse	Polyclonal IgG	ICC	Goat	Abcam	ab6786
Rabbit	Polyclonal IgG	ICC	Goat	Abcam	ab6717

2.2 Bacterial cell transformation and induction study

Competent *Escherichia coli* BL21 (DE3), NiCo21 (DE3) and SHuffle® T7 Express cells were transformed with the pET28a plasmid containing DNA encoding the p53 binding domain of RBBP6 with a polyhistidine tag. Competent BL21 (DE3) and SHuffle® T7 Express *Escherichia coli* cells were transformed with the pET28a plasmid containing DNA encoding the p53 binding domain of RBBP6 without any tags. The recombinant domain was expressed with and without a polyhistidine tag as a tag can help simplify purification. However, the addition of a purification tag to a protein can sometimes cause protein instability, incorrect folding or insoluble expression of the protein of interest. Although a polyhistidine tag is not known to regularly cause these problems, the expression of the RBBP6 p53BD without the presence of a tag was still investigated. Competent *Escherichia coli* cells were thawed on ice for 15 minutes. Then 3 µl of pET28a plasmid DNA (100 $ng.\mu l^{-1}$) was added to 100 µl of competent cell mixture and placed on ice for 30 minutes. The cells were then heated at 42 °C for 45 seconds using a heating block and rapidly transferred onto the ice for two minutes.

Next, 500 µl of SOC outgrowth media (New England Biolabs, B9020) was added to the cell mixture and was incubated for 90 minutes at 37 °C with 230 rpm shaking. Using the spread plate technique, all cells were plated on LB-agar plates supplemented with 30 µg/ml kanamycin. Agar plates were then incubated at 37 °C for 12-16 hours. Single colonies were taken from each cell line and added into 20 ml of sterile, fresh LB and grown for 12-16 hours, after which a 1:50 dilution was added to fresh LB and grown to mid-log. Glycerol stocks were created by adding equal volumes of 30 % autoclaved glycerol and cell culture. The glycerol-cell mixture was frozen at -80 °C until needed. Minipreps and restriction digests were carried out to confirm plasmid presence, using New England Biolabs (Ipswich, Massachusetts, USA) NdeI and XhoI for RBBP6 p53BD with polyhistidine tag and NdeI and NotI for RBBP6 p53BD without a tag. With cutsmart buffer, the plasmid and enzymes were incubated for 1 hour at 37 °C. The whole plasmid and digests were analysed using agarose gel electrophoresis (section 2.4.1).

BL21 (DE3) and NiCo21 (DE3) cells contain the λDE3 lysogen, which contains the gene for T7 RNA polymerase that is controlled by an IPTG inducible lac UVS promoter (Studier and Moffatt, 1986). In addition, the pET28a plasmid is inducible by IPTG as it contains a lac UV5 promoter upstream from the target gene, as well as the repressor *lacI* gene and has kanamycin antibiotic resistance, which acts as a selection marker. The system controlling gene expression in this plasmid involves the T7 promoter from the bacteriophage T7, which is not acknowledged by bacterial mRNA polymerase. Instead, the activity of the T7 promoter is regulated by the lac UV5 promoter, which is situated upstream from the gene of interest (Sørenson and Mortensen, 2005). The plasmid

contains the *LacI* gene, which encodes the LacI repressor and allows for its production. The LacI repressor blocks the expression of T7 RNA polymerase by binding to the lac operator. IPTG binds to the LacI repressor, resulting in structural changes that cause the lac operator to be released. This frees the lac UV5 promoter and allows T7 RNA polymerase to be transcribed (Sørenson and Mortensen, 2005). The expressed T7 RNA polymerase interacts with the T7 promoter, situated upstream of the target gene within the plasmid. In this case, the gene coding for RBBP6 p53BD, which is then translated into RBBP6 p53BD protein and overexpression occurs.

Mammalian proteins are notoriously difficult to express, with correct folding, in bacterial cell lines, especially proteins that require disulphide bond formation or post-translational modification. SHuffle® T7 Express cells are genetically engineered to have an altered redox state that allows for the formation of stable disulphide bonds within the bacterial cell cytoplasm and express DsbC in the cytoplasm, which assists the cells to isomerise mis-oxidized protein to their native states. This is because DsbC is an oxidoreductase chaperone that is capable of assisting in the oxidative folding of proteins (Lobstein *et al*., 2012). Even though RBBP6 p53BD does not contain a disulphide bond (it only has a single cysteine residue), difficult proteins incorrectly folded or expressed insolubly have been found to be correctly folded when expressed in SHuffle® T7 Express cells (Shoae *et al*., 2021).

Glycerol stocks (50 µl) of all *Escherichia coli* cell lines containing the pET28a plasmid (with the sequence insert) were added to 20 ml sterile, fresh LB, inoculated with 30 µg/ml kanamycin for all cell lines. All cell lines were grown for 12-16 hours at 37 ˚C with 230 rpm shaking before being inoculated into fresh LB to a dilution of 1:50, containing kanamycin (30 µg/ml) for all cell lines. Induction was performed when the cell culture produced a reading between 0.5 and 0.8 computed using optical density readings with an Implen P330 NanoPhotometer (München, Germany) at a wavelength of 600 nm. IPTG concentrations between 0.1 mM and 1.0 mM were evaluated. All cells were grown at a 37 ˚C, and various post-induction times from two to 16 hours were evaluated.

After induction, whole-cell samples were collected by centrifugation of 1 ml of cell culture for five minutes at 12,100 x g. The whole-cell pellet obtained from this centrifugation was suspended in 400 µl 50 mM sodium phosphate, pH 7.4. To analyse the extent of soluble protein expression, the soluble (supernatant) and insoluble (pellet) fractions were separated by taking 5 ml of cell culture and centrifuging it at 3000 x g for 15 minutes at 4 ˚C. The supernatant was discarded, and the cell pellet was suspended in 700 µl of 50 mM sodium phosphate, pH 7.4. Suspended cells were then sonicated with a Qsonica Q700 sonicator (Newtown, USA) at 60 amperes for six, 10 second rounds (pulsed at two seconds on, one second off) and placed on ice for two minutes in between each

cycle. The sonicated cell mixture was then centrifuged for 20 minutes at 12,100 x g at 4 ˚C before removing the supernatant. The pellet was then re-suspended in 700 µl 50 mM sodium phosphate, pH 7.4. Sonication and centrifugation were repeated for samples taken at various time intervals between two and 16 hours post-induction, depending on the cell line. Whole cells, supernatant (soluble fraction) and pellet (insoluble fraction) samples were investigated using SDS-PAGE (section 2.4.2).

For purification, a cell pellet from 100-200 ml LB at a time was centrifuged and frozen at -20 °C before use. When defrosted, the cell pellet was re-suspended in 10 ml of the necessary buffer. The cell mixture was then sonicated with a Qsonica Q700 sonicator (Newtown, USA) at 80 amperes for 16, 30 second rounds (pulsed at two seconds on, one second off) and placed on the ice during and in between each cycle. The sonicated cell mixture was then centrifuged for 25 minutes at 3000 x g at 4 ˚C before removing the supernatant for further use. Supernatant and pellet samples were analysed using SDS-PAGE to ensure successful lysis via sonication.

2.3 Purification

2.3.1 Hydrophobic interaction

Hydrophobic interaction chromatography separates molecules based on their hydrophobicity, which is the repulsion found between a non-polar compound and the polar environment surrounding it (Queiroz *et al*., 2001). It relies on the presence of a salt in the binding buffer to cause a reduction of the solvation of the sample protein molecules, which results in the exposure of the protein molecule's hydrophobic regions on the surface of the protein molecule. This enables the protein to interact with the alkyl or aryl ligands in the column resin. Lowering the salt concentration in the buffer results in the interaction between the protein molecule and the resin becoming weaker, causing the bound proteins to elute off the column (Ochoa, 1978; Queiroz *et al*., 2001).

2.3.1.1 Salt precipitation trials

Before hydrophobic interaction chromatography could be performed, a protein precipitation trial needed to be performed to estimate the salt concentration that the protein of interest precipitates out of the solution. This indicates the salt concentration range that could be used for chromatography. The trials used ammonium sulphate and tested a number of different concentrations between 50 mM and 2 M. A stock solution of 50 mM sodium phosphate with 3 M ammonium sulphate, pH 7 was added dropwise to the soluble fraction of NiCo21 (DE3) cells in 50 mM sodium phosphate, pH 7, until each concentration was reached. Samples were incubated at room temperature for 30 minutes with rotation before being centrifuged for 15 minutes at 12,100 x g at 22 °C to separate the precipitated proteins. The supernatant was removed, and the protein

pellet was suspended in 50 mM sodium phosphate, pH 7, and both fractions were analysed using SDS-PAGE (section 2.4.2).

2.3.1.2 Hydrophobic interaction purification trials

A small hydrophobic interaction chromatography trial was performed using 0.4 M, 1.0 M and 1.2 M ammonium sulphate. Briefly, using a BioRad NGC™ Chromatography system, a Cytiva HiTrap Phenyl high performance (Uppsala, Sweden) column was equilibrated with 10 column volumes of 50 mM sodium phosphate, pH 7 with either 0.4 M, 1.0 M, or 1.2 M ammonium sulphate (binding buffer). The soluble fraction from NiCo21 (DE3) cells was incubated in the desired ammonium sulphate concentration for 30 minutes at room temperature, with rotation, before being centrifuged for 20 minutes at 3000 x g. The supernatant was then removed and used further as the prepared protein sample. The prepared protein sample was then loaded onto the column, followed by the column being washed with 10 column volumes of respective binding buffer. The protein was next eluted with 50 mM sodium phosphate, pH 7 (elution buffer), using a linear gradient (five column volumes) so that column conditions reached 0 M ammonium sulphate, followed by six isocratic column volumes of 50 mM sodium phosphate, pH 7. The prepared protein sample, flow-through and fractions with significant A_{280} values were collected and analysed using SDS-PAGE (section 2.4.2).

2.3.1.3 Two-step hydrophobic interaction chromatography

Two hydrophobic interaction chromatography purifications were performed in series, namely, Step one and Step two. Firstly for Step one, after sonication, the soluble fraction was incubated in 1.0 M ammonium sulphate for 30 minutes with rotation before being centrifuged for 20 minutes at 3000 x g at 20 ˚C to remove precipitated proteins. NiCo21 (DE3) *Escherichia coli* cells were used for RBBP6 p53BD with a polyhistidine tag and SHuffle® T7 Express *Escherichia coli* cells for RBBP6 p53BD without a tag. The prepared protein sample was then loaded onto the phenol cross-linked agarose resin from Cytiva, namely HiTrap Phenyl high performance (Uppsala, Sweden).

Using a BioRad NGC™ Chromatography system, the Cytiva HiTrap Phenyl high performance (Uppsala, Sweden) column was equilibrated with 10 column volumes of binding buffer (50 mM sodium phosphate, pH 7 with 1 M ammonium sulphate). The prepared protein sample was then loaded onto the column, followed by the column being washed with 10 column volumes of binding buffer (50 mM sodium phosphate, pH 7 with 1 M ammonium sulphate). Next, the protein was eluted using a linear gradient from 1 M to 0 M ammonium sulphate, followed by six isocratic column volumes of elution buffer (50 mM sodium phosphate, pH 7). The gradient was produced by mixing the binding buffer (50 mM sodium phosphate, pH 7 with 1 M ammonium sulphate) with

elution buffer (50 mM sodium phosphate, pH 7). All buffers were filtered using a 0.2 µm filter before use.

Secondly, for Step two, the flow-through from Step one had ammonium sulphate 3 M stock solution added to it to reach a final concentration of 1.4 M ammonium sulphate. The protein sample was then incubated in 1.4 M ammonium sulphate for 30 minutes with rotation before being centrifuged for 20 minutes at 3000 x g at 20 ˚C to remove any precipitated proteins. The prepared protein sample was then loaded onto the Cytiva HiTrap Phenyl high performance (Uppsala, Sweden) column pre-equilibrated with 10 column volumes of binding buffer (50 mM sodium phosphate, pH 7 with 1.4 M ammonium sulphate). The column was then washed with eight column volumes of binding buffer. Bound proteins were eluted using a gradient (six column volumes) from 1.4 M to 0 M ammonium sulphate, followed by six isocratic column volumes of 50 mM sodium phosphate, pH 7. The gradient was produced by mixing the binding buffer (50 mM sodium phosphate, pH 7 with 1.4 M ammonium sulphate) with elution buffer (50 mM sodium phosphate, pH 7). Fractions collected were analysed using SDS-PAGE (section 2.4.2) before further use.

2.3.2 Immobilised metal affinity chromatography (IMAC)

Immobilized metal affinity chromatography (IMAC) is an affinity method where a specific metal-ligand is coupled with a support molecule within a resin. A mixture of proteins can then be filtered through the resin, and those with the affinity can bind to the resin. Non-affinity molecules flow straight through the column without interaction. The bound molecules are then eluted from the column by changing the conditions within the affinity column, often by adding a competitive agent. An affinity tag, which is a sequence that has a binding affinity to the IMAC resin, is often added to a protein in the plasmid design. Polyhistidine is one of the most commonly used tags (Yip *et al.,* 1989). The amino acid histidine can interact and form a complex with the nickel ion (Ni^{2+}), with additional histidine residues increasing a protein's affinity for nickel ions (Ni^{2+}) (Yip *et al.,* 1989; Hutchens and Yip, 1990). Histidine can interact with the metal ions as histidine residues contain imidazole rings that can donate electrons, forming bonds with the immobilized metal ions.

Fractions identified to contain RBBP6 p53BD with a polyhistidine tag from hydrophobic interaction chromatography Step two (Section 2.3.1.3) were collected and pooled before being dialysed into 50 mM sodium phosphate, pH 7.4 with 500 mM sodium chloride and 30 mM imidazole. Dialysis of protein samples was performed using three buffer changes, four, five and 18 hours apart, respectively. Dialysis was performed at approximately 4 ˚C with a buffer volume 10 times the sample size volume. The protein sample was then loaded onto a nickel cross-linked agarose resin from Cytiva, namely Histrap high performance (Uppsala, Sweden). Cytiva Histrap high-performance

columns (Uppsala, Sweden) were equilibrated with 10 column volumes of binding buffer (50 mM sodium phosphate, pH 7.4 with 500 mM sodium chloride and 30 mM imidazole). Sodium chloride and a low imidazole concentration were added to reduce nonspecific hydrophobic protein interactions with the nickel affinity resin (Bornhorst and Falke, 2000). After loading the prepared protein sample, the column was then washed with 10 column volumes of the binding buffer (50 mM sodium phosphate, pH 7.4 with 500 mM sodium chloride and 30 mM imidazole).

The bound proteins were eluted off the column using a linear gradient (six column volumes) from 30 to 500 mM imidazole followed by five isocratic column volumes of elution buffer (50 mM sodium phosphate, pH 7.4 with 500 mM sodium chloride and 500 mM imidazole). The gradient was produced by mixing binding buffer (50 mM sodium phosphate, pH 7.4 with 500 mM sodium chloride, 30 mM imidazole) with elution buffer (50 mM sodium phosphate, pH 7.4 with 500 mM sodium chloride and 500 mM imidazole). All buffers were filtered using a 0.2 µm filter before use. All chromatography was conducted using a BioRad NGC™ Chromatography system with a computer loaded with ChromLab software (Hercules, USA). RBBP6 p53BD was detected using SDS-PAGE (section 2.4.2) analysis of fractions with high 280 nm absorbance readings. Fractions that were found to contain RBBP6 p53BD were then combined and concentrated using Sartorius Vivaspin centrifugal concentrators, 30 MWCOs (Göttingen, Germany).

2.3.3 Cation exchange chromatography

Ion-exchange chromatography utilises the ability of proteins to hold a charge and the reversible reaction that is possible between a charged molecule and an oppositely charged matrix (Adams and Holmes, 1935). Proteins are amphoteric due to the presence of an N-terminal amine group, a C-terminal carboxyl group and ionisable side chain groups of amino acid residues. This means a protein's net surface charge can be manipulated by its buffer environment's pH or ionic strength. A protein's isoelectric point (pI) is the pH value at which it has no net charge, and at a pH above a protein's pI, the protein is negatively charged, and at a pH below, the protein holds a positive charge. (Lampson and Tytell, 1965). An oppositely charged resin is used, and bound proteins can be eluted off the column by changing pH or increasing ionic strength (Karlsson *et al*., 1998). In cation exchange chromatography, the binding ions on the proteins have a positive charge, and the immobilized functional groups in the resin have a negative charge (Adams and Holmes, 1935). The isoelectric point for RBBP6 p53BD is predicted to be pH 9.01 by the ProtParam tool on the ExPASy proteomics server (Figure A3 in appendix) (Gasteiger *et al*., 2005).

Fractions identified to contain RBBP6 p53BD without a tag from hydrophobic interaction chromatography Step two, using 1.4 M ammonium sulphate (Section 2.3.1.3), were collected and

pooled before being dialysed into 50 mM sodium phosphate, pH 8 or 7. Cytiva CM sepharose high-performance column (Uppsala, Sweden) was equilibrated with 10 column volumes of 50 mM sodium phosphate with pH 8 or pH 7 (binding buffer). After loading the protein sample, the column was washed with 10 column volumes of binding buffer. The protein was eluted using a linear gradient (six column volumes) from 0 to 1 M sodium chloride followed by five isocratic column volumes of elution buffer (50 mM sodium phosphate, pH 8 or 7 with 1 M sodium chloride, respectively). All buffers were filtered using a 0.2 µm filter before use. Purification was conducted using a BioRad NGC™ Chromatography system with a computer loaded with ChromLab software (Hercules, USA). RBBP6 p53BD was detected using SDS-PAGE (section 2.4.2) analysis of fractions with high A_{280} absorbance readings.

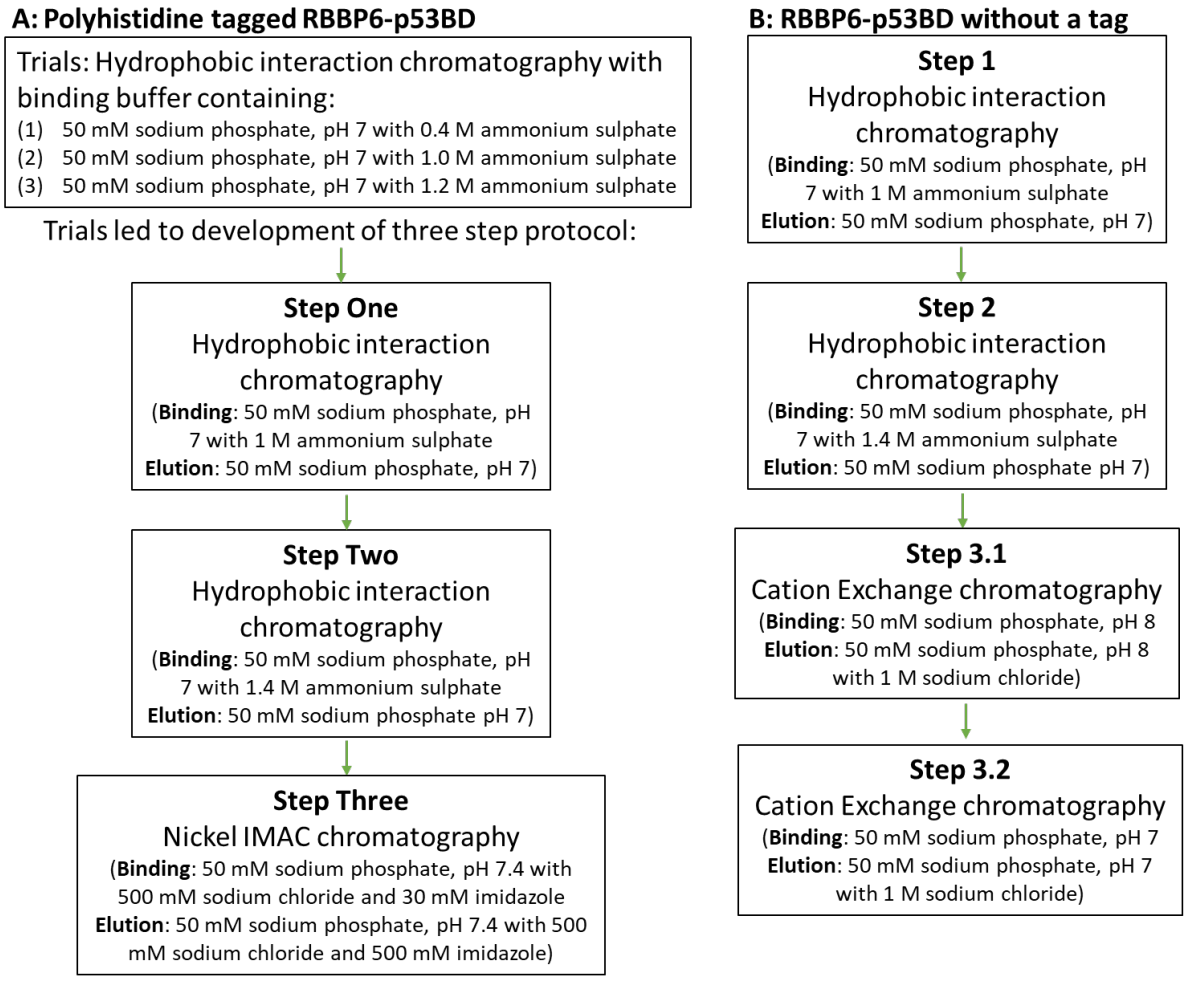

Figure 2.1. Summary of the purification process.

A summary of the trials and purification steps taken for the purification of ***(A)*** *polyhistidine tagged RBBP6 p53BD and* ***(B)*** *non-tagged RBBP6 p53BD.*

2.4 Gel electrophoresis

2.4.1 Agarose

Gels containing 1.0 % (w/v) of agarose in 1 x TAE buffer (40 mM Tris-acetate, pH 8.3 with 1 mM EDTA) were used for the separation of DNA fragments. Before the loading, DNA samples were mixed with a 1:5 volume of 6 x Novel Juice (Bio-Helix), which acts as both the loading dye and the fluorescent dye. GeneRuler 1 kb DNA ladder (Thermo Scientific) was used. The agarose gel was performed in 1 x TAE buffer (40 mM Tris-acetate, pH 8.3 with 1 mM EDTA), at 90 V, for approximately 1 hour and 30 minutes. A BioRad, Universal Hood III (Hercules, USA) gel imaging system was used.

2.4.2 SDS-PAGE

SDS-PAGE was used to visualise the solubility and purity of RBBP6 p53BD and Western blot analysis. SDS-PAGE uses electrophoresis to separate proteins based on their molecular mass (Laemmli, 1970). A 10 or 12.5 % separating gel and 4 % stacking gel was used in a BioRad Mini-PROTEIN Electrophoresis Cell (Hercules, USA). The protein samples were diluted two-fold with SDS-PAGE sample buffer (0.5 M Tris-HCl, pH 6.8 with 10 % (w/v) glycerol, 2 % (w/v) SDS, 5 % (w/v) β-mercaptoethanol and 0.05 % (w/v) bromophenol blue). Protein in the SDS-PAGE sample buffer was boiled for 5 minutes. The gel was performed in an SDS-PAGE running buffer (0.5 M Tris-HCl, pH 8.3 with 7.2 % (w/v) glycine and 0.5 % SDS (w/v)) at 160 volts for approximately 1 hour.

Three molecular weight markers were used, firstly the Pierce™ Unstained Protein MW Marker (Thermo Scientific, 26610) with a molecular weight range from 116 kDa to 14.4 kDa. The second ladder used was the Spectra™ Multicolour Broad Range Protein Ladder (Thermo Scientific, 26623) with a molecular weight range from 260 kDa to 10 kDa. Lastly the Perfect Protein™ Markers (Merck, 69079) with a molecular weight range of 10 kDa to 225 kDa. Each gel was then stained with 0.05 % R250 Coomassie Brilliant blue, 10 % acetic acid and 50 % methanol for an hour and then de-stained with 5 % ethanol and 7 % acetic acid solution overnight. A BioRad, Universal Hood III (Hercules, USA) gel imaging system was used.

2.4.3 Clear native PAGE

Clear native PAGE samples are prepared in a non-reducing, non-denaturing sample buffer, and the proteins are separated based on molecular mass, structure and charge. Two types of clear native PAGE were performed in a BioRad Mini-PROTEIN Electrophoresis Cell (Hercules, USA). Firstly, a continuous 8 % Tris-HCl gel was used, with a native PAGE sample buffer (62.5 mM Tris-HCl, pH 8 with 40 % (w/v) glycerol and 0.01 % (w/v) bromophenol blue) and a running buffer of 25 mM Tris-HCl, pH 8 with 192 mM glycine. Secondly, a native continuous 8 % Hepes-Imidazole gel was used with a native PAGE sample buffer (35 mM Hepes, pH 7.4 with 43 mM imidazole, 10 % (w/v) glycerol,

and 0.05 % (w/v) bromophenol blue) and native PAGE running buffer (35 mM Hepes, pH 7.4 with 43 mM imidazole) as described in McLellan (McLellan, 1982).

Due to RBBP6 p53BD having a predicted pI of 9, by ProtParam tool on the ExPASy proteomics server (Figure A3 in appendix) (Gasteiger *et al*., 2005), the electrodes were reversed. The gels were performed at 140 volts for approximately two hours. Each gel was then stained with 0.05 % R250 Coomassie Brilliant blue, 10 % acetic acid and 50 % methanol for an hour and then de-stained with 5 % ethanol and 7 % acetic acid solution overnight. A BioRad, Universal Hood III (Hercules, USA) gel imaging system was used to photograph the gels.

2.4.4 Western blot

Following the separation of proteins by SDS-PAGE (as described in section 2.4.2), proteins were transferred onto a polyvinylidene difluoride (PVDF) membrane by placing the following layers into the transfer cassettes: a sponge, filter paper, polyvinylidene difluoride (PVDF), SDS-PAGE gel, filter paper and a sponge. A SuperSignal™ Enhanced Molecular Weight Protein Ladder (Thermo Scientific, 84786) or Spectra™ Multicolor Broad Range Protein Ladder (Thermo Scientific, 26634) was used in gels where protein transfer to membranes was going to occur. Transfer cassettes were fully immersed in TruPAGE™ transfer buffer (Sigma, PCG3011) within the transfer tank and ran at 40 V for 16 hours at 4 °C. The SDS-PAGE gels were stained and de-stained after the transfer as described in section 2.4.2 to check for successful transfer.

The polyvinylidene difluoride (PVDF) membrane was then incubated in casein blocking buffer (Sigma, B6429) for one hour at room temperature, with agitation, before being incubated in primary antibody (Table 2.2) diluted in casein blocking buffer (1:10000) for 16 hours at 4 °C, with agitation. Following incubation with primary antibodies, the polyvinylidene difluoride (PVDF) membranes were washed in TBST three times for five minutes each time, with agitation. The polyvinylidene difluoride (PVDF) membranes were then incubated with secondary antibodies (Table 2.3) diluted in blocking buffer (1:10000) for at least one hour at room temperature, with agitation. After this incubation, the membranes were washed three times, for five minutes, in TBST, with agitation. Proteins were visualised by incubating the membrane in SuperSignal™ West Pico PLUS Chemiluminescent Substrate (Thermo Scientific, Massachusetts, United States) for five minutes and photographed using a BioRad, Universal Hood III (Hercules, USA) gel imaging system.

2.4.5 Mass spectrometry

Partially purified RBBP6 p53BD with polyhistidine tag proteins was analysed using SDS-PAGE (Section 2.4.2). The protein bands of interest were excised and placed in ultrapure water at 4 °C. The samples were then sent to CSIR (Pretoria, South Africa) for trypsin digested LC-MS analysis.

2.5 Spectroscopic techniques

2.5.1 Protein concentration determination

2.5.1.1 Qubit® Protein Assay

According to the manufacturer's instructions, the fluorescent Qubit® Protein Assay Kit developed by Thermo Scientific (Waltham, Massachusetts, USA) was used as a method to quantify proteins. Briefly, Qubit® Protein reagent was mixed with Qubit® Protein buffer in a 1:200 ratio and added to protein samples and Qubit® standards (10 µl sample to 190 µl of Qubit® working solution) before incubation at room temperature for 15 minutes. A standard curve was generated from the standards provided in the kit using the Qubit® 2.0 Fluorometer (Waltham, Massachusetts, USA). Finally, all sample tubes were read. Quantification data was generated automatically by the Qubit® 2.0 Fluorometer software by comparing the absorbance measured in each sample to the standard curve.

2.5.1.2 Absorbance

Protein concentration can be calculated from absorbance spectroscopy using the Beer-Lambert law:

$$A = \varepsilon\lambda cl \quad (5)$$

where A is the absorbance at the respective wavelength, ελ is the molar extinction coefficient of the absorber at wavelength λ (L. mol^{-1}. cm^{-1}), c is the concentration of the absorber (mol. L^{-1}), and l is the path length of the cuvette (cm).

To calculate the molar extinction coefficient ε of a protein, the number of tryptophan, tyrosine and cysteine disulphide bonds are obtained and used in the following equation described by Perkins (Perkins, 1986):

$$Ɛ280\ M^{-1}.\ cm^{-1}=[5550 \times (\Sigma Trp\ residues)]+[1340 \times (\Sigma Tyr\ residues)]+[150 \times (Cys\ residues)] \quad (6)$$

The molar extinction coefficient for RBBP6 p53BD was determined to be 8940 $M^{-1}.cm^{-1}$ using formula 6 with RBBP6 p53BD containing 0 Trp, 6 Tyr and 1 Cys residues.

Protein concentration was determined prior to other spectroscopic techniques using an Applied Photophysics Chirascan Plus (Leatherhead, United Kingdom) with Photophysics Pro-Data software. A quartz cuvette with a path length of 10 mm was used. A bandwidth of 1 mm was used, and a measurement was recorded for every 1 nm between 360 nm and 220 nm. For every sample, three spectra repeats were recorded and averaged. All spectra had buffer contributions subtracted.

2.5.2 Far-UV circular dichroism

Far-UV circular dichroism (CD) spectra were obtained with an Applied Photophysics Chirascan Plus (Leatherhead, United Kingdom) with Photophysics Pro-Data software. Wavelengths between 250 nm to 190 nm were evaluated at 22 ˚C. Measurements were recorded every 1 nm, at a bandwidth of 1 nm and a 2 nm per second scan speed. Lastly, a 1 mm quartz cuvette was used.

Spectra values collected were converted to mean residue ellipticity with the following formula:

$$[\theta] = 100\ (signal)/\ Cnl \qquad (7)$$

where C is the concentration of protein in mM, n is the number of amino acid residues, and l is the path length in cm. For every sample, three spectra repeats were recorded and averaged. All spectra had buffer contributions subtracted.

2.5.3 Unfolding

Heat and denaturants such as urea and guanidinium chloride are capable of unfolding native proteins (Schmid, 2001). Therefore a protein's stability can be tested by subjecting it to the different conditions and measuring the far-UV circular dichroism spectrum for the presence or absence of characteristic secondary structure measurements (Kelly and Price, 2000). Far-UV CD was used to monitor the stability of the protein by displaying how the secondary structure changed in response to changes in buffer conditions.

2.5.3.1 Thermal

Far-UV circular dichroism spectra were obtained as described in section 2.5.2 while increasing the temperature of the protein sample from 20 ˚C to 90 ˚C. The temperature was maintained by a PCS.3 Single Cell Peltier Temperature Controller, with a circulating chiller unit programmed by Chirascan's Pro-Data software (Leatherhead, United Kingdom).A spectrum was recorded every two degrees between 20 ˚C and 90 ˚C. A final spectrum was recorded when the protein sample was cooled to 20 ˚C after being heated to 90 ˚C. The spectrum was recorded between 195 nm and 250 nm. All spectra had buffer contributions subtracted.

2.5.3.2 Denaturants

RBBP6 p53BD was tested in the presence of urea and guanidinium chloride. All urea used was prepared as described by Nozaki, and guanidinium chloride was prepared as described by Pace using 10 mM sodium phosphate, pH 7.4 (Nozaki, 1972; Pace, 1986). The pH was adjusted before being filtered with a 0.4 µm filter. Stock solution concentrations were confirmed using an Atago R5000 Refractometer (Tokyo, Japan) through refractive indices. Stock solutions were used within a week of being made. Samples were prepared by adding denaturant stock solutions to the given concentration and incubated for one hour before spectra were recorded. For refolding studies,

protein samples were diluted back down from 6 M to 1 M guanidinium chloride and 8 M to 0.5 M urea by adding 10 mM sodium phosphate, pH 7.4. Protein samples were allowed to fold for one hour before spectra were recorded at each new concentration. Far-UV circular dichroism spectra were obtained as described in section 2.5.2. The spectrum was recorded between 195 nm and 250 nm. All spectra had buffer contributions subtracted.

2.6 Computational analysis of protein structure

2.6.1 Using amino acid sequence

I-TASSER (Yang *et al*., 2015) is an online resource that can assist in protein structure prediction. I-TASSER identifies structural templates from the PDB library using a multiple threading alignment approach called LOMETS (Wu and Zhang, 2007). Structural models are constructed by iterative fragment assembly simulations. The lowest free-energy conformations are identified by SPICKER to refine the structural models, with the low free-energy conformations further refined by full-atomic simulations using FG-MD and ModRefiner (Yang and Zhang, 2015).

The confidence of the 3D structures returned is estimated by the confidence score (C-score), which is given as a value between -5 and 2, with a score greater than -1.5 indicating a model of correct global topology. RMSD scores are also given, with larger RMSD scores showing greater dissimilarity to the structures used. TM-score measures the degree of similarity between two proteins containing different tertiary structures. The TM-score measures this similarity using a score ranging from 0 – 1, where 1 indicates a perfect match, and a value above 0.5 is seen as globally relevant. The structure of RBBP6 p53BD was estimated using I-TASSER using the primary amino acid sequence of residues 409-1792 of full-length RBBP6 (NM_006910.4). PyMOL Molecular Graphics System ((2.5.2 Edu), Schrodinger, LLC) was used to visual residues 1380-1726 constituting the recombinant RBBP6 p53BD in this study.

2.6.2 2struc secondary structure prediction server

The top three 3D models generated by I-TASSER from the RBBP6 p53BD sequence were analysed using 2struc secondary structure prediction (Klose *et al*., 2010) server to estimate the percentage of alpha-helices, beta-strands and random coil for RBBP6 p53BD.

2.6.3 Using far-UV circular dichroism spectrum

Far-UV CD spectrum collected was analysed using open-source software CONTIN (Van Stokkum *et al*., 1990), SELCON3 (Sreerema *et al*., 1999) and CDSSTR (Manavalan and Johnson., 1987) in DichroWeb (Miles *et al*., 2021). Each software used several reference sets to predict the percentages of alpha-helices, beta-strands, turns, and random coils. NRMSD (normalized root-mean-square deviation) is a parameter used to measure the fit of data. It is a measure of the

correspondence between the experimental and calculated spectra, and it is one way that can be used to judge the quality of the results. NRMSD generally needs to be below 0.1 to be deemed acceptable; however, various programs give higher or lower NRMSD scores on average. Therefore, the fit to spectra also needs to be taken into consideration.

2.7 Mammalian cell culture

2.7.1 Recovery, maintenance and storage

Cell lines used in this study are shown in Table 2.1. To recover frozen cells, the frozen stocks were defrosted at room temperature and then placed in a sterile flask with recovery media (79 % DMEM, 20 % FBS and 1 % pen/strep). Cells were grown in a humidified incubator at 37 °C, with 5 % CO_2. Once cells reached a confluency of approximately 80 %, the media was removed, and the cells were washed twice with PBS buffer before adding trypsin-EDTA. Cells were then incubated for 10-15 minutes at 37 °C until cells had detached. Media (89 % DMEM, 10 % FBS and 1 % pen/strep) was then added to stop the trypsin-EDTA reaction. The cells were then centrifuged at 600 x g for three minutes at 4 °C. The supernatant was removed before the cells were suspended in either maintenance media (89 % DMEM, 10 % FBS and 1 % pen/strep) for further seeding or freezing media (10 % DMSO and 90 % FBS) at a density of approximately 6×10^6 cells mL^{-1}. Cells were frozen at -80 °C and used within a month. Cells were counted using a hemocytometer.

2.7.2 Cell lysis

Unless otherwise stated, mammalian cells were lysed by sonication at 60 A for five, 10 second cycles, with each cycle consisting of two seconds pulse on and one-second pulse off. Cells were kept on ice during and in between sonication cycles. Lysed cells were then centrifuged at 12,100 x g for 20 minutes at 4 °C. The supernatant was removed and used for further studies after adding 50 µl of protease inhibitor cocktail (Sigma-Aldrich, St. Louis, USA).

2.8 Immunocytochemistry

Coverslips (Lasec, South Africa) were autoclaved at 121 °C for 20 minutes and placed into six-well plates before being further sterilized under UV light for 60 minutes before use. Cells were prepared as described in section 2.7.1 and seeded at a density of 2×10^5 cells/ml in each well. Cells were then grown until they reached a confluency of between 70 and 80 %. The cells were fixed by incubation in 3 % formaldehyde (Sigma, F8775) in PBS at room temperature for 15 minutes. The fixative was then aspirated, and the coverslips were washed four times in PBS buffer, with five minutes of incubation each time. Next, the cells were permeabilized by incubation in 0.25 % Triton X-100 in PBS at room temperature for 10 minutes. The triton X-100 solution was then aspirated, and the coverslips were washed in PBS three times, with a five minute incubation each time.

Next, cells were blocked using 10 % normal animal serum (of the host in which the secondary antibody was produced) with 0.1 % BSA. The cells were incubated at room temperature in the blocking buffer for 90 minutes before removing the blocking buffer and adding the primary antibody diluted in 1 % normal animal serum (of the host that the secondary antibody was produced in) with 0.1 % BSA and incubating at 4 °C for 12-16 hours. After incubation, the primary antibody was aspirated from the coverslips, and they were washed five times in PBS with 0.1 % tween, with a five minute incubation each time. Next, the cells were incubated in the conjugated secondary antibody for one hour and 30 minutes at 37 °C in the dark. The secondary antibody was then aspirated from the coverslips, and the coverslips were washed five times in PBS, for five minutes each time, in the dark. For dual stained cells, the process would be repeated; however, the primary antibody incubation would now be performed in the dark as well in order to prevent photo-bleaching the first secondary antibody. When dual staining, the primary antibodies would be derived from different species to ensure the correct identification of the protein of interest. Multiple dilutions between 1:50 and 1:5000 of both primary and secondary antibodies were tested to optimise staining. Primary and secondary antibodies used are shown in Table 2.2 and Table 2.3.

Prolong Gold Anti-fade reagent with DAPI (Invitrogen, P36935) was used as mounting media, and coverslips were mounted cell side down on microscope slides. Slides were cured for 24 hours before being sealed. Slides were kept at 4 °C in the dark until needed. Slides were visualised using a Zeiss (Oberkochen, Germany) LSM 710 series confocal fluorescence microscope using Zen Black imaging software and analysed further using Zen Blue imaging software and ImageJ software (Schneider *et al*., 2012). The ImageJ plugin, JACoP, was used for quantitative colocalisation analysis (Bolte and Cordelières, 2006).

Bleed-through or crosstalk is a common phenomenon in fluorescent staining where the emission of one of the fluorophores can be detected in a chancel reserved for a different fluorophore. This creates the illusion of a false positive colocalisation. To prevent this, several precautions were taken. Firstly, fluorophores were carefully chosen so that desired wavelengths were as far from each other as possible. Secondly, band-pass filters were used to ensure the correct wavelength entered the detector. Lastly, controls were performed for every immunocytochemistry experiment to ensure bleed-through was not occurring. These controls include cells stained with (1) no antibodies for auto-fluorescence in cell preparation procedure, (2) secondary antibodies only, (3) one primary antibody, with other species secondary antibody, (4) single staining in colocalisation studies and (5) a range of concentrations of both primary and secondary antibodies. Channels were then checked to confirm the absence of any signal in the reciprocal channel. Controls were

repeated for each antibody used. Any signal present not being produced by the protein of interest can then be removed by adjusting thresholds, as it is background staining. The procedure was followed for all channels.

2.9 Co-immunoprecipitation

Immunoprecipitation is a technique that purifies a protein of interest (antigen) out of a mixture of proteins using an antibody that specifically interacts with the protein of interest. Agarose beads are used as a support to which a Protein A is added and bound. Protein A can recognise the primary antibody and bind to it. Co-immunoprecipitation (Co-IP) is a form of immunoprecipitation performed under non-denaturing, non-reducing conditions. Co-IP is used to investigate protein interactions as a protein of interest is chosen, and the immuno-complexes isolated during elution can be probed for proteins that interact with the protein of interest.

2.9.1 Co-immunoprecipitation with endogenous protein in normal and cancer cell lines

Approximately 8.4 x 10^6 cells were cultured and lysed as described in section 2.7.2. A primary antibody was added to the cell lysate, and the mixture was incubated for five hours at 4 °C with rotation. Protein A agarose (Abcam, ab193254) was pre-washed with PBS three times before being incubated in 0.1 % BSA in PBS for one hour at 4 °C with rotation. The agarose beads were then washed three to five times with PBS before the cell lysate, and the antibody mixture was added and further incubated for 12-16 hours at 4 °C with rotation.

Next, the agarose beads were washed five times in PBS, with centrifugation at 1000 x g for five minutes each wash. Two types of elution steps were carried out, the first a non-reducing elution using non-reducing sample buffer (0.5 M Tris-HCl, pH 6.8 with 10 % (w/v) glycerol, 2 % (w/v) SDS and 0.05 % (w/v) bromophenol blue) and the second a reducing elution with sample buffer (0.5 M Tris-HCl, pH 6.8 with 10 % (w/v) glycerol, 2 % (w/v) SDS, 5 % (w/v) β-mercaptoethanol and 0.05 % (w/v) bromophenol blue). Antibody heavy and light chains are detected in a Western blot when the same secondary antibody species is used for the Co-IP and the Western blot. The heavy and light chains appear at approximately 50 kDa and 25 kDa. Therefore, when a protein was investigated with a molecular weight similar to the weight of the light or heavy chain, both elution steps were performed in series. If the protein of interest was not a similar molecular weight, then only the reducing elution step was performed. The agarose beads were incubated in the respective sample buffer for 10 minutes at 95 °C and centrifuged at 1000 x g for five minutes at 4 °C. The supernatant was removed and analysed using SDS-PAGE (section 2.4.2) and Western blot (section 2.4.4).

2.9.2 Co-immunoprecipitation with Recombinant RBBP6 p53BD and endogenous p53

Approximately 8.4 x10^6 cells were cultured and lysed as described in section 2.7.2. Recombinant RBBP6 p53BD was prepared and purified as described in sections 2.3.1.3 and 2.3.2. Purified RBBP6 p53BD was added to the cell lysate, and the mixture was incubated at 4 °C with rotation for three hours. Next, the primary antibody was added to the cell lysate and RBBP6 p53BD mixture and was incubated for three hours at 4 °C with rotation. Protein A agarose (Abcam, ab193254) was pre-washed with PBS three times before being incubated in 0.1 % BSA in PBS for one hour at 4 °C with rotation. The agarose beads were then washed three times with PBS before the cell lysate, RBBP6 p53BD and antibody mixture was added and further incubated for 12-16 hours at 4 °C with rotation.

Next, the agarose beads were washed five times in PBS, with centrifugation at 1000 x g for five minutes each wash. Two kinds of elution steps were carried out, the first a non-reducing elution using sample buffer (0.5 M Tris-HCl, pH 6.8 with 10 % (w/v) glycerol, 2 % (w/v) SDS and 0.05 % (w/v) bromophenol blue) and the second a reducing elution with sample buffer (0.5 M Tris-HCl, pH 6.8 with 10 % (w/v) glycerol, 2 % (w/v) SDS, 5 % (w/v) β-mercaptoethanol and 0.05 % (w/v) bromophenol blue). Both elution steps were performed for the Co-IP assay that used the p53 antibodies as the probe. For the Co-IP assay that used polyhistidine antibodies as a probe, just a reducing elution was performed. The agarose beads were incubated in the respective sample buffer for 10 minutes at 95 °C and centrifuged at 1000 x g for 5 minutes at 4 °C., The supernatant was removed and analysed using SDS-PAGE (section 2.4.2) and Western blot (section 2.4.4).

2.9.3 Co-immunoprecipitation in the presence of NADH

A stock solution of NADH (Roche, 10 107 735 001) was prepared in distilled water and concentrations between 50 µM and 500 µM were investigated. Approximately 8.4 x 10^6 cells per NADH concentration were cultured and lysed as described in section 2.7.2, and recombinant RBBP6 p53BD was prepared and purified as described in sections 2.3.1.3 and 2.3.2. NADH and purified RBBP6 p53BD were added to the cell lysate, and the mixture was incubated at 4 °C with rotation for three hours. Next, the primary antibody was added to the cell lysate, NADH and RBBP6 p53BD mixture and was incubated for 12-16 hours at 4 °C with rotation. Protein A agarose (Abcam, ab193254) was pre-washed with PBS three times before being incubated in 0.1 % BSA in PBS for one hour at 4 °C with rotation. The agarose beads were then washed three times with PBS before the cell lysate, RBBP6 p53BD, NADH and antibody mixture was added and further incubated for 12-16 hours at 4 °C with rotation.

The agarose beads were then washed five times in PBS, with centrifugation at 1000 x g for five minutes each wash. Two elution steps were carried out, the first a non-reducing elution step using

non-reducing sample buffer (0.5 M Tris-HCl, pH 6.8 with 10 % (w/v) glycerol, 2 % (w/v) SDS and 0.05 % (w/v) bromophenol blue) and the second a reducing elution with sample buffer (0.5 M Tris-HCl, pH 6.8 with 10 % (w/v) glycerol, 2 % (w/v) SDS, 5 % (w/v) β-mercaptoethanol and 0.05 % (w/v) bromophenol blue). The agarose beads were incubated in the respective sample buffer for 10 minutes at 95 °C and centrifuged at 1000 x g for 5 minutes at 4 °C. The supernatant was removed and analysed using SDS-PAGE (section 2.4.2) and Western blot (section 2.4.4).

3. Results

3.1 Overview of results

RBBP6 is involved in the degradation of p53, either by directly causing p53 ubiquitination or by facilitating the interaction between p53 and its prototypical negative regulator, MDM2. As degradation of p53 results in uncontrolled cell proliferation in cancer cells that retain wild type p53, the interaction between p53 and RBBP6 is a potential cancer therapy target. The main objective of this study was to characterise the p53 binding domain of RBBP6 to further understand RBBP6's ability to interact with p53. This study procured plasmids containing inserts that encoded the RBBP6 p53BD, with and without a polyhistidine tag. A bacterial expression system was chosen because it is economical and relatively easy to use. Recombinant RBBP6 p53BD expression was investigated in a number of bacterial cell lines under varying expression conditions such as inducer concentration and post-induction time. These conditions were investigated to obtain the best expression conditions for RBBP6 p53BD.

RBBP6 p53BD needed to be isolated from the bacterial cell proteins after expression, and therefore, different chromatography techniques were considered. Multiple purification steps were performed in series to optimise a purification protocol for RBBP6 p53BD for the domain to be used in further studies. Once pure, the recombinant RBBP6 p53BD was investigated for the presence of structure, using clear native-PAGE and spectroscopic techniques. Clear native-PAGE can determine if a protein occurs in one or more oligomeric states as it investigates a protein in its native form, using electrophoresis. Far-UV CD is a spectroscopic technique that investigates the secondary structure of a protein, as the spectrum produced by a protein has known characteristics based on the presence of secondary structure conformations such as alpha-helices or beta-strands or simply random coil. Far-UV CD was used to probe the secondary structure of recombinant RBBP6 p53BD, and the spectrum produced was further used to estimate the secondary structure using an online severer DichroWeb (Miles *et al*., 2021). Next, the stability of the RBBP6 p53BD was studied. A protein's stability is vital for a number of downstream experiments, including drug interaction studies and structural determination through techniques such as X-ray crystallography. The

recombinant domain's stability was analysed in the presence of denaturants and an increase in temperature. As Far-UV CD can be used to evaluate a protein's secondary structure, it can also be used to investigate the change in the structure of a protein under different conditions. Therefore, far-UV CD was used to analyse RBBP6 p53BD for chemical and thermal unfolding.

Along with studying the recombinant RBBP6 p53BD, it is important to investigate the subcellular location of endogenous p53 and RBBP6 in normal and cancer cell lines. To achieve this, immunocytochemistry was used. By dual staining the cells with antibodies that can recognise RBBP6 and p53, quantitative colocalisation analysis was conducted using an ImageJ plugin known as JACoP (Bolte and Cordelières, 2006). To investigate whether endogenous RBBP6 and p53 can interact *in vitro*, co-immunoprecipitation (Co-IP) assays were performed. The presence of endogenous MDM2 in the endogenous p53-RBBP6 complexes isolated during Co-IP assays was also investigated using Western Blot. In addition the functionality of the recombinant RBBP6 p53BD produced in this study was investigated using Co-IP assays. Lastly, Twala performed *in silico* studies on the p53 binding domain of RBBP6, and found that NADH is likely to bind to the p53 binding domain of RBBP6 and could potentially interfere with its ability to bind p53 (Twala, 2017). To investigate this, Co-IP assays were performed to determine if different concentrations of NADH in the Co-IP assay reaction could interfere with the binding of the recombinant RBBP6 p53BD and endogenous p53.

3.2 Identification of successful transformation

Several cell lines were transformed with a pET28a plasmid containing the gene insert that encodes RBBP6 p53BD with or without a polyhistidine tag. Successful transformation was confirmed by agarose gel electrophoresis (Figure 3.1A, lane 2). The plasmid extracted during the miniprep was also subjected to a double restriction digest, and these results were also analysed using agarose gel electrophoresis (Figure 3.1B, lanes 3 and 4). The plasmid extracted via miniprep showed the classic formation of a plasmid that takes on at least three conformations based on different levels of structure taken by the circular DNA plasmid (Figure 3.1A, lane 2). The plasmid was digested using XhoI and NdeI for the plasmid containing RBBP6 p53BD with a polyhistidine tag (Figure 3.1B, lane 3) and XhoI and NotI for the plasmid containing RBBP6 p53BD without a tag (Figure 3.1B, lane 4). The restriction digests produced two DNA segments of approximately 5298 bp and 1050 bp, which are seen in the agarose gel. However, the band at 6348 bp indicates the whole plasmid, which has been digested with a single restriction enzyme and is, therefore, a linear piece of DNA. Potentially the NdeI restriction enzyme was not fully functional in the buffer used, as both plasmid digest reactions have this single linear piece of DNA present, and NdeI was the only enzyme used in both digests.

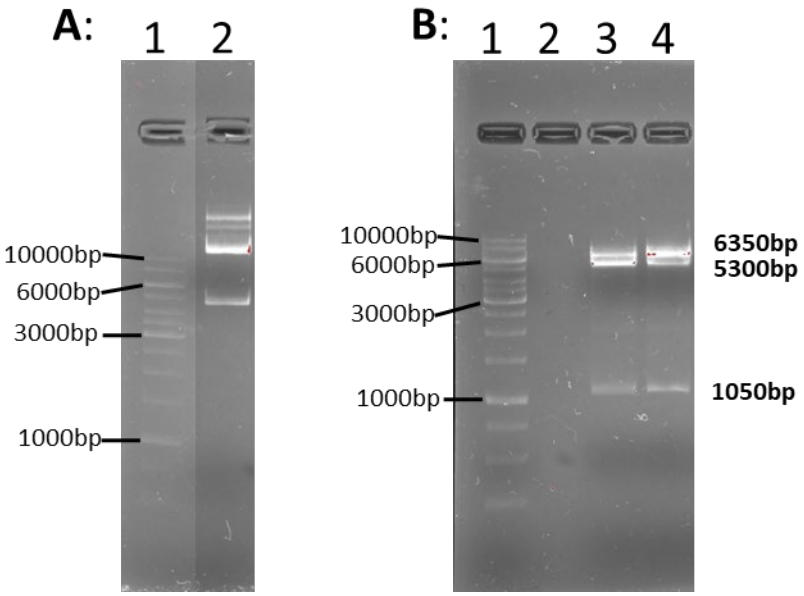

Figure 3.1. Electrophoresis of extracted pET28a DNA containing RBBP6 p53BD gene insert.

(A) *Lane 1 shows the DNA ladder (Thermo Scientific, SM0311). Lane 2 shows the unrestricted plasmid DNA.* ***(B)*** *Lane 1 shows the DNA ladder (Thermo Scientific, SM0311). Lane 2 is a negative control containing restriction enzymes with no plasmid. Lane 3 shows a pET28a plasmid containing a gene insert encoding RBBP6 p53BD with a polyhistidine tag, digested using restriction enzymes XhoI and NdeI. Lane 4 shows pET28a plasmid containing a gene insert encoding RBBP6 p53BD without a tag, digested using restriction enzymes NotI and NdeI. Selected base pair values for the DNA ladder are indicated on the left-hand side for both (A) and (B). Base pair values for digested DNA fragments are indicated on the right-hand side of (B).*

This data supports that the cells were successfully transformed and that the pET28a plasmid contains the gene insert encoding RBBP6 p53BD. Controls conducted include the plasmid without the restriction enzymes (Figure 3.1A, lane 2) and the restriction enzymes on their own (Figure 3.1B, lane 2).

3.3 The heterologous expression and purification of RBBP6 p53BD with polyhistidine tag

In order to investigate the RBBP6 p53BD, the recombinant protein needs to be expressed in a bacterial expression system and then successfully purified to be used in downstream experiments. A polyhistidine tag is commonly utilised to simplify protein purification while not interfering with protein structure or folding, as it is a small tag consisting of only six histidine residues.

3.3.1 Recombinant expression of RBBP6 p53BD with polyhistidine tag

RBBP6 p53BD with a polyhistidine tag on its N-terminal end was expressed in BL21 (DE3), NiCo21 (DE3) and SHuffle® T7 Express *Escherichia coli* cells. Protein expression was evaluated using two variables: post-induction time (Figure 3.2A) and inducer concentration (Figure 3.2B). Honours students also evaluated different post-induction temperatures under my supervision (results not shown). Negligible variation in expression was seen with temperature changes, and therefore, 37 °C was chosen to conduct the experiments reported in this thesis. Soluble (supernatant) and insoluble (pellet) fractions were visualised using SDS-PAGE (section 2.4.2). Two overexpressed proteins were seen in the soluble fraction (marked with pink arrows in Figure 3.2), with estimated molecular weights of 48 kDa and 44 kDa. The calibration curve used to calculate these molecular weights is shown in Figure 3.2E. This is bigger than the predicted 39 kDa for RBBP6 p53BD with a polyhistidine tag. However, there are several reasons why a protein may migrate at an unexpected rate through SDS-PAGE, including amino acid sequence composition, protein hydrophobicity, ability to bind SDS, secondary structural composition and stability (Banker and Cotman, 1972; Rath *et al*., 2013; Yarawsky *et al*., 2017).

When the post-induction time was evaluated, expression in NiCo21 (DE3) cells (Figure 3.2A) showed an increase in RBBP6 p53BD expression from two to 16 hours, with the highest expression seen at 16 hours post-induction. The majority of the expression was also found within the soluble fraction. When inducer concentration was tested (Figure 3.2B), a similar level of expression was seen for all three concentrations (0.1 mM, 0.5 mM and 1.0 mM) tested in NiCo21 (DE3) cells. Lower inducer concentrations place less stress on the cells and are also more economical (Malakar and Venkatesh, 2012). Lastly, when evaluating the expression in the three cell lines (Figure 3.2C), BL21(DE3) and NiCo21 (DE3) cells had similar levels of expression, and SHuffle® T7 Express cells had remarkably less expression even at 16 hours post-induction at all IPTG concentrations.

A Western blot was performed using polyhistidine antibodies on the soluble fractions of the three cell lines taken 16 hours post-induction. This confirmed the presence of polyhistidine residues in both overexpressed proteins (Figure 3.2E, indicated by the pink box), further confirming the presence of recombinant RBBP6 p53BD. As this Western blot was performed using crude cell lysate, the presence of background protein bands is expected. The expression conditions chosen for future studies were NiCo21 (DE3) cells, 37 °C, 0.1 mM IPTG and 16 hours post-induction growth. NiCo21 (DE3) cells were chosen as they have been genetically modified to reduce non-specific protein binding during Nickel IMAC purification (Robichon *et al*., 2011). This is supported by the NiCo21 (DE3) cells displaying the lowest number of background protein bands in the anti-polyhistidine Western blot performed (Figure 3.2E).

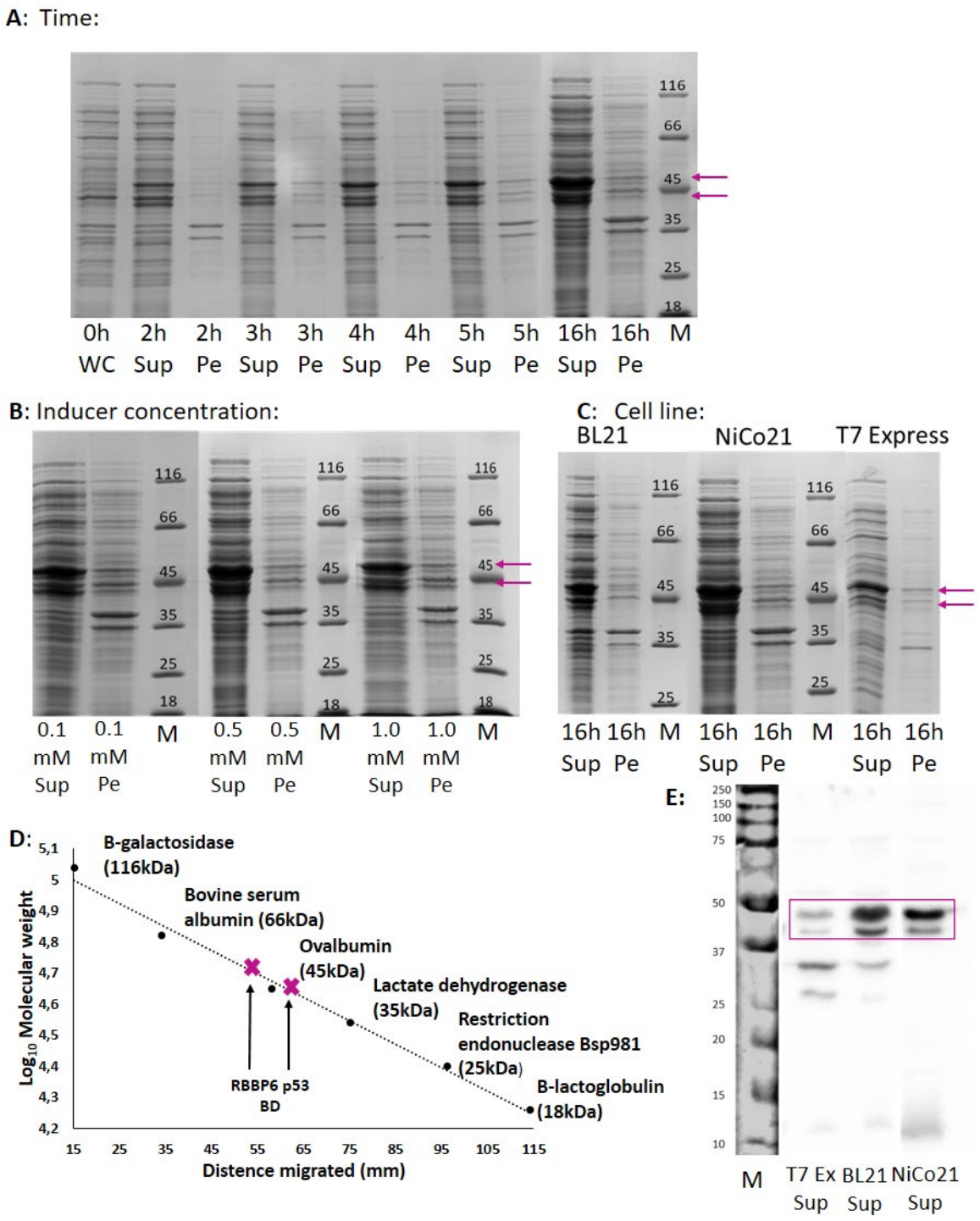

Figure 3.2. Induction study of RBBP6 p53BD with a polyhistidine tag.

SDS-PAGE analysis of the expression of RBBP6 p53BD with polyhistidine tag where "Sup" represents the soluble fraction and "Pe" represents the insoluble fraction after cell lysis. All studies were conducted at 37 °C. The positions of overexpressed proteins are marked with pink arrows. The molecular mass marker ("M") (Thermo Scientific, 26610) has sizes in kDa, marked on the gel. ***(A)*** *NiCo21 E.coli cells over a post-induction time of 2 hours to 16 hours, where post-induction time is indicated as the number of hours followed by an "h".* ***(B)*** *NiCo21 (DE3) cells induced with different*

concentrations of IPTG, with IPTG concentration indicated per lane in mM. ***(C)*** *Expression in three cell lines, namely BL21(DE3), NiCo21(DE3) and SHuffle® T7 Express cells, with all cells grown at 37 °C, 16 hours post-induction and 0.5 mM IPTG.* ***(D)*** *Calibration curve showing RBBP6 p53BD with polyhistidine tag, with an estimated molecular weight of 48 kDa and 44 kDa (positions marked with an "x"). Size and protein names in the protein marker are indicated on the curve.* ***(E)*** *Western blot analysis using anti-polyhistidine to confirm the presence of a protein with a polyhistidine tag at the corresponding molecular weight of overexpressed proteins (pink box) found in the soluble fraction of the cell lines used.*

3.3.2 Purification of RBBP6 p53BD using hydrophobic interaction

Recombinant RBBP6 p53BD needed to be purified before it can be structurally characterised. Chromatography techniques exploit the properties of a protein in order to purify a protein of interest out of a protein mixture. Hydrophobic chromatography relies on the presence of a salt in the buffer to cause the exposure of the protein's hydrophobic groups, thus allowing the protein to interact with the resin in the column. By changing the type of salt or salt concentration in the buffer, the behaviour of the proteins in the protein mixture can be altered, therefore creating favourable conditions for the protein of interest.

3.3.2.1 Protein precipitation test

Before hydrophobic interaction chromatography could be performed, the salt concentration at which RBBP6 p53BD precipitates out of solution was determined. A salt precipitation trial was conducted where the soluble fraction of NiCo21 (DE3) cells was incubated in several ammonium sulphate concentrations with rotation for 30 minutes. After centrifugation, the supernatant was removed and analysed using SDS-PAGE (Figure 3.3). After resuspension in 50 mM sodium phosphate, pH 7, the pellet was also analysed using SDS-PAGE. The pellet samples showed the proteins that precipitated out of the solution at each ammonium sulphate concentration (Figure 3.3). It was found that RBBP6 p53BD stayed in the soluble fraction after protein precipitation in up to 2 M ammonium sulphate when a 3 M stock was used.

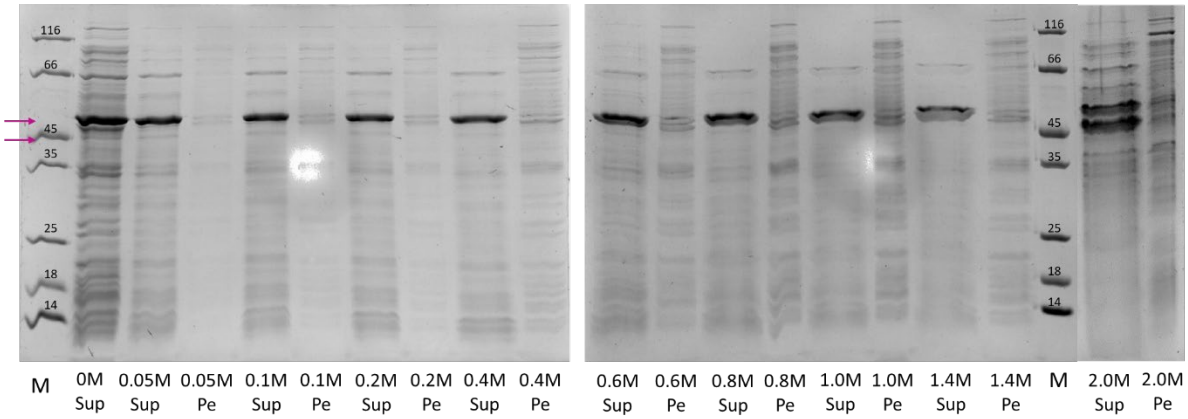

Figure 3.3. SDS-PAGE analysis of salt precipitation trials on recombinant RBBP6 p53BD.

Recombinant RBBP6 p53BD was subjected to a range of ammonium sulphate concentrations (0.05 M -2 M) marked under each lane. The supernatant (Sup) and pellet (Pe) samples were analysed. The molecular mass marker (marked as "M") (Thermo Scientific, 26610) has sizes in kDa, marked on the gel. RBBP6 p53BD is marked with pink arrows.

3.3.2.2 Hydrophobic interaction chromatography trials

Hydrophobic interaction chromatography relies on the buffer's salt concentration, causing the exposure of hydrophobic regions on the protein molecule's surface. Therefore optimization for the protein of interest is necessary within the salt concentration range that does not cause precipitation of the protein of interest out of solution. For RBBP6 p53BD, several different concentrations of ammonium sulphate in the binding buffer were tested. Presented here are trials using the supernatant from the lysate of NiCo21 (DE3) cells that were transformed with a plasmid encoding RBBP6 p53BD with a polyhistidine tag. Cytiva HiTrap Phenyl high performance (Uppsala, Sweden) columns were used for 0.4 M, 1.0 M and 1.2 M ammonium sulphate. The results are shown in Figure 3.4.

Figure 3.A and B show that RBBP6 p53BD did not bind the column when either 0.4 M or 1.0 M ammonium sulphate was included in the binding buffer. In the flow-through collected, the prepared protein sample loaded onto the column is diluted through the process of the protein mixture interacting with the column and the column being washed. Consequently, protein concentration appears less in the flow-through compared to the prepared protein sample used. For 1.2 M ammonium sulphate (Figure 3.4C), most of the RBBP6 p53BD still did not bind to the column and was found in the flow-through. However, it appeared that some of the recombinant RBBP6 p53BD bound to the column and was eluted in the fractions indicated with a blue box in "fractions collected during elution" in Figure 3.4C. At all three concentrations, some non-specific binding

occurred as non-recombinant proteins bound to the column and were eluted off when ammonium sulphate concentration was decreased.

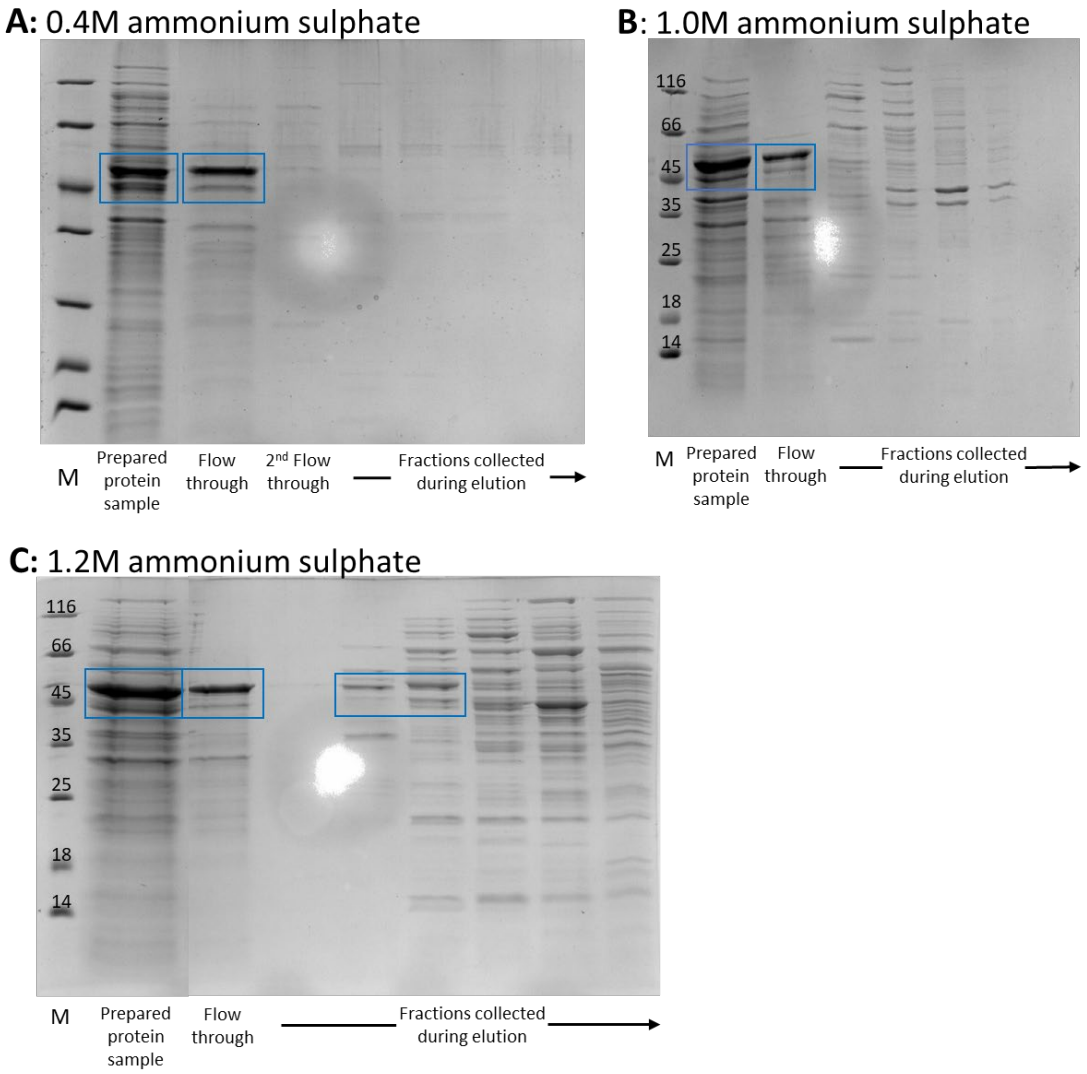

Figure 3.4. Hydrophobic interaction chromatography trials on recombinant RBBP6 p53BD with a polyhistidine tag.

*SDS-PAGE analysis of purification trials with **(A)** 0.4 M ammonium sulphate in the binding buffer, **(B)** 1.0 M ammonium sulphate in the binding buffer and **(C)** 1.2 M ammonium sulphate in the binding buffer. The "Prepared protein sample" consists of the soluble fraction of NiCo21 (DE3) cells prepared in the respective ammonium sulphate concentration. "Flow-through" samples consist of the proteins that did not bind the column, and "Fractions collected during elution" are proteins collected when the ammonium sulphate concentration was decreased from the binding buffer's concentration to 0 M, using a gradient. Ammonium sulphate concentration in the binding buffer is indicated above each gel. RBBP6 p53BD is marked with blue boxes. The molecular mass marker (marked as "M") (Thermo Scientific, 26610) has sizes in kDa, marked on the gel.*

3.3.3 Three-step purification protocol of polyhistidine-tagged RBBP6 p53BD

As a high protein purity is needed for downstream experiments, more than one chromatographic technique was necessary to isolate recombinant RBBP6 p53BD from the bacterial cell lysate. For p53BD of RBBP6, three independent purifications were performed in series utilizing a phenol hydrophobic interaction column followed by a nickel IMAC column.

3.3.3.1 Step One

Soluble fractions taken from NiCo21 (DE3) cells were incubated in 1.0 M ammonium sulphate before being centrifuged and loaded onto a pre-equilibrated Cytiva HiTrap Phenyl high performance (Uppsala, Sweden) column. Columns are equilibrated with 10 column volumes of binding buffer. Proteins were eluted off the column by decreasing the ammonium sulphate concentration in a gradient from 1.0 M to 0 M (Figure 3.5A). Fractions with high A_{280} absorbance readings were analysed with SDS-PAGE (Figure 3.5B). RBBP6 p53BD was found not to bind to the column when 1.0 M ammonium sulphate was present in the binding buffer but instead was found in the flow-through (FT), which contains the proteins that move through the column without binding (Figure 3.5A and B). Smudging of the samples in SDS-PAGE (Figure 3.5B) is caused by high concentrations of ammonium sulphate in the samples. Multiple non-specific bacterial cellular proteins could bind to the column and were eluted when the ammonium sulphate concentration was decreased. This is often called reverse purification, as non-specific proteins bind under the conditions instead of the protein of interest. However, the protein of interest still becomes purer than in the original sample loaded onto the column.

3.3.3.2 Step two

The flow-through from Step one (section 3.3.3.1) was incubated in 1.4 M ammonium sulphate before being loaded onto a pre-equilibrated Cytiva HiTrap Phenyl high performance (Uppsala, Sweden) column. Proteins were eluted off the column by decreasing the ammonium sulphate concentration in a gradient from 1.4 M to 0M (Figure 3.6A). Fractions with high A_{280} absorbance readings were analysed with SDS-PAGE (Figure 3.6B). At 1.4 M, ammonium sulphate RBBP6 p53BD was found to bind to the column and be eluted when the ammonium sulphate concentration was decreased to approximately 0.85 M, as seen in fractions 4 and 5 (Figure 3.6A and B). However, several non-specific bacterial cellular proteins bound and were eluted from the column under the same conditions as RBBP6 p53BD, despite a gradient elution being used. Smudging of the samples in SDS-PAGE (Figure 3.6B) is caused by high concentrations of ammonium sulphate in the samples.

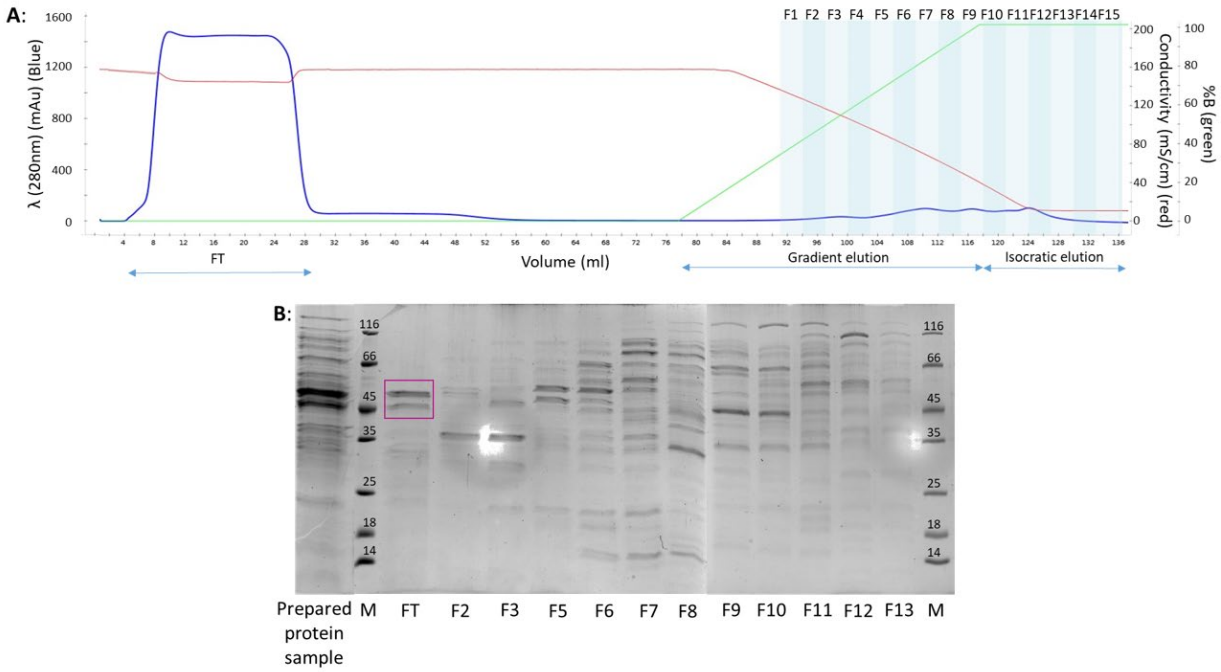

Figure 3.5. Hydrophobic interaction purification of polyhistidine-tagged RBBP6 p53BD with 1.0 M ammonium sulphate in the binding buffer.

(A) *Chromatograph with A_{280} effluent (blue), negative salt gradient (green), conductivity (red) as well as Flow-through (FT), elution and fractions collected (F'X') depicted.* ***(B)*** *SDS-PAGE analysis of the "Prepared protein sample" loaded onto the column, the Flow-through (FT) and specific fractions collected "FX" where X represents the fraction number. The prepared protein sample is the soluble fraction of NiCo21 (DE3) cell lysate prepared in 1.0 M ammonium sulphate. RBBP6 p53BD is indicated in flow-through (FT) with a pink box. The molecular mass marker (marked as "M") (Thermo Scientific, 26610) has sizes in kDa, marked on the gel. Purification was performed using a BioRad NGC™ Chromatography system with a computer loaded with ChromLab software (Hercules, USA).*

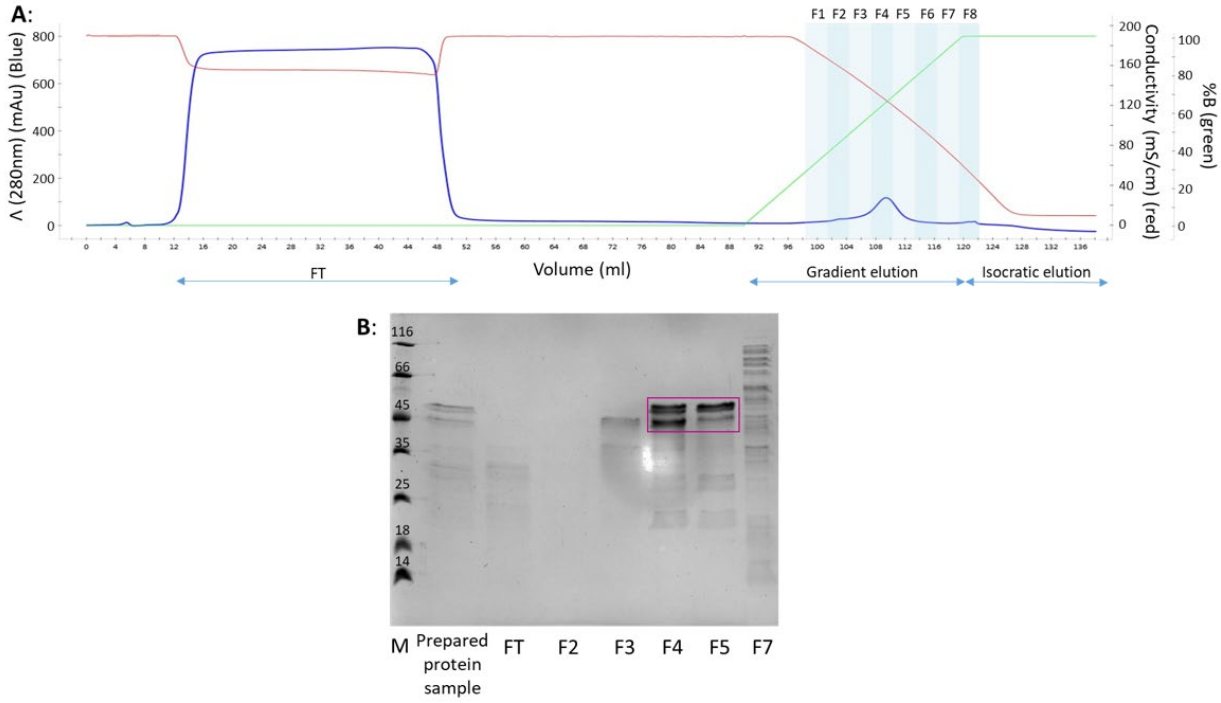

Figure 3.6. Hydrophobic interaction purification of polyhistidine-tagged RBBP6 p53BD with 1.4 M ammonium sulphate in the binding buffer.

(A) *Chromatograph with A_{280} effluent (blue), negative salt gradient (green), conductivity (red) as well as Flow-through (FT), and fractions collected (F'X') are depicted.* ***(B)*** *SDS-PAGE analysis of "Prepared protein sample" that was loaded onto the column, the Flow-through (FT) and specific fractions collected "FX" where X represents the fraction number. The prepared protein sample was the flow-through from Step one, prepared in 1.4 M ammonium sulphate. RBBP6 p53BD is indicated on gel with a pink box. The molecular mass marker ("M") (Thermo Scientific, 26610) has sizes in kDa, marked on the gel. Purification was performed using a BioRad NGC™ Chromatography system with a computer loaded with ChromLab software (Hercules, USA).*

3.3.3.3 Step three

As the protein percentage purity was not high enough for downstream experiments, a third purification step was performed using nickel IMAC to purify RBBP6 p53BD utilising its polyhistidine tag. Fractions 4 and 5 from Step two (section 3.3.3.2) were dialysed against 50 mM sodium phosphate, pH 7.4 with 500 mM sodium chloride and 30 mM imidazole. Dialysis was performed at 4 °C, with a buffer volume 10 times that of the sample and three buffer changes. After that, the dialysed protein sample was loaded onto a pre-equilibrated Cytiva HisTrap high performance (Uppsala, Sweden) column. Bound proteins were eluted from the column by increasing the imidazole concentration (Figure 3.7A), and fractions with high A_{280} absorbance readings were analysed with SDS-PAGE (Figure 3.7B).

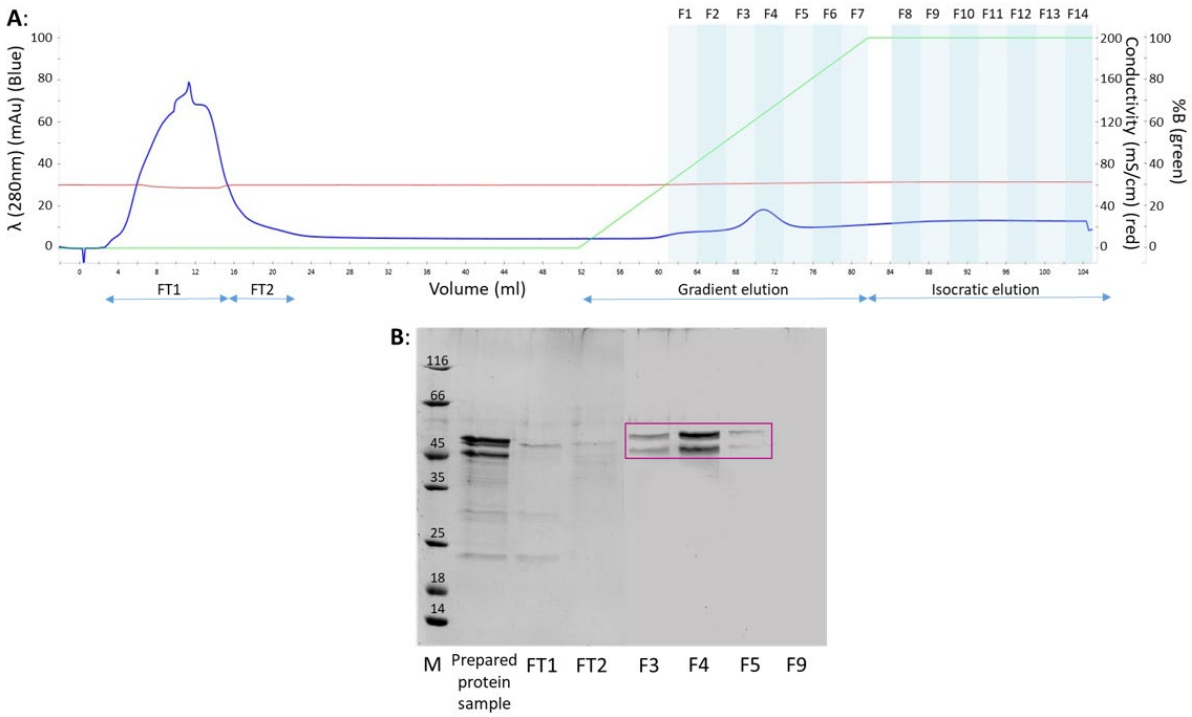

Figure 3.7. Nickel IMAC purification of RBBP6 p53BD with a polyhistidine tag.

(A) *Chromatograph with A_{280} effluent (blue), imidazole gradient (green), conductivity (red) as well as Flow-through (FT) and fractions collected (FX) depicted.* ***(B)*** *SDS-PAGE analysis of 'Prepared protein sample' that was loaded onto the column, the Flow-through (FT) and specific fractions collected "FX" where X represents the fraction number. The Prepared protein sample consisted of the dialysed fractions 4 and 5 from Step two. RBBP6 p53BD is indicated on gel with a pink box. The molecular mass marker (marked as "M") (Thermo Scientific, 26610) has sizes in kDa, marked on the gel. Purification was performed using a BioRad NGC™ Chromatography system with a computer loaded with ChromLab software (Hercules, USA).*

The binding buffer used during purification contained 500 mM sodium chloride and 30 mM imidazole to help prevent non-specific binding. RBBP6 p53BD was found to bind the column and was eluted off at approximately 300 mM imidazole, as seen in fractions 3, 4 and 5 (Figure 3.7A and B). After Step three, Nickel IMAC purification, fractions 3, 4 and 5 were pooled and concentrated, and RBBP6 p53BD was estimated to be approximately 95% pure when using BioRad Image Lab™ software version 6.0.1 (Hercules, USA) "Relative Quantity" tool. This was calculated taking the two protein bands of RBBP6 p53BD into consideration.

3.4 The heterologous expression and purification of RBBP6 p53BD without a tag

Adding a tag to the C or N terminal of a protein can sometimes cause protein instability, incorrect folding or insoluble expression of the protein of interest. Although a polyhistidine tag is not known

to regularly cause these problems, the expression of the RBBP6 p53BD without the presence of a tag was still investigated.

3.4.1 Recombinant expression of RBBP6 p53BD without a tag

RBBP6 p53BD without a tag was expressed in BL21 (DE3) and SHuffle® T7 Express *E.coli* cells, where two conditions were evaluated, namely post-induction time (Figure 3.8A and B) and inducer concentration (Figure 3.8C). Soluble (supernatant) and insoluble (pellet) fractions were visualised using SDS-PAGE (section 2.4.2). In the soluble fraction, two overexpressed proteins, marked with pink arrows in Figure 3.8, were seen with estimated molecular weights of 46 kDa and 43 kDa using a calibration curve (Figure 3.8D). These are bigger than the predicted 39 kDa for RBBP6 p53BD; however, there are several reasons why a protein may migrate at an unexpected rate through SDS-PAGE, as discussed in section 3.3.1.

For RBBP6 p53BD expressed without a tag, overall expression was higher in SHuffle® T7 Express cells over the BL21 (DE3) cells (Figure 3.8A and B). For BL21 (DE3) cells (Figure 3.8B), expression was low from two to four hours and slightly increased at 16 hours. For SHuffle® T7 Express cells (Figure 3.8A), expression was relatively high from two hours but appeared highest at five hours post-induction, with little increase seen at 16 hours post-induction. In SHuffle® T7 Express cells, when inducer concentrations were tested, similar expression levels were seen at both 0.1 mM and 1.0 mM IPTG (Figure 3.8C). SHuffle® T7 Express cells were chosen for further studies, with the chosen conditions being 37 °C, 0.1 mM IPTG and five hours post-induction growth. This places less stress on the cells as both shorter growth times and lower inducer concentration reduce the stress placed on cells during recombinant protein expression as well as make it more economical (Malakar and Venkatesh, 2012).

3.4.2 Purification of RBBP6 p53BD without a tag

Based on the findings in section 3.3.2, two hydrophobic purifications were carried out in series. The soluble fraction taken from SHuffle® T7 Express cells was incubated in 1.0 M ammonium sulphate before being centrifuged and supernatant loaded onto a pre-equilibrated Cytiva HiTrap Phenyl high performance (Uppsala, Sweden) column. Proteins were eluted off the column by decreasing the ammonium sulphate concentration. Fractions with high A_{280} absorbance readings were analysed with SDS-PAGE (Figure 3.9A). RBBP6 p53BD without a tag could not bind the column under these conditions and was found in the flow-through. Again several non-specific bacterial proteins bound and were eluted off of the column under these conditions, resulting in a reverse purification where RBBP6 p53BD becomes purer than the original sample loaded, without the protein of interest binding the column.

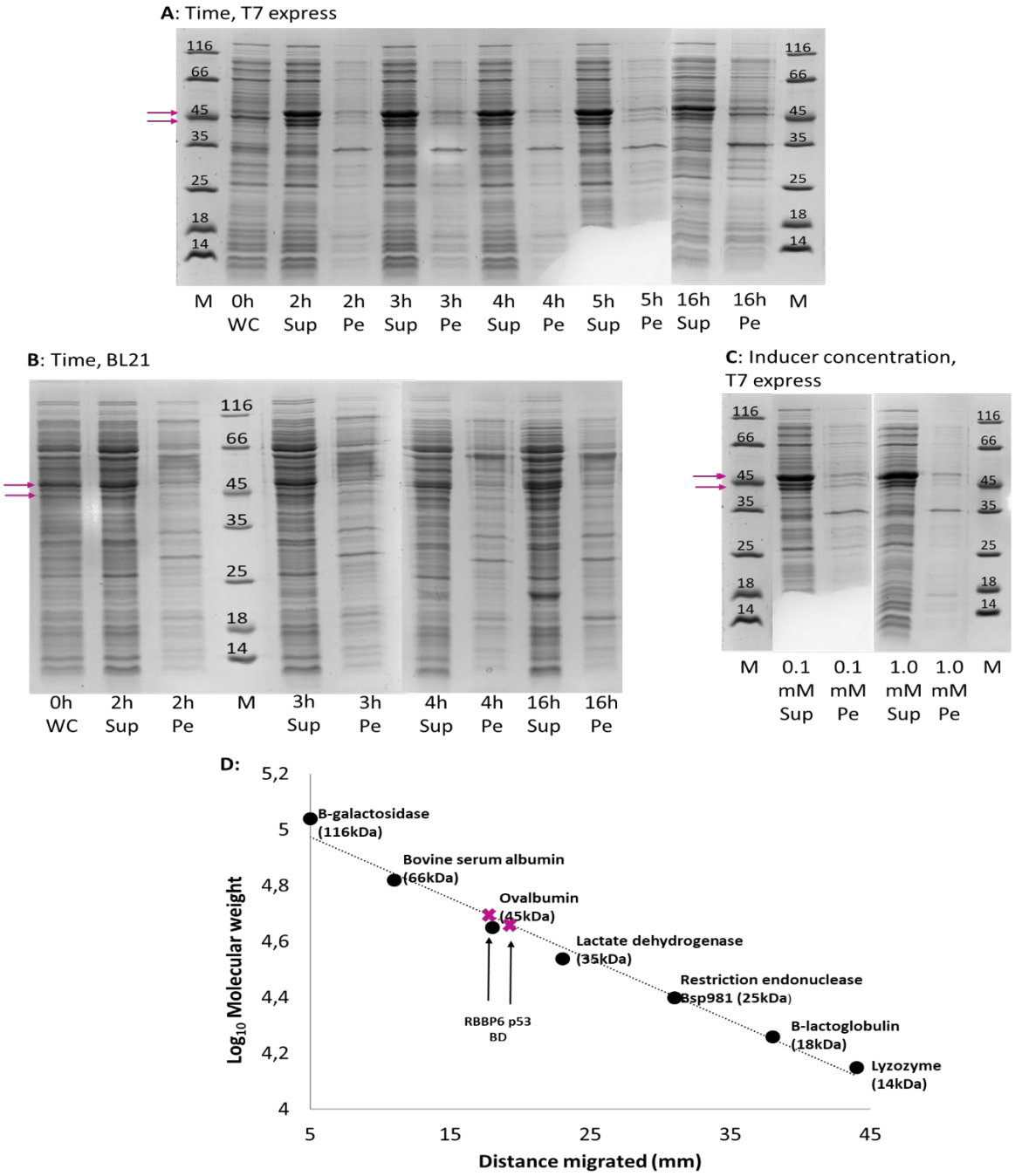

Figure 3.8. Induction study of RBBP6 p53BD without a tag.

SDS-PAGE analysis of the expression of RBBP6 p53BD without a tag in ***(A)*** *T7 express E.coli cells and* ***(B)*** *BL21 E.coli cells, over a post-induction time of two hours to 16 hours where post-induction time is indicated as the number of hours followed by an "h". "Sup" represents the soluble fraction and "Pe" represents the insoluble fraction after cell lysis.* ***(C)*** *Different inducer concentrations in T7 express cells. All studies were conducted at 37 °C, and the position of overexpressed proteins are indicated with pink arrows.* ***(D)*** *Calibration curve showing RBBP6 p53BD without a tag with an estimated molecular weight of 46 kDa and 43 kDa (position marked with an "x"). Size in kDa and protein names in the protein marker are indicated on the curve.*

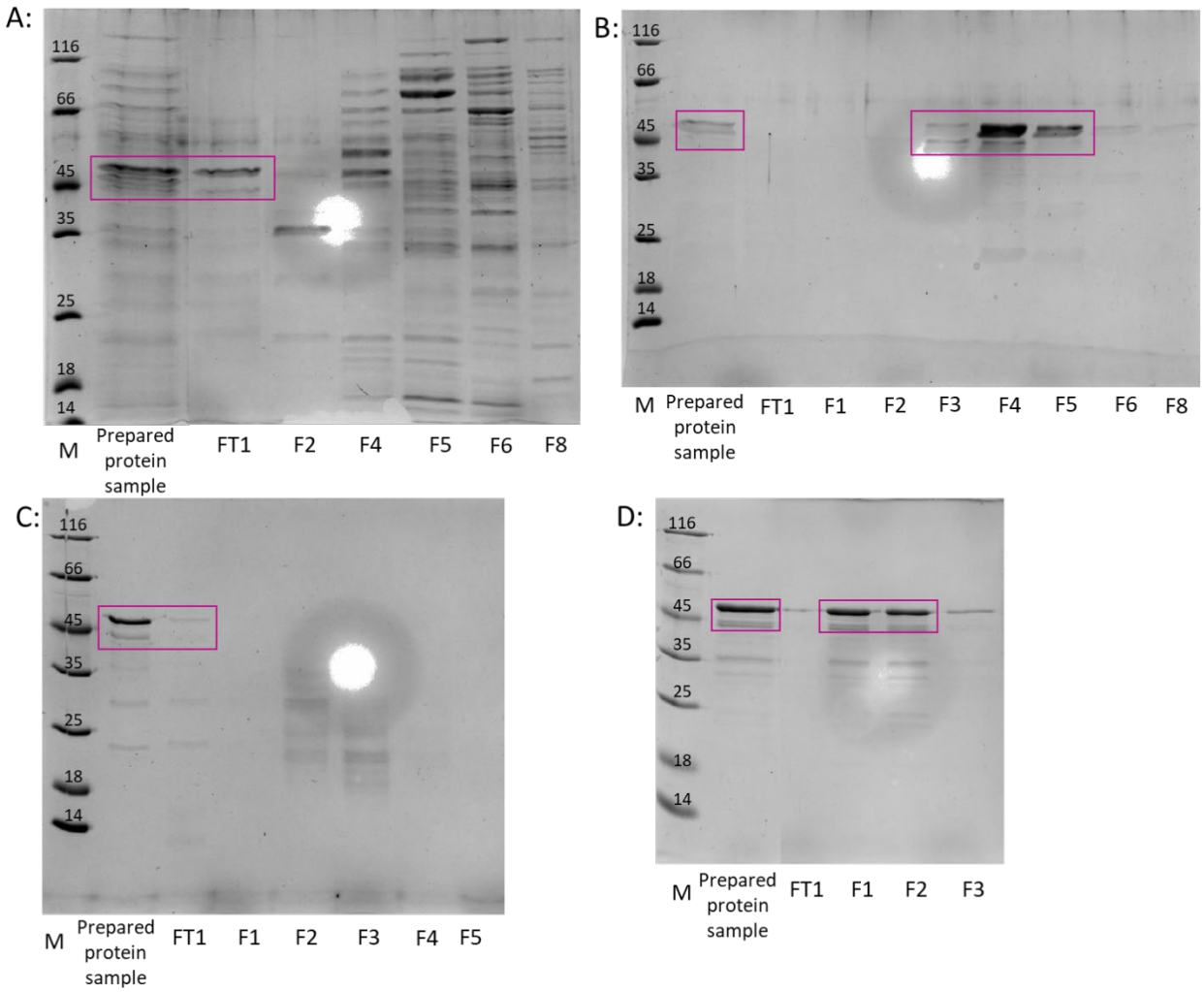

Figure 3.9. SDS-PAGE analysis of purification trials of recombinant RBBP6 p53BD without a tag. *SDS-PAGE analysis of the prepared protein sample that was loaded onto the column, the flow-through (FT1) and specific fractions collected (F"X") where X represents the fraction number for* ***(A)*** *Hydrophobic interaction chromatography with 1.0 M ammonium sulphate in binding buffer.* ***(B)*** *Hydrophobic interaction chromatography with 1.4 M ammonium sulphate in the binding buffer.* ***(C)*** *Ion exchange chromatography, with a pH of 8 in the binding buffer and* ***(D)*** *Ion exchange chromatography with a pH of 7 for the binding buffer. RBBP6 p53BD is indicated on gels in the 'Prepared protein sample', flow-through (FT1) or fractions collected (F"X") with pink boxes. The molecular mass marker ("M") (Thermo Scientific, 26610) has sizes in kDa, marked on the gel.*

Next, the flow-through collected using 1.0 M ammonium sulphate in the binding buffer (Figure 3.9A) was incubated in 1.4 M ammonium sulphate before being loaded onto a pre-equilibrated Cytiva HiTrap Phenyl high performance (Uppsala, Sweden) column. Proteins were again eluted off the column by decreasing the salt concentration. Fractions with high A_{280} absorbance readings were analysed with SDS-PAGE (Figure 3.9B). At 1.4 M ammonium sulphate RBBP6 p53BD without a tag

was found to bind the column and be eluted when the ammonium sulphate concentration was decreased to approximately 0.9 M in fractions 3, 4 and 5 (Figure 3.9B). However, multiple non-specific bacterial cellular proteins were bound and eluted from the column under the same conditions. Therefore, fractions 3, 4 and 5 from Figure 3.9B were pooled and dialysed into 50 mM Sodium phosphate, pH 8. The dialysed protein sample was loaded onto a pre-equilibrated Cytiva (Uppsala, Sweden) HiTrap® CM Fast Flow column. RBBP6 p53BD without a tag could not bind the column under these conditions and was instead found in the flow-through (Figure 3.9C).

The flow-through seen in Figure 3.9C was collected, concentrated, and dialysed into 50 mM Sodium phosphate, pH 7, before being loaded onto a pre-equilibrated Cytiva (Uppsala, Sweden) HiTrap® CM Fast Flow column. RBBP6 p53BD was found to bind to the column and be eluted when the sodium chloride concentration was increased to approximately 0.25 M, seen predominantly in fractions 1 and 2 (Figure 3.9D). However, several non-specific bacterial cellular proteins were bound and eluted from the column under the same conditions as RBBP6 p53BD. The protein purity was estimated to be approximately 78 % when using BioRad Image Lab™ software version 6.0.1 (Hercules, USA) "Relative Quantity" tool. RBBP6 p53BD with polyhistidine tag had an estimated purity of 95 %; therefore, it was used for all subsequent studies.

3.5 Identification of the recombinant protein by Mass Spectrometry

After purification, two prominent protein bands were observed and would bind and elute together regardless of the chromatography technique applied. Before further studies could be undertaken, mass spectrometry analysis was conducted to determine if the two protein bands were RBBP6 p53BD (with polyhistidine tag). The samples were prepared by purifying the supernatant of NiCo21 (DE3) cells using hydrophobic interaction chromatography, as explained in section 2.3.1.3. The samples sent for mass spectrometry analysis were not purified by nickel IMAC after hydrophobic interaction chromatography, which is why there are numerous other proteins seen on the gel in addition to the protein bands of interest indicated (Figure 3.10). After trypsin digested LC-MS analysis, it was confirmed that both bands were RBBP6 p53BD. This allowed studies to be conducted using the pure protein samples containing both protein bands obtained from the three-step purification protocol (Section 3.3.3).

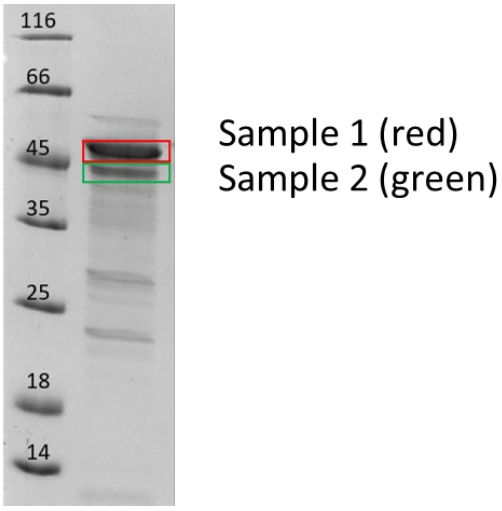

Figure 3.10. SDS-PAGE of samples sent for analysis by mass spectrometry.

Two protein bands marked samples 1 and 2 were excised from the SDS-PAGE pictured and placed in ultrapure water before being sent for trypsin digested LC-MS analysis. The molecular mass marker's protein band sizes are shown on the gel in kDa (Thermo Scientific, 26610).

3.6 Physicochemical and structural characterization of the recombinant protein

3.6.1 Clear native PAGE

Clear native PAGE prepares samples in a non-denaturing, non-reducing buffer so that the proteins reserve their native form. Clear native PAGE is used to investigate the presence of multimeric forms of a protein. Two separate buffer systems were used independently, namely a Tris-HCl buffer system at a pH of 8.3 and an imidazole-HEPES buffer system with a pH of 7.4. In a standard native electrophoresis set up for proteins, the proteins migrate from the anode (negative) to the cathode (positive). RBBP6 p53BD has a predicted pI of 9, and therefore, RBBP6 p53BD will carry a positive charge at the pH of 8.3 in the Tris-HCl buffer and pH of 7.4 in the imidazole-HEPES buffer used. Therefore the electrodes were reversed so that the current flows from the cathode (positive) to the anode (negative), allowing RBBP6 p53BD to enter the gel.

When using the Tris-HCl buffer at pH 8.3 (Figure 3.11A), it was observed that the RBBP6 p53BD appears in a single form (lane 1), and the single form is still present after the domain was heated to 90 °C and cooled to 20 °C (lane 2). Lane 3 showed a single form present even when RBBP6 p53BD was in the presence of 2 M urea. As the pH of 8.3 of the Tris-HCl buffer was close to the pI of 9 for the RBBP6 p53BD, there was little migration into the gel. Therefore a second clear native PAGE was performed using an imidazole-HEPES buffer system with a pH of 7.4 (Figure 3.11B). This showed that RBBP6 p53BD appears in a single form before (lane 1) and after being heated to 90 °C and cooled (lane 2). However, a greater migration into the gel is seen at the lower pH.

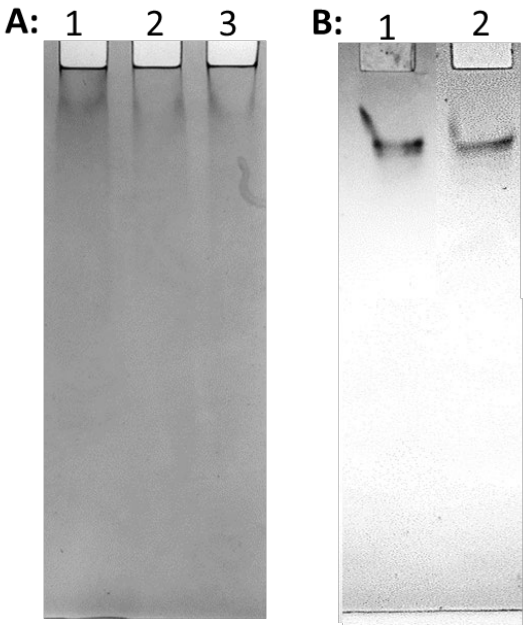

Figure 3.11. Clear native PAGE analysis of RBBP6 p53BD.

Clear native PAGE analysis of purified p53 binding domain of RBBP6. ***(A)*** *Tris-HCl buffer, with pH 8.3. Lane 1 is the p53 binding domain of RBBP6 in 50 mM sodium phosphate, pH 7. Lane 2 is the p53 binding domain of RBBP6 in 50 mM sodium phosphate, pH 7 after being heated to and cooled from 90 °C to 20 °C, as described in section 2.5.3.1. Lane 3 is the p53 binding domain of RBBP6 in 50 mM sodium phosphate, pH 7 with 2 M urea.* ***(B)*** Imidazole-HEPES buffer, pH 7.4. *Lane 1 is the p53 binding domain of RBBP6 in 50 mM sodium phosphate, pH 7, and Lane 2 is the p53 binding domain of RBBP6 in 50 mM sodium phosphate, pH 7 after being heated to and cooled from 90 °C to 20 °C, as described in section 2.5.3.1. Protein sample concentrations were not equalised before loading onto the gels.*

The exact molecular weight cannot be determined from a clear Native PAGE, as movement through the gel is based on charge and size. However, the results suggest that the domain is present in a monomer form, as in 2 M urea or after being heated, a single band is seen to migrate to a similar distance as the protein without denaturants.

3.6.2 Secondary structure characterisation

Investigating the far-UV circular dichroism spectrum (approximately from 250 nm-180 nm) produced by a protein can give information on a protein's secondary structure based on characteristic features caused by the presence of secondary structure conformations in proteins, such as beta-strands and alpha-helices (Woody, 1995). Characteristic troughs in a far-UV CD spectrum of a protein that consists of alpha-helices are at 208 nm and 222 nm. For a protein consisting of beta-strands, the trough is at 215 nm, and the random coil trough is found at

approximately 200 nm and is usually stronger than other structural signals. The positive band seen for alpha-helices is 190 nm, and for beta-strands, it is 195 nm (Ranjbar and Gill, 2009).

Far-UV circular dichroism was used to study the secondary structure of purified RBBP6 p53BD. The spectrum produced has two troughs at approximately 222 nm and 200 nm, with a positive band heading up to the 195 nm mark (Figure 3.12). This spectrum suggests a protein that is a mix of alpha-helices, beta-strands and random coils. CD spectra were recorded to approximately 195 nm, as the noise to signal ratio was too high below this wavelength, as detected by the dynode voltage. RBBP6 p53BD does not contain any tryptophan residues, so an accurate tertiary structure estimation could not be obtained using fluorescence spectrometry.

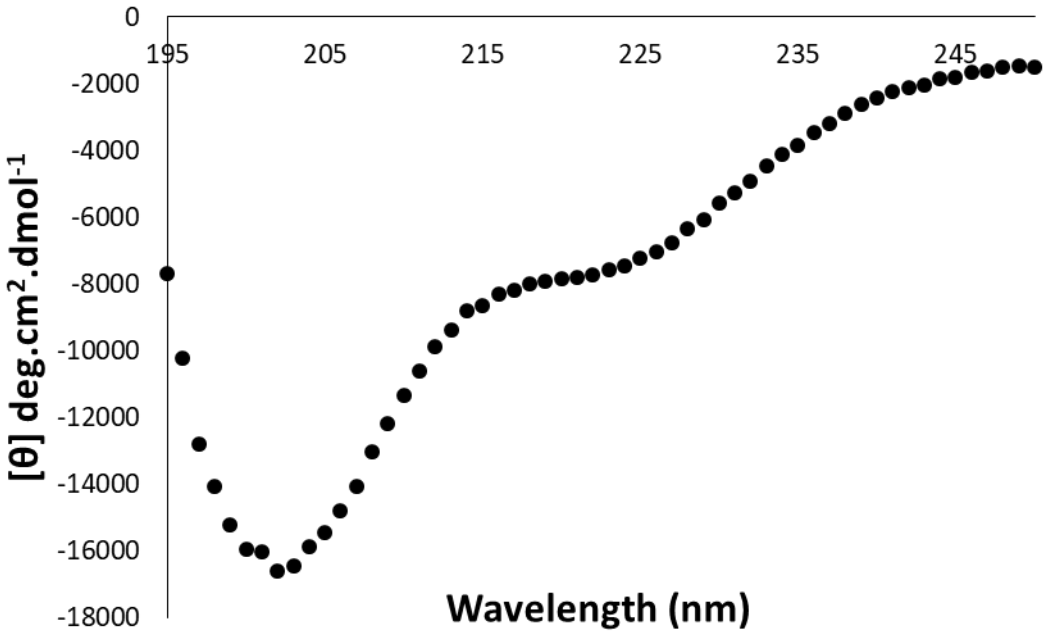

Figure 3.12. Far-UV circular dichroism spectrum of RBBP6 p53BD.

Far-UV circular dichroism spectra of RBBP6 p53BD, obtained between 250 and 195 nm for 2.6 µM RBBP6 p53BD in 20 mM sodium phosphate, pH 7.

Using DichroWeb (Miles *et al*., 2021), a secondary structure prediction was generated based on the Far-UV circular dichroism spectrum (Figure 3.12). Several reference sets were utilised to evaluate the far-UV CD spectrum in three programs: CONTIN, SELCON3 and CDSSTR. The percentage predictions for alpha-helices, beta-strands, turns, and random coils are found in Table 3.1. Reference set 7 consistently had the lowest NRMSD (Normalised Root Mean Squared Deviation) values across the CONTIN, SLECON3 and CDSSTR. An average prediction from these three programs using reference set 7 is 19 % alpha-helical, 9 % beta-strands, 13 % turns and 59 % random coil. NRMSD is a score of how accurate the prediction is. Usually, an NRMSD of less than 0.1 is

considered a good fit. However, SELCON3 is notorious for having higher NRMSD than the other programs, and CDSSTR has a slightly lower value; however, this is not indicative of better or worse predictions. However, it should be noted that CDSSTR NRMSD readings for reference set sp175 and 4 are within an acceptable range. Their readings predict a higher alpha-helical percentage and significantly higher beta-strand percentage for RBBP6 p53BD than reference set 7.

Table 3.1: DichroWeb secondary structure predictions.

DICHROWED (Miles et al., 2021) predicted secondary structure components using three different software server programs: CONTIN, SELCON3 and CDSSTR. The reference set used in each prediction is indicated in the table. NRMSD is a score of how accurate the prediction is.

Program	Reference set used	NRMSD	% Alpha helix	% beta strands	% turns	% coil
CONTIN	sp175	0,71	21	17	16	46
CONTIN	7	0,103	20	3	12	65
CONTIN	4	0,117	23	17	27	33
SELCON3	sp175	0,604	22	18	16	44
SELCON3	7	0,442	16	14	13	57
SELCON3	4	0,604	25	16	25	34
CDSSTR	sp175	0,019	23	17	18	42
CDSSTR	7	0,024	21	10	14	55
CDSSTR	4	0,019	18	21	26	35

3.6.3 Computational protein structure prediction

The top three 3D models representing RBBP6 p53BD structural conformation produced by LOMETS (Wu and Zhang, 2007) in I-TASSER software (Yang *et al*., 2015) are shown in Figure 3.13**.** It was predicted that RBBP6 p53BD consists predominantly of random coil, with alpha-helical and beta-strand structures varying from model to model (Figure 3.13). The confidence of each model is measured using the c-score and is shown on each model in Figure 3.13. The c-score is generated based on the significance of the treading template alignment and convergence of parameters of the structure assembly simulations. The acceptable range for a c-score is -5 to 2, with a higher score signifying a model with higher confidence; however, a score greater than -1.5 indicates a model of correct global topology. Global accuracy prediction is made using c-score and protein length for model 1 by I-TASSER and consists of a TM-Score and RMSD value. For model 1, the estimated TM-score was 0.65±0.13, and the estimated RMSD was found to be 10.9±4.6Å. A TM-score is between 0 and 1, with a TM greater than 0.5 indicating a model of correct topology (Xu and Zhang, 2010).

Models 2 and 3 generally have lower TM scores than model 1 and therefore are not reported by I-TASSER. The predicted structure in this study is significantly different from the previous study done (Twala, 2017); however, it must be noted that Twala's predictions were based on a much smaller portion of the domain.

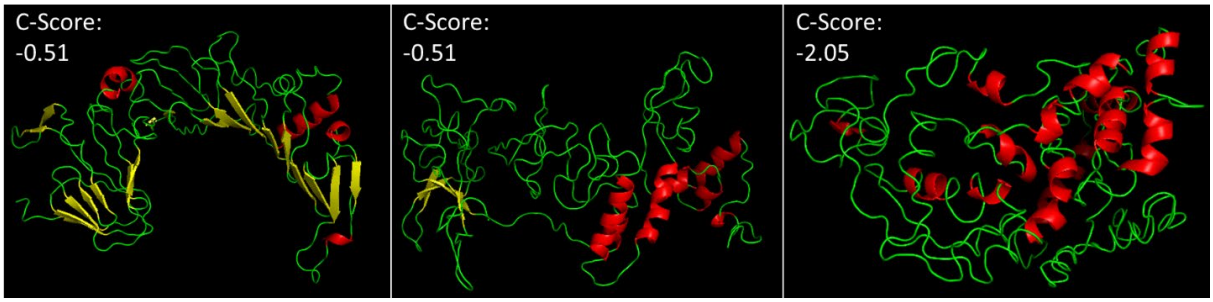

Figure 3.13. I-TASSER software prediction of secondary and tertiary structure.

Top three 3D conformation models predicted by I –TASSER, with predicted C-Score shown on each model. Alpha-helices are shown in red, beta-strands in yellow, and loops shown in green. The structure was obtained from the protein data bank (PDB) files produced by I-TASSER and viewed with PyMOL Molecular Graphics System (2.5.2 Edu), Schrödinger, LLC.

A secondary structure server, namely 2Struc (Klose *et al*., 2010), predicted the percentage of alpha-helices and beta-strands for the RBBP6 p53BD models using the protein data bank files generated by I-TASSER (Table 3.2)**.** Percentages of alpha-helices, beta-strands and other (a mixture of turns and random coil) varied significantly from model to model, with the highest alpha-helical content found in model 3 and the highest beta-strand prediction found in model 1. Model 2 showed the highest random coil percentage prediction and three times the alpha-helical content compared to its beta-strand content (Table 3.2)**.** According to I-TASSER, model 1 is the most likely protein conformation for the amino acid sequence submitted for RBBP6 p53BD. However, when comparing the models to the prediction made by DichroWeb (Miles *et al*., 2021), it is seen that model 2 has a similar ratio of alpha-helices to beta-strands as seen in predictions made from the far-UV CD spectrum. However, I-TASSER did predict a lower percentage of structure overall, with 14 % alpha-helices to 4 % beta-strand for model 2 compared to an average of 19 % alpha-helices to 9 % beta-strand from the far-UV CD spectrum using DichroWeb.

The amino acid composition of a protein can indicate the likelihood of intrinsic order or disorder. Order-promoting amino acids (Trp, Met, Cys, Phe, Ile, Tyr, Val, Leu and Asn) are frequently found in folded globular proteins. In contrast, a high percentage of polar and charged amino acids (Gln, Ser, Pro, Glu, Lys, Gly, Ala and Arg), are known to indicate disorder and are overrepresented in

unstructured proteins (Dunker *et al*., 2001; Dyson and Wright, 2005). RBBP6 p53BD sequence investigated in this study comprises of 63.6 % amino acid residues that promote disorder and only 19.8 % amino acid residues that promote order as depicted by ExPASy (Table A1 in appendix), (Gasteiger *et al*., 2005).

Table 3.2: Prediction of alpha-helical and beta-strand protein content for I-TASSER predicted structures of RBBP6 p53BD.

2Struc secondary structure server (Klose et al., 2010) predicated alpha-helical and beta-strand content of RBBP6 p53BD for the three top models predicted by I-TASSER software.

Model	Program	% Alpha helix	% beta strands	%Other
Model 1	DSSP	12,9	28,6	58,5
	STRIDE	10,5	28,3	61,2
Model 2	DSSP	14,4	3,9	81,6
	STRIDE	14,2	5,2	80,6
Model 3	DSSP	25,2	0	74,8
	STRIDE	26,5	1,0	72,4

3.7 Conformational stability

Investigating a protein's stability is essential for protein storage and undertaking functional or structural investigations. A protein's stability can affect early investigations such as expression and purification. Once purified, determining protein stability is important for a number of techniques, including protein-drug interaction studies and structural determination techniques such as protein crystallization studies. Protein aggregation, often a result of protein unfolding, can affect many downstream experiments. Therefore, determining a protein's stability before further studying a protein's characteristics is important to save time and expense. The far-UV circular dichroism spectrum (approximately 250-180 nm) can evaluate the secondary structural content of a protein based on characteristic features produced by secondary structural conformations. Therefore, it can be used to evaluate any structural changes for a protein of interest by evaluating the spectrum produced by the protein under different conditions and comparing them to the spectrum produced by the native protein.

3.7.1 Thermal-induced unfolding

Far-UV CD evaluated RBBP6 p53BD secondary structure's stability when heating the protein sample from 20 to 90 °C. With an increase in temperature, there is an increase in ellipticity between 200 nm and 210 nm. However, ellipticity between 210 nm and 250 nm decreased, showing structural changes upon heating that are suggestive of the protein structure becoming more compact in parts (Figure 3.14A and B). The spectrum's negative maximum shifted from 202 nm to approximately 206 nm upon heating. The negative maximum for a random coil is at approximately 200 nm, and for alpha-helices, there are negative maxima at 208 nm and 222 nm. This shift further supports the increase in secondary structure with increased temperature. The negative maximum of a random coil frequently has a greater magnitude than that of structural compositional negative maxima, potentially explaining the increase in ellipticity at these lower wavelengths. The spectra also present an isodichroic point at the wavelength 210 nm, where the far-UV CD signal is not dependent on temperature and remains constant throughout the temperature range investigated.

When comparing the native sample spectrum at 20 °C (blue) to the spectrum of the sample having been heated to 90 °C (red) and subsequently been cooled back down to 20 °C (black) (Figure 3.14B), it is observed that thermal unfolding is reversible for RBBP6 p53BD. The recovery percentages at different wavelengths (Table 3.3) showed over 90 % recovery at all wavelengths investigated, with near-perfect (99.6 %) recovery seen at 208 nm (Figure 3.14A and B). Percentage structural changes are also shown in Table 3.3, showing little structural change (10-30 %) when the protein is heated to 90 °C.

When looking at temperature dependence curves at 222 nm (Figure 3.14C) and 215 nm (Figure 3.14D), the curves show a negative linear relationship with temperature across 20 to 90 °C, suggesting a monotonous change in structure with an increase in temperature (Figure 3.14C and D). At 208 nm (Figure 3.14E), the curve shows small ellipticity changes between 20 and 50 °C, suggesting minor structural arrangements at these temperatures, followed by a greater secondary structural change from 50 to 90 °C. The curves are similar for RBBP6 p53BD at two concentrations, namely 2.6 µM and 4.1 µM at all investigated wavelengths.

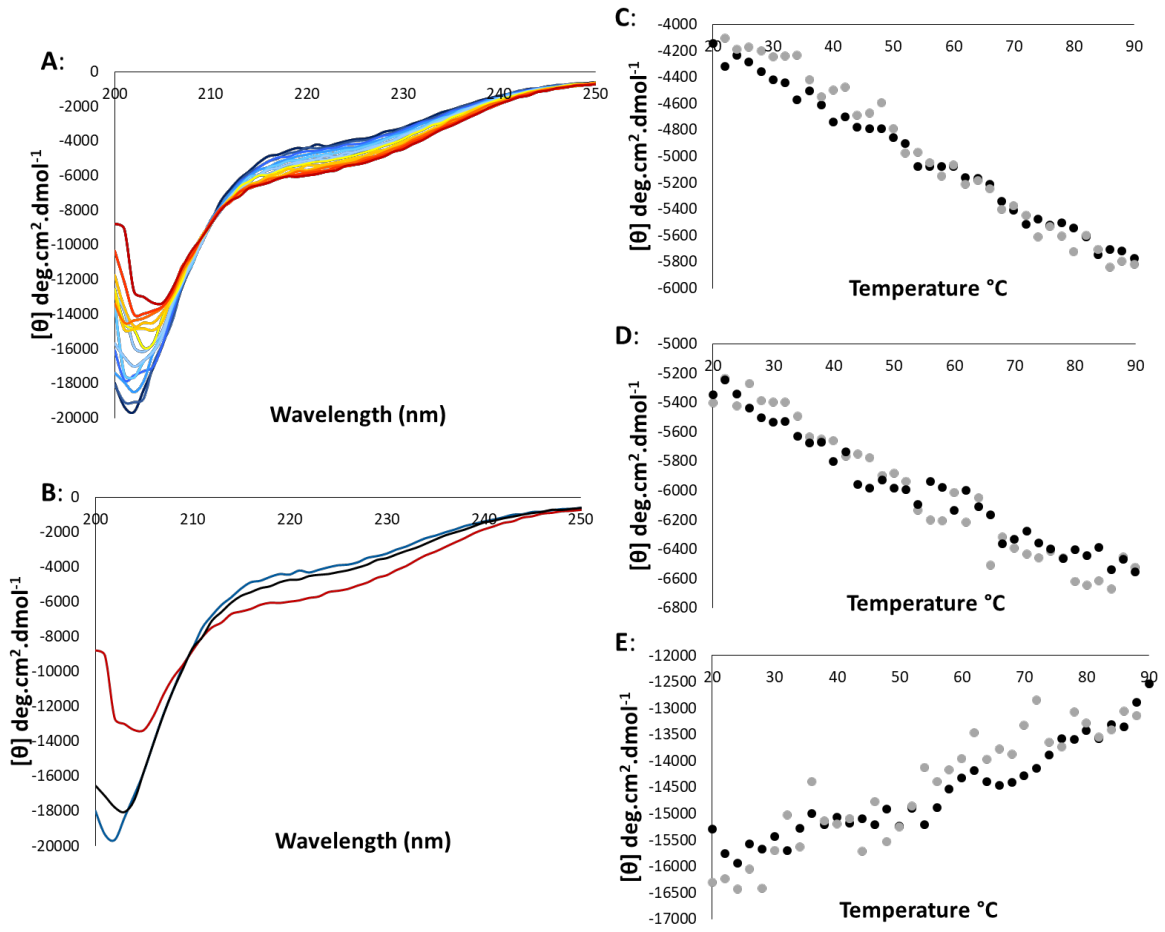

Figure 3.14. Far-UV circular dichroism monitoring of thermal unfolding of RBBP6 p53BD.

(A) *Far-UV CD spectrum between 20 ˚C and 90 ˚C (dark blue to dark red) for 2.6 µM RBBP6 p53BD in 20 mM Sodium phosphate, pH 7.* ***(B)*** *Protein refolding after heating shown in black, protein at 20 °C in blue and protein at 90 °C in red for RBBP6 p53BD in 20mM Sodium phosphate, pH 7. Heat unfolding curves for RBBP6 p53BD in 20 mM Sodium phosphate, pH 7, at 2.6 µM (black) and 4.1 µM (grey) for* ***(C)*** *222 nm,* ***(D)*** *215 nm and* ***(E)*** *208 nm between 20 ˚C and 90 ˚C.*

Table 3.3: The percentage recovery of RBBP6 p53BD after thermal unfolding study.

Percentage structural change and recovery were calculated between 20 °C and 90 °C spectrum values at 222 nm, 215 nm and 208 nm.

Wavelength (nm)	% structural change	% recovery
222	29	91
215	19	94
208	7	99,6

3.7.2 Characterization of RBBP6 p53BD in the presence of urea

Far-UV CD spectra were recorded for purified RBBP6 p53BD in the presence of urea (Figure 3.15A). Urea is a known denaturant, which is known to cause proteins to unfold. RBBP6 p53BD was placed into 8 M urea and then diluted to 0.5 M urea to check for refolding. The far-UV CD spectra could only be recorded to between 215 nm and 205 nm in the presence of urea as the noise to signal ratio was too high at wavelengths lower than this, identified using turbidity. There is a substantial loss of structure at 8 M urea and high recovery when diluted back to 0.5 M urea (Figure 3.15A). Ellipticity at 208 nm, 215 nm and 222 nm was utilised to investigate the recovery of the domain's secondary structure (Figure 3.15B) with the percentage structure change and percentage recovery at different wavelengths shown in Table 3.4. A much larger percentage structural change was seen in the presence of urea compared to the protein being heated to 90 °C, and recovery was found to be lower than thermally unfolded RBBP6 p53BD (Table 3.3). In Figure 3.15B**,** the increase in mean residue ellipticity at both 215 nm and 222 nm indicates significant structural changes occurring consistently up to 8 M urea.

3.7.3 Characterization of RBBP6 p53BD in the presence of guanidinium chloride

Far-UV spectra were recorded for purified RBBP6 p53BD in guanidinium chloride (Figure 3.16A). Guanidinium chloride is another well-known denaturant that is known to cause proteins to unfold. RBBP6 p53BD was placed into 6 M guanidinium chloride and then diluted down to 1 M guanidinium chloride to check for refolding. The far-UV CD spectra could only be recorded to between 215 nm and 205 nm in the presence of guanidinium chloride as the noise to signal ratio was too high at wavelengths lower than this, identified using turbidity.

There is a substantial loss of structure at 6 M guanidinium chloride and high recovery when diluted back to 1 M guanidinium chloride. Again ellipticity at 208 nm, 215 nm and 222 nm was utilised to investigate the recovery of the domain's secondary structure (Figure 3.16B) with percentage structure change and percentage recovery at different wavelengths shown in Table 3.5**.** A larger percentage structural change for RBBP6 p53BD was seen in the presence of guanidinium chloride compared to the protein in the presence of urea, and recovery was found to be lower in guanidinium chloride than in urea (Table 3.4). In Figure 3.16B**,** the increase in mean residue ellipticity at 215 nm and 222 nm indicates larger structural changes occurring until 3 M guanidinium chloride and minor structural changes occurring from 3 M to 6 M.

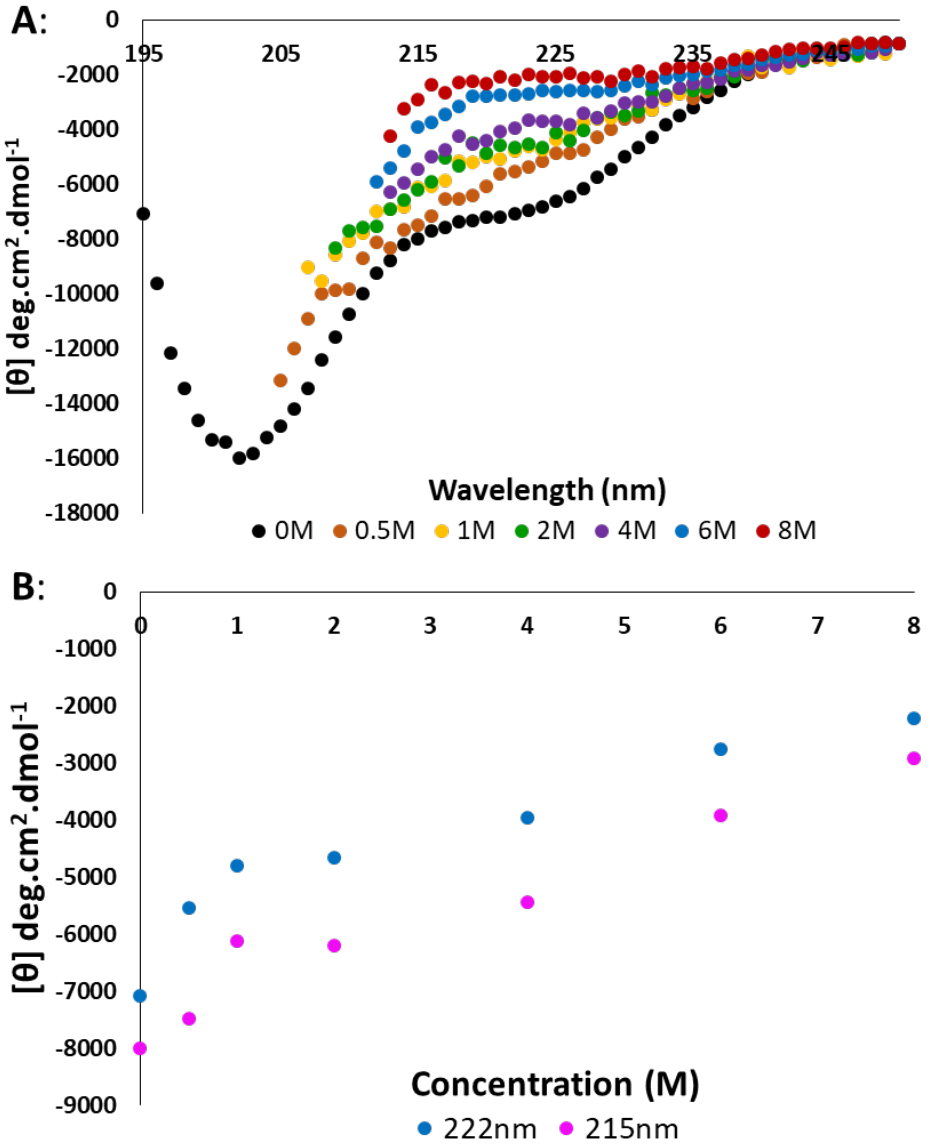

Figure 3.15. RBBP6 p53BD in the presence of urea.

(A) *Far-UV CD Spectra between 250 nm and 195 nm for RBBP6 p53BD in 10 mM sodium phosphate, pH7 with 0 to 8 M urea.* ***(B)*** *Far-UV CD for 215 nm (pink) and 222 nm (blue) at urea concentrations between 0 and 8 M.*

Table 3.4: The percentage recovery of RBBP6 p53BD after exposure to 8M urea.

Percentage structural change and recovery were calculated between 8 M and 0.5 M urea spectrum values at 222 nm, 215 nm and 208 nm.

Wavelength (nm)	% structural change	% recovery
222	69	78
215	64	93
208	n.a	80

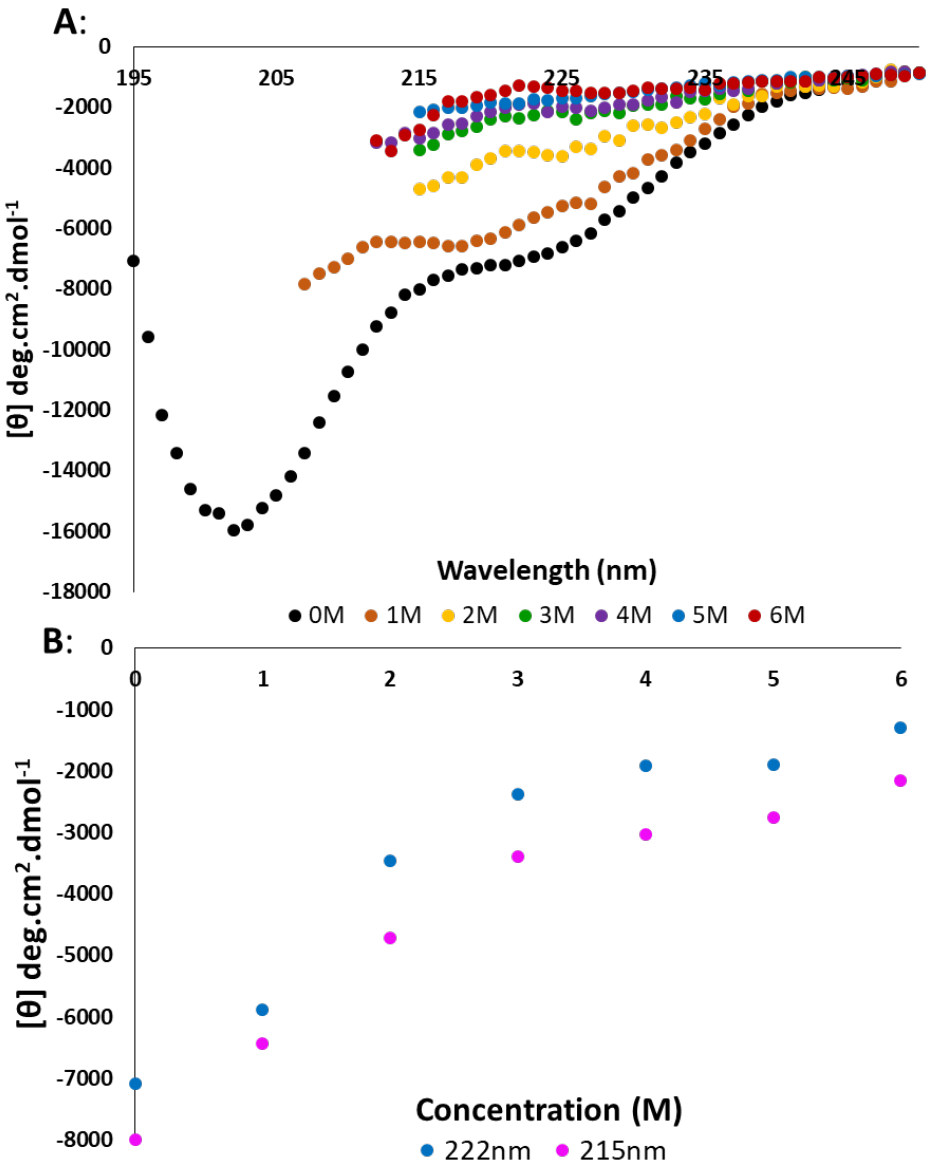

Figure 3.16. RBBP6 p53BD in the presence of guanidinium chloride.

(A) *Far-UV CD Spectra between 250 nm and 195 nm for RBBP6 p53BD in 10 mM sodium phosphate, pH7 with 0 to 6 M* guanidinium chloride*.* ***(B)*** *Far-UV CD for 215 nm (pink) and 222 nm (blue) at various* guanidinium chloride *concentrations between 0 and 6 M.*

Table 3.5: The percentage recovery of RBBP6 p53BD after exposure to 6M guanidinium chloride.

Percentage structural change and recovery were calculated between 6 M and 1 M guanidinium *chloride spectrum values at 222 nm, 215 nm and 208 nm.*

Wavelength (nm)	% structural change	% recovery
222	74	83
215	73	80
208	n.a	60

3.8 Subcellular Localisation of RBBP6 and p53 in normal and cancer cell lines

To investigate the subcellular localisation of RBBP6 and p53 in normal and cancer cell lines, immunocytochemistry was performed using secondary antibodies conjugated with fluorophores. The primary antibodies used were rabbit anti-RBBP6 (Novusbio NBP1-49535) and mouse anti-p53 (Abcam ab1101). The secondary antibodies used were anti-rabbit (FITC conjugated) (Abcam ab6717) and anti-mouse TRITC conjugated (Abcam ab6786). DAPI was used as a DNA dye to distinguish the nucleus from the cytoplasm. It is noteworthy that the anti-RBBP6 primary antibody can recognise isoforms 1, 2 and 4 based on the epitope specified by the manufacturer. This means this antibody cannot recognise isoform 3, the shortest isoform of RBBP6, which contains just the DWNN and an unstructured C-terminal region. Isoform 3 has been found to be expressed in the cytoplasm and be pro-apoptotic.

In HEK293 T cells, RBBP6 (Figure 3.17A) was predominately localised in the nucleus, particularly in characteristic speckle-like bodies. Previous studies have found that RBBP6 is present in nuclear speckles, supporting its involvement in pre-mRNA splicing (Simons *et al*., 1997). Very little RBBP6 was found in the cytoplasm. For p53 (Figure 3.17B), localisation was seen in the cytoplasm and the nucleus. p53 localisation levels varied from cell to cell, potentially due to different cells being in different levels of development and stress.

For MCF7 cells, RBBP6 (Figure 3.18A) was found to be localised in both the nucleus as well as the cytoplasm.RBBP6 was still more prominent in the nucleus, with speckle-like bodies present. For p53 (Figure 3.18B), localisation was found in the cytoplasm and the nucleus, with slightly higher localisation found in the nucleus. In A549 cells, RBBP6 (Figure 3.19A) was again localised in the nucleus and cytoplasm, this time with no remarkable difference between the two locations. For p53 (Figure 3.19B), localisation was seen in the cytoplasm and the nucleus; however, p53 levels were remarkably higher in the nucleus than in the cytoplasm.

Interestingly, in MDA-MB-231 cells, RBBP6 (Figure 3.20A) localisation is seen in the cytoplasm and nucleus, with little difference in localisation seen between the two locations. Furthermore, p53 (Figure 3.20B) localisation was found in the cytoplasm and the nucleus. It should be noted that MDA-MB-231 ($p53^{R280K}$) cells have a mutated p53, where the mutation is present in the DNA binding domain of p53 without causing destabilisation of p53's structure.

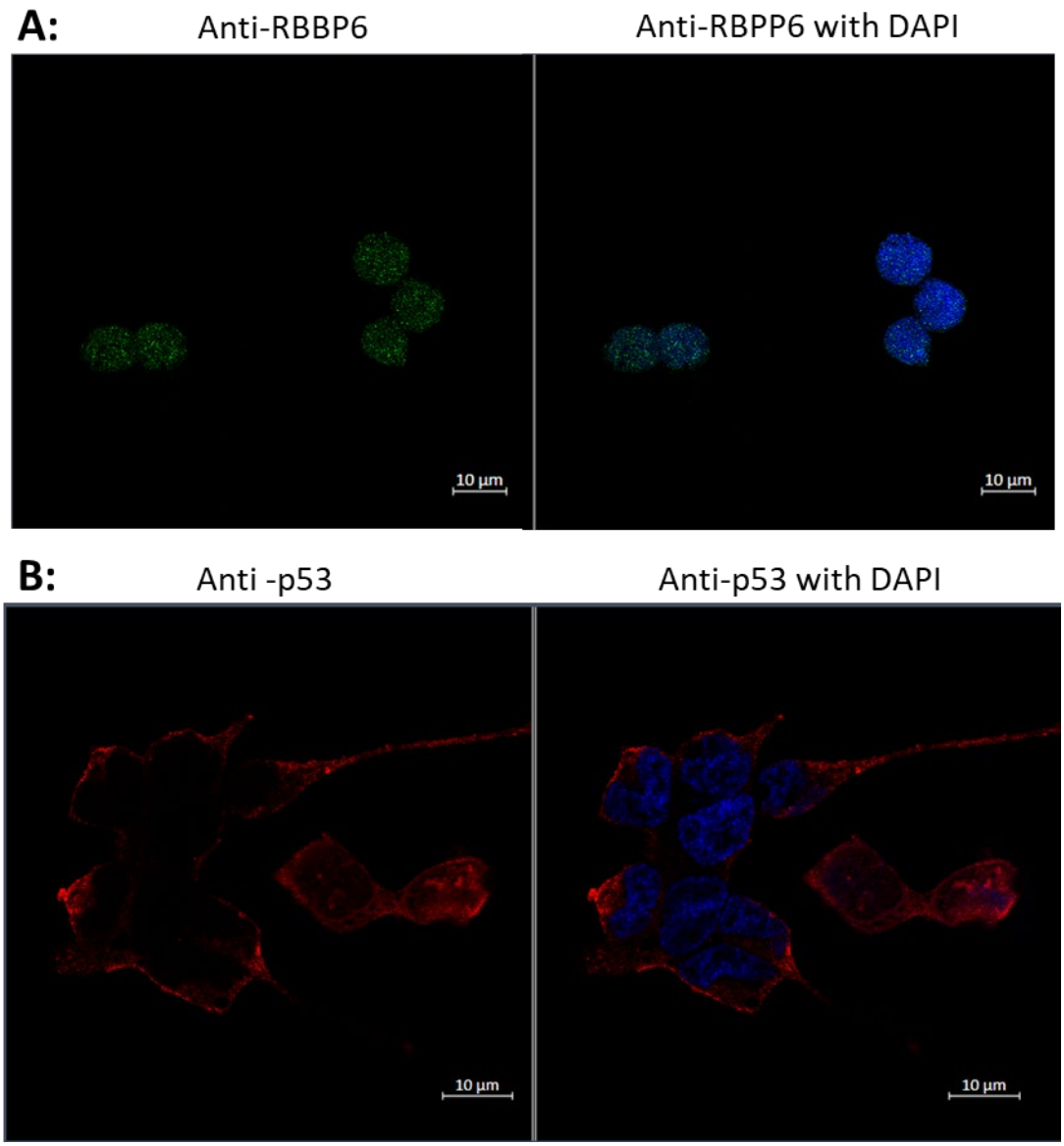

Figure 3.17. Localisation of p53 and RBBP6 in HEK293 T cells.

*HEK293 T cells were stained with **(A)** polyclonal anti-RBBP6 (green) and **(B)** monoclonal anti-p53 (red). DAPI (blue) shows the stained cell nucleus. The scale bar is 10 µm.*

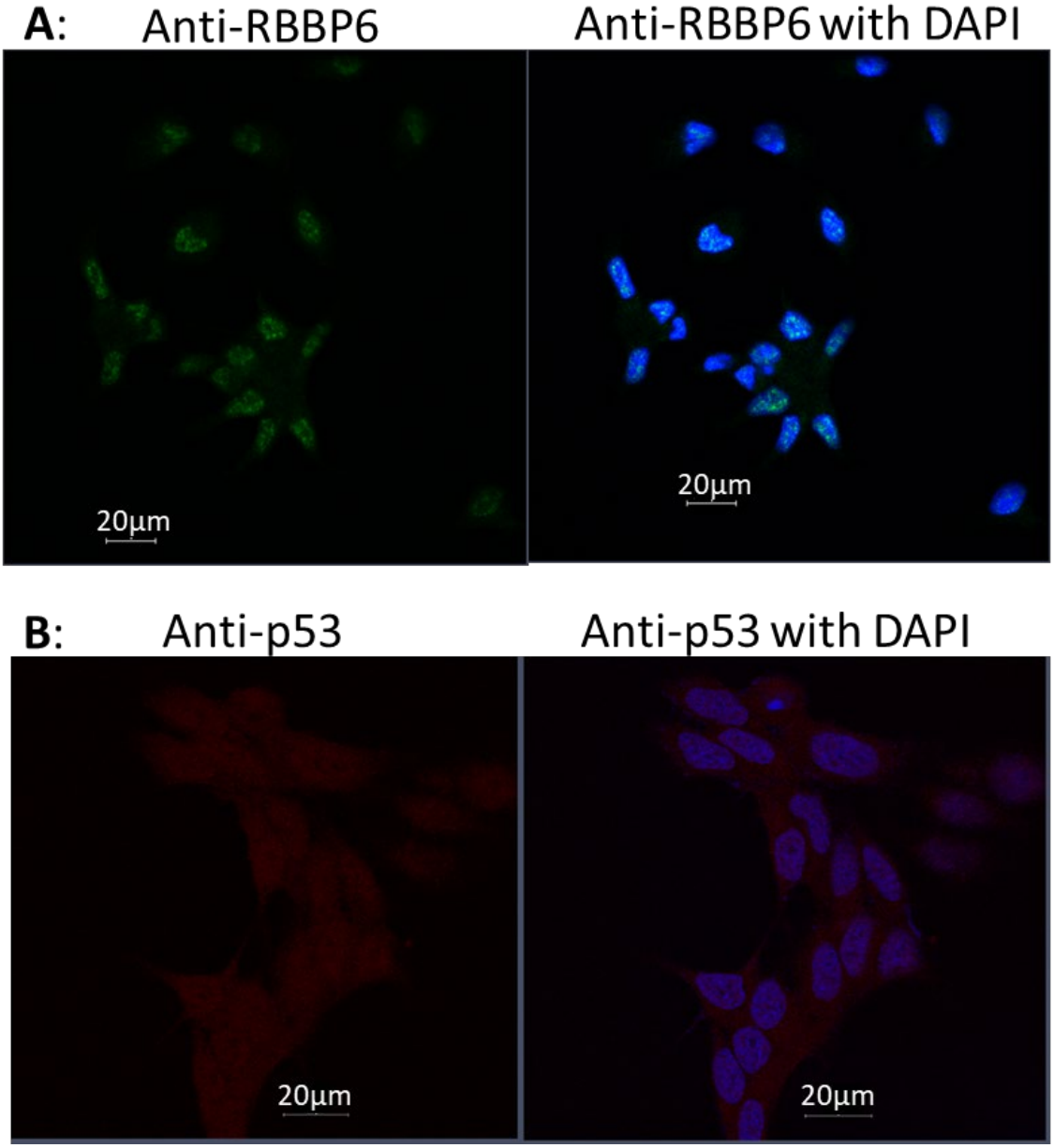

Figure 3.18. Localisation of p53 and RBBP6 in MCF7 cells.

*MCF7 cells were stained with **(A)** polyclonal anti-RBBP6 (green) and **(B)** monoclonal anti-p53 (red). DAPI (blue) shows the stained cell nucleus. The scale bar is 20 µm.*

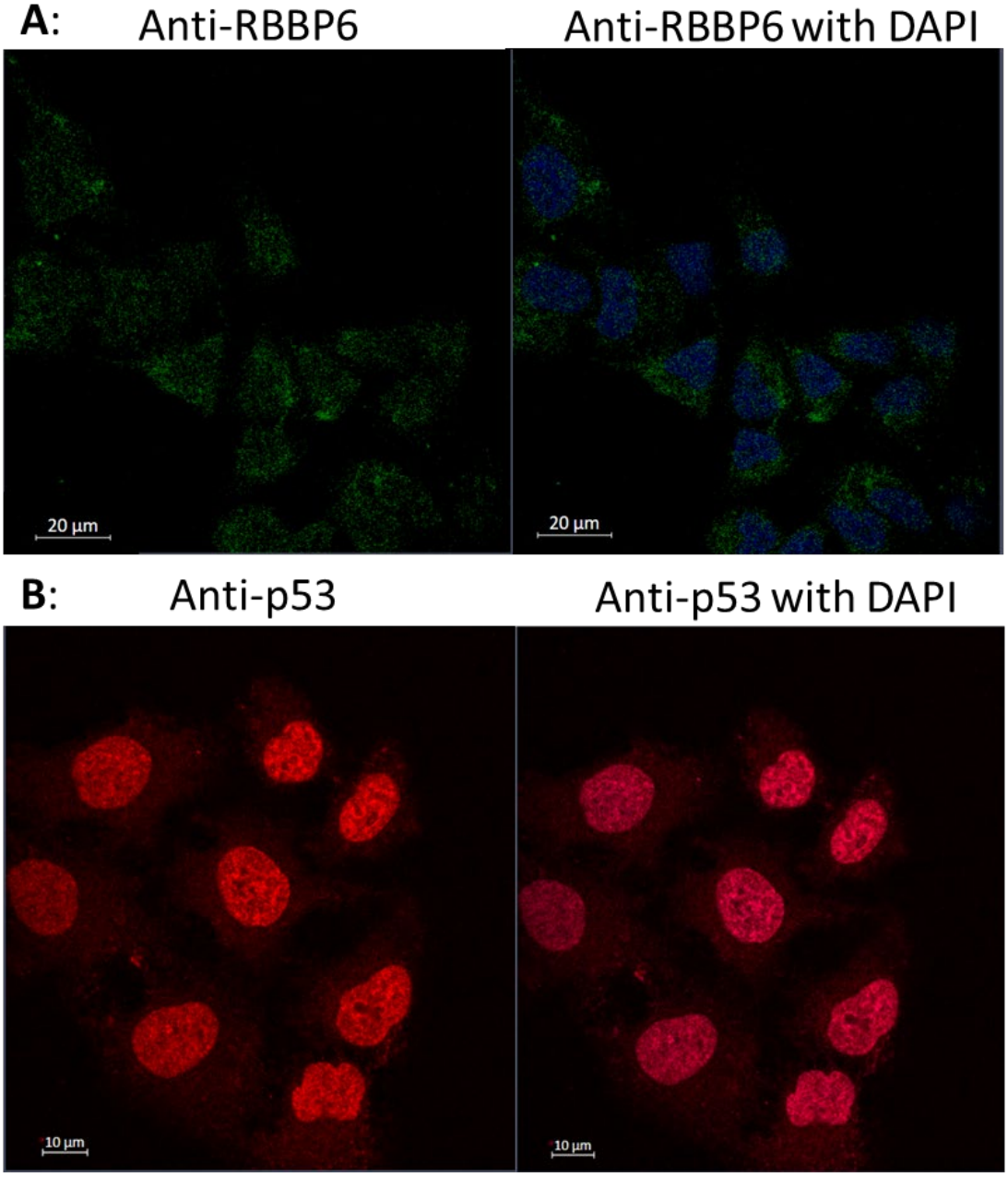

Figure 3.19. Localisation of p53 and RBBP6 in A549 cells.

*A549 cells were stained with **(A)** polyclonal anti-RBBP6 (green), with a scale bar of 20 µm, and **(B)** monoclonal anti-p53 (red), with a scale bar of 10 µm. DAPI (blue) shows the stained cell nucleus.*

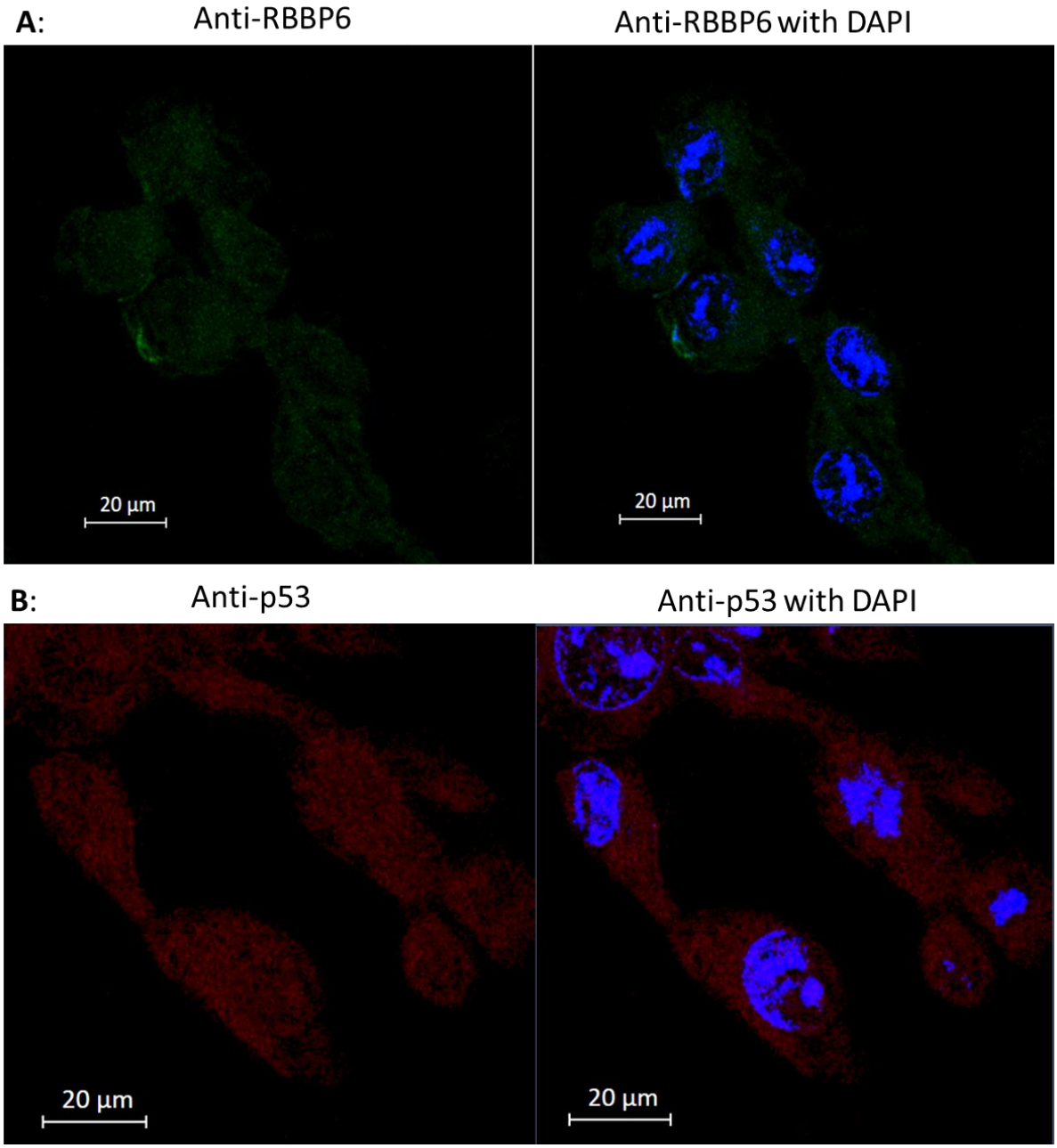

Figure 3.20. Localisation of p53 and RBBP6 in MDA-MB-231 cells.

*MDA-MB-231 cells were stained with **(A)** polyclonal anti-RBBP6 (green) and **(B)** monoclonal anti-p53 (red). DAPI (blue) shows the stained cell nucleus. The scale bar is 20 µm.*

3.9 Colocalisation of RBBP6 and p53 in cancer cell lines

Immunocytochemistry can be taken further to investigate the localisation of more than one protein at a time and therefore determine whether two or more proteins localise in similar subcellular regions. In order for two proteins to be able to interact within the cell, they need to be within close proximity to one another. The antibodies that recognise the different proteins being studied need to be from different species for colocalisation studies. The antibodies must also be conjugated to different fluorophores, which have excitation and visualisation wavelengths that are far enough

apart to not create cross-talk. Again, the primary antibodies used were rabbit anti-RBBP6 (isoforms 1, 2 and 4) (Novusbio, NBP1-49535) and mouse anti-p53 (Abcam, ab1101). The secondary antibodies used were anti-mouse TRITC conjugated (Abcam, ab6786) and anti-rabbit (FITC conjugated) (Abcam, ab6717). DAPI was used as a DNA dye to distinguish the nucleus from the cytoplasm.

Cells were dual stained with antibodies that recognise RBBP6 and p53 in MCF7 cells (Figure 3.21) and A549 cells (Figure 3.22). There are several colocalisation coefficients that can be calculated to predict the probability of two protein molecules colocalising. Quantitative colocalisation analysis was performed using ImageJ colocalisation JACoP plugin software, where Manders and Pearson's coefficients were generated. The background threshold was set automatically using the Costes method (Costes *et al.,* 2004) to ensure an unbiased measurement. The experiments were repeated at least twice, and the average values are reported here (Table 3.6). Colocalisation of RBBP6 to p53 was measured, and the colocalisation of p53 to RBBP6.

Manders overlap coefficient measures if the two separate fluorophores are in the same place in the image, in other words, the co-occurrence. Pearson's correlation coefficient measures if there is a relationship between the two fluorophore intensities, in other words, if there is a correlation. Manders overlap coefficient has a value from 0 to 1, indicating a fraction of pixels with positive values above the threshold in both channels. With Pearson's correlation coefficient, its value can range from -1 to 1. A value of 1 indicates perfect correlation; that is, the two channels' fluorescent intensities are perfectly linearly related. A value of -1 indicates a perfect inverse correlation; that is, the two channels' fluorescent intensities are perfectly but inversely related to each other and 0 indicates a lack of correlation between any of the pixels in both channels. A value over 0.5 is seen as positive colocalisation occurring.

Table 3.6 shows the Manders coefficient values that indicate a higher colocalisation of RBBP6 to p53 than p53 to RBBP6 in both MCF7 and A549 cells. They do not indicate a perfect colocalisation value of 1. However, this is expected as both p53 and RBBP6 are involved in several biological functions within the cell that do not relate to their interaction. The Pearson's coefficient shows significant colocalisation from a value of 0.5 to 1. For both MCF7 and A549, the Pearson's coefficients were above 0.5, and therefore, this shows positive colocalisation occurring in both cell lines. Again a perfect score of 1 is not seen; however, this can be explained by these proteins serving multiple other biological functions within the cell. These measurements suggest that RBBP6 and p53 are in close enough proximity that interaction is likely possible.

On basic visual inspection, p53 and RBBP6 colocalise in the nucleus and cytoplasm, but they do not appear to colocalise in the nuclear speckles. Nuclear speckles are linked to mRNA processing, and RBBP6's localisation in nuclear speckles has supported its involvement in mRNA processing. Further studies would need to be conducted using an antibody that can recognise a key splicing factor such as SC35, a well-established localisation marker in nuclear speckles. Investigating p53 colocalisation to a factor such as SC35 could help determine whether p53 could colocalise with RBBP6 within the nuclear speckles.

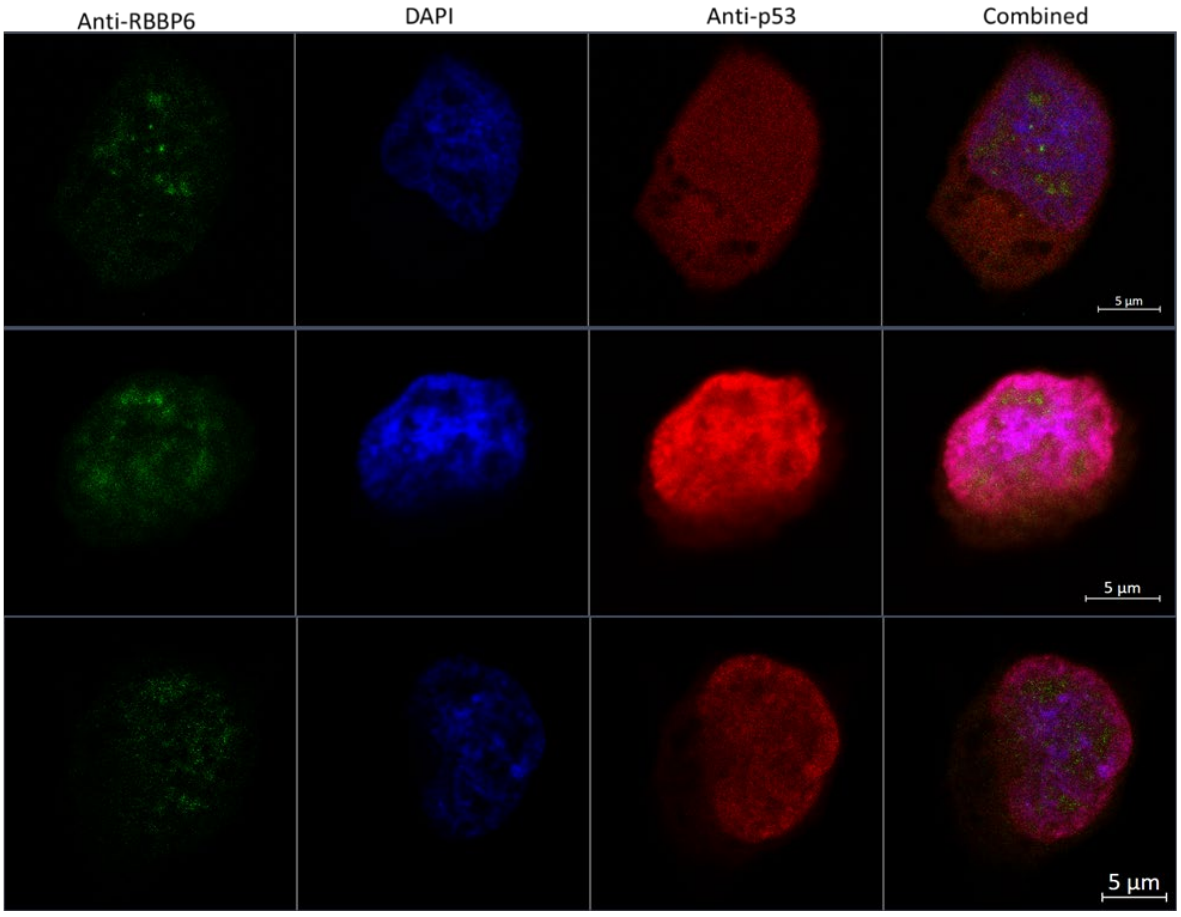

Figure 3.21. Colocalisation of p53 and RBBP6 in MCF7 cells.

MCF7 cells were stained with polyclonal anti-RBBP6 (green) and monoclonal anti-p53 (red). A fluorescent signal was found for RBBP6 and p53 in the cytoplasm and the nucleus. DAPI (blue) shows the stained cell nucleus. The scale bar is 5 µm.

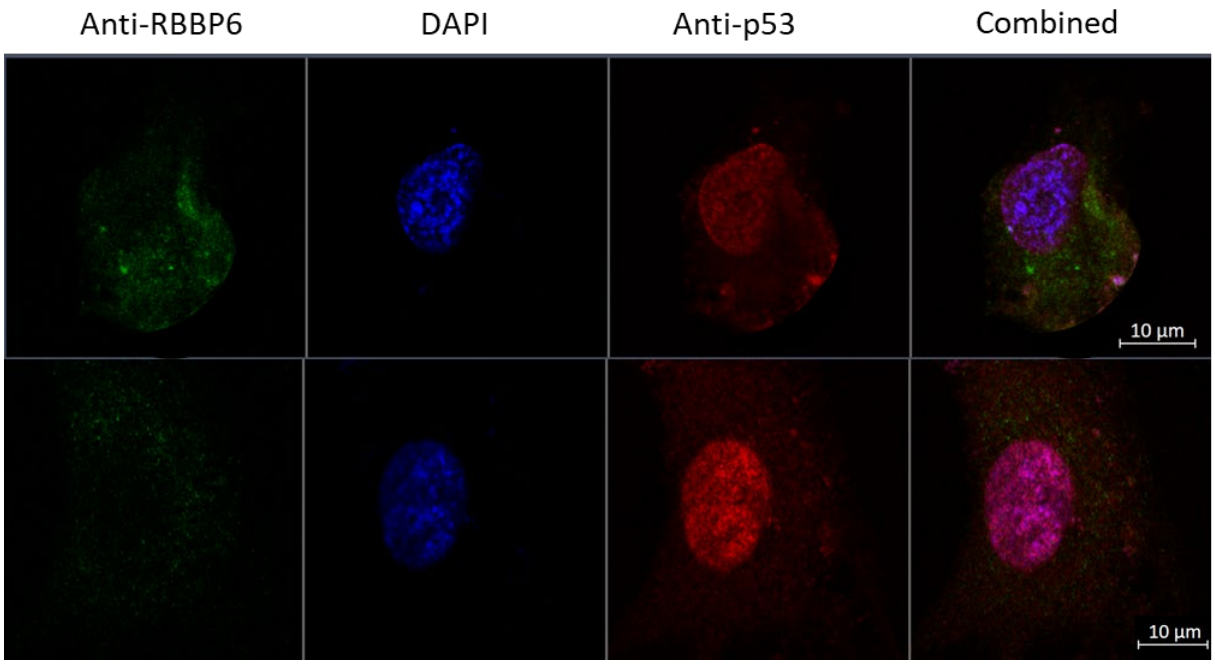

Figure 3.22. Colocalisation of p53 and RBBP6 in A549 cells.

A549 cells were stained with polyclonal anti-RBBP6 (green) and monoclonal anti-p53 (red). The fluorescent signal was found for both RBBP6 and p53 in the cytoplasm and the nucleus. DAPI (blue) shows the stained cell nucleus. The scale bar is 10 µm.

Table 3.6: Quantitative colocalisation measurements.

Manders and Pearson's coefficients were calculated using the JACoP plugin of ImageJ (Bolte and Cordelières, 2006) for MCF7 and A549 cells.

Measurement	MCF7	A549
Mean Manders coefficient of RBBP6 to p53	0.904	0.834
Mean Manders coefficient of p53 to RBBP6	0.761	0.784
Mean Pearson's coefficient	0.759	0.630

3.10 Investigating the nature of the potential RBBP6-p53-MDM2 interaction

Colocalisation studies are not enough to prove protein interactions, as even a microscope with the highest resolution possible cannot determine the precise location of two separate protein molecules. Therefore, to further investigate the interaction between p53 and RBBP6, co-immunoprecipitation (Co-IP) assays were performed. Co-IP assays can investigate potential protein interactions as they are performed under non-denaturing conditions. Co-IP assays utilise an antibody that can recognise a protein of interest and, through interaction with Protein A agarose beads, results in the isolation of immuno-complexes from a protein mixture. The isolated immuno-complexes can then be investigated for proteins that can interact with the protein of interest using Western blot or mass spectrometry. Co-IP assays have been performed in mice (Li *et al*., 2007), which identified that the mouse homologue of RBBP6, known as PACT, could bind to p53. Further, Xiao and colleagues showed that in human colorectal cell lines SW620 and HT29, when an anti-MDM2 Co-IP assay was performed, RBBP6 was present in the immuno-complexes isolated (Xiao *et al*., 2018a). In the anti-p53 Co-IP assay, MDM2 was found in the immuno-complexes isolated. To our knowledge, the interaction of RBBP6 to p53 and MDM2 has not been shown through Co-IP assays in the normal cell line HEK293T or breast cancer cell line MCF7. The interaction between endogenous p53 and the recombinant RBBP6 p53BD produced in this study is also presented.

3.10.1 Endogenous RBBP6-p53-MDM2

To investigate the potential interaction between p53, MDM2 and RBBP6, co-immunoprecipitation (Co-IP) assays were performed using cell lysates from normal and cancer cell lines. For HEK293 T cells, two independent Co-IP assays were performed, one using an anti-p53 antibody and one using an anti-RBBP6 antibody. The immune complexes were isolated from cell lysate using Protein A agarose beads. Both Co-IP assays were analysed using Western blot to determine the presence of p53, RBBP6 and MDM2 in the immuno-complexes isolated after elution (Figure 3.23). As seen in Figure 3.23, in the RBBP6 Co-IP assay, the proteins p53, MDM2 and RBBP6 were found in the immuno-complexes isolated (lane 2), suggesting that these three proteins interact and can form a complex *in vitro*. This is further supported as p53, MDM2 and RBBP6 were identified in the immuno-complexes isolated during the anti-p53 Co-IP assay (lane 5). p53, MDM2 and RBBP6 are not present in the flow-through (lanes 1 and 4), which contains the proteins that did not interact with the Protein A agarose bound antibodies. The lack of protein detection in the cell lysate sample (lane 3) could be due to the lysate being diluted compared to the eluents.

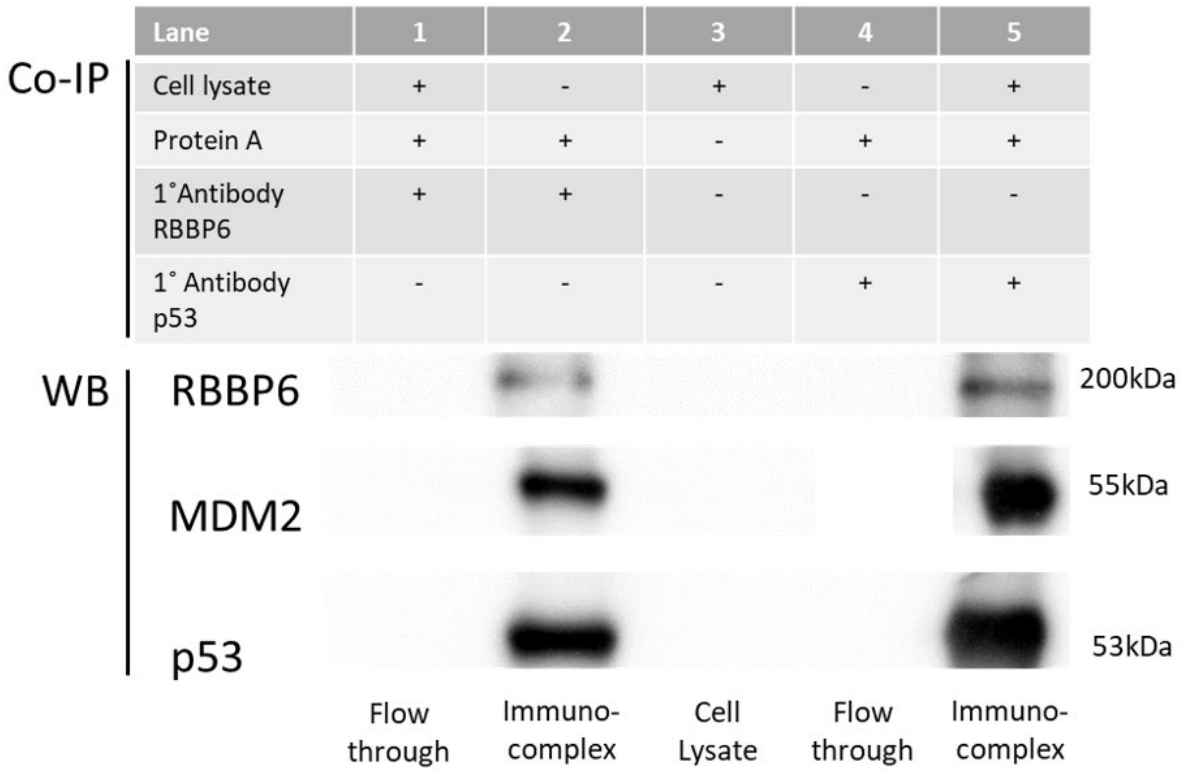

Figure 3.23. Western blot analysis of samples collected from Co-IP assays performed using RBBP6 and p53 antibodies independently on HEK293 T cells.

Three independent Western blots were performed to investigate the presence of p53, RBBP6 and MDM2 in Co- IP assays performed using Protein A agarose and anti-RBBP6 (lanes 1 and 2) and anti-p53 (lanes 4 and 5). Lane 1 is the flow-through from the anti-RBBP6 Co-IP assay, which contains the proteins in the cell lysate that did not interact with the Protein A agarose bound antibody. Lane 2 contains the immuno-complexes isolated during the anti-RBBP6 Co-IP assay. Lane 3 is the HEK293 T cell lysate used in Co-IP assays. Lane 4 contains the flow-through from the anti-p53 Co-IP assay. Lane 5 contains the immuno-complexes isolated during the anti-p53 Co-IP assay.

p53 is known for migrating to a distance of 53 kDa in SDS-PAGE despite having a molecular weight of 43 kDa. Isoform 1 of RBBP6 often appears at approximate 200 kDa on SDS-PAGE. MDM2 is often reported at 55 kDa or 90 kDa on SDS-PAGE despite having a molecular weight of 55 kDa. The manual from the manufacturer of the MDM2 antibody used (Abcam-ab16895) states it recognises the epitope within amino acids 294-339 of MDM2, and during Western blot analysis that the antibody recognises a protein of 55 kDa that is MDM2 with the apparent weight of 90 kDa. Many articles do not give a molecular weight in Western blot analysis, including publications that used this specific antibody. However, reviews in the manufacturer's manual and published articles using anti-MDM2 (Abcam-ab16895) report a band for MDM2 at approximately 66 kDa and 55 kDa, respectively (Tabata *et al*., 2009; Sun *et al*., 2019). Therefore, the band at 55 kDa was taken as representing

MDM2. It should also be noted that the identified isoforms of MDM2 with lower molecular weights, expressed in cancer cells, lack the p53 binding domain of MDM2 and therefore would not be likely to appear in the immuno-complexes isolated during Co-IP assays.

Similarly, three independent Co-IP assays were performed on MCF7 cells using anti-RBBP6, anti-MDM2 and anti-p53 antibodies, respectively, to determine whether the proteins p53, RBBP6 and MDM2 can interact in a cancer cell line. The immuno-complexes formed were isolated using Protein A agarose beads and subjected to Western blot analysis for the proteins p53, MDM2 and RBBP6 (Figure 3.24). MCF7 is a breast adenocarcinoma with wild type p53. In Figure 3.24**,** it can be seen that p53, MDM2 and RBBP6 were present in the immuno-complexes isolated in the anti-p53 Co-IP assay (lane 2). Similarly, in the immuno-complexes isolated from the anti-MDM2 (lane 4) and anti-RBBP6 (lane 6) Co-IP assays, you can see that all three proteins are present. The flow-through for each assay (lanes 1, 3 and 5) contains the proteins that did not interact with the Protein A agarose bound antibodies in each respective assay. The three proteins being investigated were not found in the flow-through samples analysed. This further supports that p53, MDM2 and RBBP6 are able to interact as a complex *in vitro* in normal and cancer cell lines.

3.10.2 Recombinant RBBP6 p53BD interaction with endogenous p53

The functionality of a recombinant protein needs to be evaluated before downstream experiments can be performed. Co-IP assays were performed to investigate whether the recombinant RBBP6 p53BD, produced in this study, was functional and able to interact with endogenous p53. Purified, recombinant RBBP6 p53BD was incubated with a HEK293 T cell lysate before adding antibodies. The immune complexes subsequently formed were isolated by Protein A Agarose and visualised using Western analysis (Figure 3.25). Two independent Co-IP assays were performed, using anti-p53 and anti-polyhistidine antibodies respectively. The anti-polyhistidine antibody was used to investigate the polyhistidine-tagged RBBP6 p53BD. In the immuno-complexes isolated during the anti-p53 Co-IP assay (lane 3), both p53 and recombinant RBBP6 p53BD were present. This suggests that the recombinant RBBP6 p53BD can bind and form a complex with endogenous p53. Similarly, in the immuno-complexes isolated during the anti-polyhistidine Co-IP assay (lane 5), both p53 and recombinant RBBP6 p53BD were present, further supporting that recombinant RBBP6 p53BD and endogenous p53 are able to interact. Endogenous p53 and recombinant RBBP6 p53BD are also seen in lane 1, which contains the cell lysate-recombinant RBBP6 p53BD mixture used in the Co-IP assays.

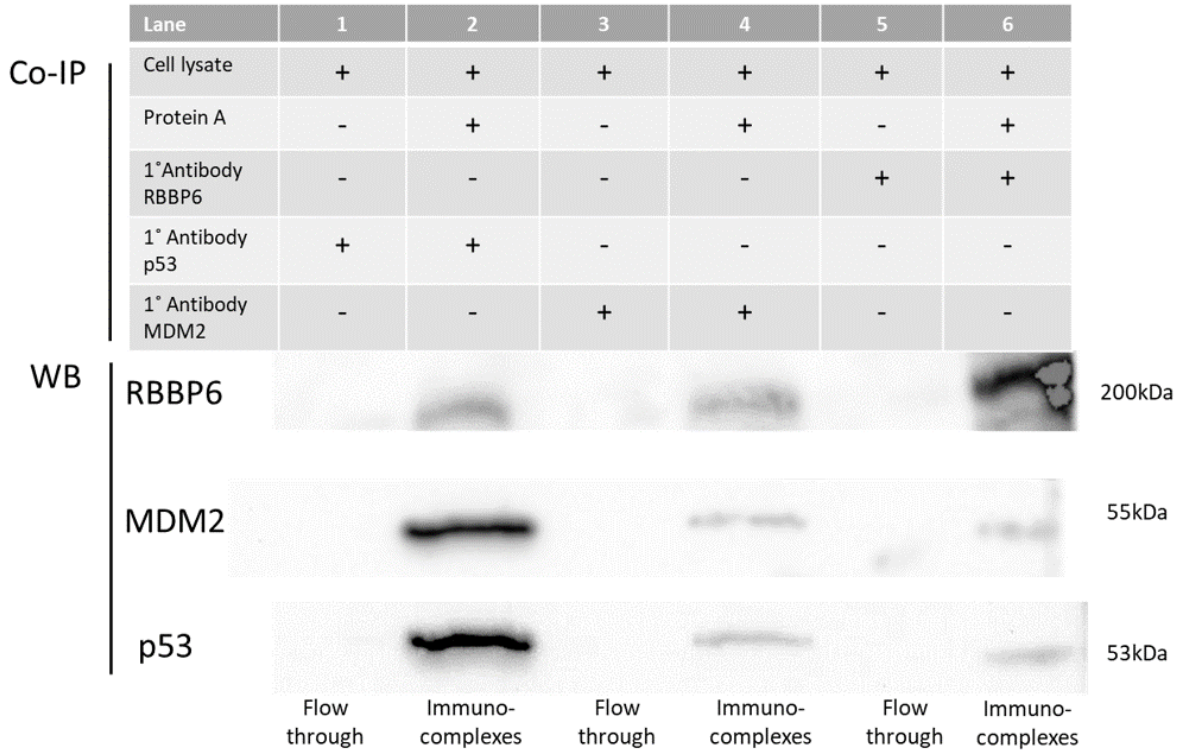

Figure 3.24. Western blot analysis of samples collected from Co-IP assays performed using p53, MDM2 and RBBP6 antibodies independently on MCF7 cells.

Three independent Western blots were performed to investigate the presence of p53, RBBP6 and MDM2 in Co-IP assays performed using Protein A agarose and anti-p53 (lanes 1 and 2), anti-MDM2 (lanes 3 and 4) and anti-RBBP6 (lanes 5 and 6). Lane 1 is the flow-through from the anti-p53 Co-IP assay, which contains the proteins in the cell lysate that did not interact with the Protein A agarose bound antibody. Lane 2 contains the immuno-complexes isolated during the anti-p53 Co-IP assay. Lane 3 contains the flow-through from the anti-MDM2 Co-IP assay. Lane 4 contains the immuno-complexes isolated during the anti-MDM2 Co-IP assay. Lane 5 contains the flow-through from the anti-RBBP6 Co-IP assay. Lane 6 contains the immuno-complexes isolated during the anti-RBBP6 Co-IP assay.

	Lane	1	2	3	4	5	6	7
Co-IP	Cell lysate	+	+	-	+	-	+	-
	RBBP6 p53BD	+	+	+	+	+	-	+
	Protein A	-	+	+	+	+	+	-
	1˚Antibody polyhistidine	-	-	-	+	+	+	-
	1˚ Antibody p53	-	+	+	-	-	+	-

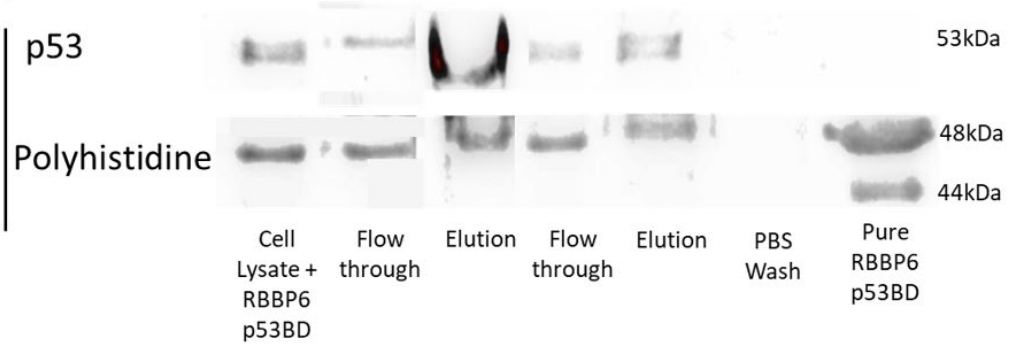

Figure 3.25. Western blot analysis of samples collected from Co-IP assays performed using p53 and polyhistidine antibodies independently on HEK293 T cells.

Two independent Western blots were performed to investigate the presence of endogenous p53 and recombinant polyhistidine-tagged RBBP6 p53BD in Co-IP assays performed using Protein A agarose with anti-p53 (lanes 2 and 3) and anti-polyhistidine (lanes 4 and 5) as probes. Lane 1 contains the HEK293 T cells cell lysate with purified RBBP6 p53BD used in Co-IP assays. Lane 2 contains the flow-through from the anti-p53 Co-IP assay, which consists of the proteins in the cell lysate that did not bind with the p53 antibody. Lane 3 contains the immuno-complexes isolated during the anti-p53 Co-IP assays. Lane 4 contains the flow-through from the anti-polyhistidine Co-IP assay, which consists of the proteins in the cell lysate that did not bind with the polyhistidine antibody. Lane 3 contains the immuno-complexes isolated during the anti-polyhistidine Co-IP assay. Lane 6 contains the PBS collected from washing the agarose beads before elution for combined Co-IP assays. Lane 7 contains the purified RBBP6 p53BD as a control.

Recombinant RBBP6 p53BD was seen in the flow-through for both Co-IP assays performed (Figure 3.25) (lanes 2 and 4). The flow-through is the proteins in the cell lysate-recombinant protein mixture that did not interact with the Protein A agarose bound antibodies. The presence of recombinant RBBP6 p53BD in the flow-through may be due to the excess recombinant protein being added to give the domain a competitive advantage over endogenous full-length RBBP6 present in the cell lysate. P53 was found in the flow-through for the anti-p53 Co-IP Assay (lane 2), suggesting that insufficient p53 antibody or agarose beads were added to bind all endogenous p53

present. p53 was also found in the flow-through for the anti-polyhistidine Co-IP Assay (lane 5), which may be due to endogenous RBBP6 being present in the HEK293 T cell lysate and competing for p53 binding, resulting in not all p53 present being able to bind the recombinant RBBP6 p53BD. As recombinant RBBP6 p53BD and p53 were found in the flow-through, the PBS wash step (lane 6) was analysed to confirm the presence of the RBBP6 p53BD and p53 in the immuno-complexes isolated (Lanes 3 and 5) was not just due to the excess protein being present. Lane 7 shows purified RBBP6 p53BD; this acts as a positive control in the anti-polyhistidine Western blot and as a negative control in the ant-p53 Western blot as it shows the anti-p53 antibody is unable to bind the purified RBBP6 p53BD. Recombinant RBBP6 p53BD's ability to bind endogenous p53 confirms that the recombinant RBBP6 p53BD has structure and is functional.

3.11 NADH interaction RBBP6 p53BD and its interference with p53 binding

During postgraduate studies, Twala computationally predicted the structure of the p53 binding domain of RBBP6, using its amino acid sequence identified by the UniprotKB database (Unique entry identifier: Q7Z6E9) and two programs, namely I-TASSER and eThread-modeller (Twala, 2017). A model predicted by eThread-modeller was used as the best representation based on parameters investigated in the study, and the predicted model consisted predominantly of alpha-helices. This model was used in *in silico* binding site prediction studies using the FTSite Webserver server, followed by drug binding studies using the Schrödinger-Maestro v10.7: Glide SP to screen the Zinc drug database (Zdd). The compound predicted to bind to the p53 binding domain of RBBP6 was Nicotinamide adenine dinucleotide (NADH). NADH is a coenzyme that is found in all living cells. It has both oxidizing and reducing properties and is very important during cellular energy metabolism.

To investigate the potential interaction between the RBBP6 p53BD and NADH and whether this interaction affects the binding of recombinant RBBP6 p53BD to endogenous p53, co-immunoprecipitation assays were used. Eight assays in total were performed, using anti-p53 and anti-polyhistidine antibodies with varying concentrations of NADH between 0 µM and 500 µM. The immuno-complexes isolated were then analysed using Western blot (Figure 3.26). The protein concentration of the samples was quantified using a Qubit Protein Assay kit and Qubit Fluorometer, and the sample concentrations were normalised before loading onto the gel. When investigating the presence of endogenous p53 in the immuno-complexes isolated, it was found that p53 levels were consistent regardless of NADH concentration in the anti-polyhistidine Co-IP assays (lanes 1-4). However, the levels of p53 in the anti-p53 Co-IP assays decreased when NADH concentration increased (lanes 5-8).

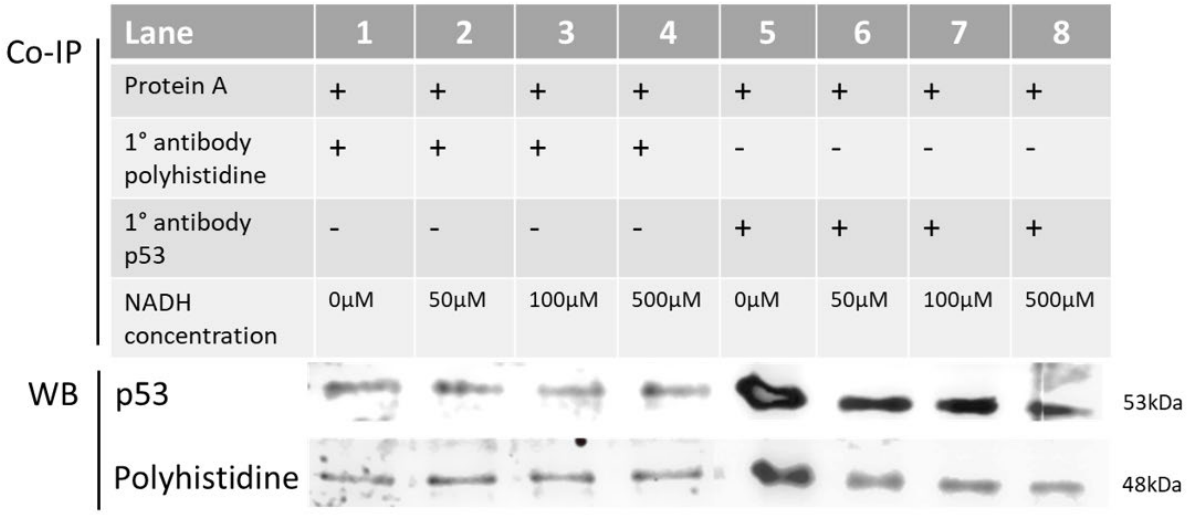

Figure 3.26. Western blot analysis of samples collected from Co-IP assays in the presence of NADH performed using p53 and polyhistidine antibodies independently on HEK293 T cells.

Two independent Western blots were performed to investigate the presence of endogenous p53 and recombinant polyhistidine-tagged RBBP6 p53BD in the immuno-complexes isolated during Co-IP assays performed using Protein A agarose and anti-polyhistidine (lanes 1-4) and anti-p53 (lanes 5-8) in the presence of a range of NADH concentrations. Concentration in µM for NADH is shown per lane and ranges from 0 µM to 500 µM.

When investigating the presence of the polyhistidine-tagged RBBP6 p53BD in the immuno-complexes isolated during the Co-IP assays, it can be seen that in the anti-polyhistidine Co-IP assays (Figure 3.26) (lanes 1-4) that levels of RBBP6 p53BD were consistent with an increase in NADH concentration. However, in the anti-p53 Co-IP assays, there is a decrease of RBBP6 p53BD with an increase in NADH concentration (Figure 3.26) (lanes 5-8). This corresponds to p53 levels in the anti-p53 Co-IP assays, showing that NADH interferes with some interaction occurring within the experiment. However, the NADH may be interfering with the binding of p53 with its antibody during the Co-IP assay rather than the interaction between p53 and RBBP6 p53BD. The decrease in RBBP6 p53BD levels seen with an increase in NADH concentration is consistent with the decrease of p53 seen in the anti-p53 Co-IP assays (lanes 5-8), suggesting the decrease in RBBP6 p53BD is a result of less p53 binding the p53 antibody during the anti-p53 Co-IP assay. However, as endogenous proteins were used from the cell lysate, it cannot be confirmed that NADH does not interact with endogenous RBBP6 and plays a role in the results.

Twala suggested that NADH may be a good lead compound to be used as a scaffold for the delivery of drugs that could disrupt the p53-RBBP6 interaction instead of causing the disruption itself (Twala, 2017). It also needs to be noted that Twala used a shorter sequence (residues 1433-1544)

for the p53 binding domain of RBBP6 than that investigated in this present study (residues 1380-1726) (Twala, 2017). Twala also predicted a considerably higher alpha-helical percentage than that predicted by I-TASSER and DichroWeb using the far-UV CD spectrum of recombinant RBBP6 p53BD in this study (Figure 3.13**,** Table 3.1 and Table 3.2) (Twala, 2017). Therefore further studies would need to be undertaken to evaluate whether NADH and RBBP6 p53BD are able to bind and whether the binding can interrupt the interaction between RBBP6 and p53. This emphasizes the need for further structural characterisation of this domain. For further testing within live cells, a few issues may also arise. These include getting NADH to cross the cell's phospholipid bilayer and potentially unbalancing the NAD+/NADH redox homeostasis within the cell. Unbalancing redox homeostasis has been linked to several pathological conditions (Wu *et al*., 2016). Thus further experimentation would need to be undertaken to determine the therapeutic usefulness of NADH.

4. Discussion

4.1 Overview

Many studies have implicated RBBP6 in tumourigenesis and poor prognosis (Yoshitake *et al*., 2004; Dlamini *et al*., 2005; Chen *et al*., 2013; Ntwasa *et al*., 2018; Xiao *et al*., 2019; Dlamini *et al*., 2019). Understanding the interaction between RBBP6 and p53 is key to effectively targeting this interaction in cancer therapy. This study presents data that supports that RBBP6, p53 and MDM2 can interact and form a complex in normal HEK293 T and breast cancer MCF7 cells. High localisation of RBBP6 isoforms 1 and 2 (and potentially 4) was observed in the nucleus of HEK293 T, MFC7, A549 and MDA-MB-231 cells, particularly in nuclear speckles. More specifically, this study shows higher cytoplasmic localisation of RBBP6 in the cancer cell lines, MCF7, A549 and MDA-MD 231, compared to the normal cell line HEK293 T, where RBBP6 localisation occurs predominantly in the nucleus alone. In addition, for the first time, significant subcellular colocalisation of RBBP6 and p53 is shown in A549 and MCF7 cancer cell lines. This supports that these two molecules could interact *in vivo*.

Additionally, this study presents an expression and purification protocol for a portion of full-length RBBP6 pertaining to the p53 binding domain, named RBBP6 p53BD. The purified recombinant protein was confirmed to have structure and be functional as it interacts and forms a complex with endogenous p53. To our knowledge, this is the first reported stable, functional recombinant RBBP6 p53BD, which utilises a polyhistidine tag. Evidence collected suggests that the RBBP6 p53BD is largely intrinsically disordered. Furthermore, the recombinant RBBP6 p53BD has shown significant stability in the presence of denaturants or when exposed to high temperatures despite having extensive random coil in its secondary structure. Protein stability is important for further structural and drug interaction studies. These findings are explained in detail in the following sections.

4.2 The heterologous expressed RBBP6 p53BD is stable, functional and appears to have an intrinsically disordered structure

Mammalian proteins are frequently challenging to express in a soluble form in bacterial expression systems. This is often due to bacterial cells lacking the ability to perform post-translational modifications. Therefore, the expression of recombinant RBBP6 p53BD was tested under multiple conditions in several *Escherichia coli* bacterial cell lines. This was to obtain optimal recombinant RBBP6 p53BD expression conditions. In addition, RBBP6 p53BD was expressed with and without a polyhistidine tag. RBBP6 p53BD was predominantly expressed in the soluble fraction in all tested cell lines and conditions.

All cell lines overexpressed recombinant proteins at approximately 48 kDa and 44 kDa for polyhistidine-tagged and 46 kDa and 43 kDa for untagged RBBP6 p53BD. Based on the amino acid sequence, these molecular weights are bigger than the predicted 39 kDa for the domain. However, a protein migrating to a distance not anticipated in SDS-PAGE is not uncommon. It can be caused by several variables, including the amino acid residues present in the primary sequence, hydrophobic regions, SDS interaction, and protein structure and stability. Protein mobility in an SDS-PAGE relies on the net charge produced by the number of SDS molecules bound to each protein. SDS denatures proteins via its interaction with the protein's hydrophobic tail and side chains. For highly hydrophilic proteins, SDS is less able to interact and bind to the protein, resulting in aberrant mobility in the gel. ExPASy predicts RBBP6 p53BD to be highly hydrophilic, with a grand average of hydropathicity (GRAVY) of -1.645, as seen in Figure A3 in appendix (Gasteiger *et al*., 2005). GRAVY values range from 2 to -2, where positive values indicate a protein that is hydrophobic and negative values indicate a hydrophilic protein. This is further supported by the ExPASy predicted aliphatic index (the relative volume occupied by aliphatic side chains) for the RBBP6 p53BD, which is low at 41.3 (Figure A3 in appendix) (Ikai, 1980). Aliphatic amino acids are hydrophobic, and therefore proteins that lack them are generally hydrophilic.

Interestingly, stunted migration of proteins in SDS-PAGE has been seen for proteins that are intrinsically disordered. Intrinsically disordered proteins (IDPs) are either unstructured along their entire length or contain significant portions of amino acids that lack structure within the protein (Tompa, 2003; Uversky, 2010). Specifically, the RBBP6 p53BD would be considered an intrinsically disordered region (IDR) as it is just a domain forming part of the full-length RBBP6. Intrinsically disordered proteins are involved in various critical biological processes such as the regulation of transcription and translation, cell cycle control and cell signalling processes (Fong *et al.,* 2009). It is estimated, in higher eukaryotes, that approximately 30% of the proteasome consists of IDP or IDRs. The highly flexible conformation of IDPs is advantageous as it enables multiple binding partners.

As conformational changes are frequently seen upon binding, there is the ability to control the timing of protein binding due to different conformational adaptations (Fong *et al.,* 2009). This means the binding of one partner can facilitate the binding of another partner, or in turn the prevention of the binding of one partner can result in the prevention of the binding of another partner. The disordered structure can also block binding sites, and the exposed and flexible residues are often sites of post-translational modifications. Post-translational modifications are common signalling pathway mediators (Wright and Dyson, 2015). The IDPs can also contain fixed structural motifs amongst the disordered structure, which can serve as binding sites. IDPs are frequently found in mediating or scaffolding roles in protein interactions and can function as central hubs in signalling networks (Dubreuil *et al.,* 2019). Lastly, it should be noted that IDPs usually have high binding specificity but modest affinity, allowing for quick binding transitions and higher control, especially in cell signalling. Aberrant expression of IDPs has been linked to many pathologies, including cancer, cardiovascular disease, diabetes and neurodegenerative disorders (Hosoya and Ohkanda, 2021). The RBBP6 p53BD would not be the first IDP/IDR involved in carcinogenesis, as it is estimated that approximately 79 % of cancer-associated proteins contain disordered regions (Iakoucheva *et al*., 2002). One example that is relevant to this study is the transactivation domain of p53, which is the domain that interacts with MDM2 and is largely disordered. (Wright and Dyson, 2015).

Looking at the primary amino acid sequence for RBBP6 p53BD, ExPASy calculated RBBP6 p53BD to contain 63.6 % amino acid residues promoting disorder and only 19.8 % amino acid residues promoting order (Table A1 in the appendix). This suggests that the domain's disorder is an intrinsic property derived from its primary amino acid sequence (Dunker *et al.*, 2001; Dyson and Wright, 2005). The UniProtKB database (RBBP6 Unique identifier: Q7Z6E9) predicts high compositional amino acid bias for the residues investigated as the RBBP6 p53BD. Additionally, as mentioned before, the GRAVY score and aliphatic index (Figure A3 in appendix) show that RBBP6 p53BD is highly hydrophilic. This further suggests that RBBP6 p53BD is an intrinsically disordered region, as intrinsically disordered proteins frequently contain biased amino acids, lack hydrophobic amino acid residues and contain a larger portion of disorder promoting amino acid residues (Uversky, 2017).

As the recombinant RBBP6 p53BD was already expressed in a soluble form, little preparation was needed before purification. However, the soluble fraction contains additional proteins over the insoluble fraction, and therefore, more vigorous purification is needed to isolate the protein of interest. This led to the development of a three-step purification protocol for RBBP6 p53BD with a

polyhistidine tag. The RBBP6 p53BD's hydrophilicity allowed it to stay in solution at a high concentration of ammonium sulphate, namely at least 2 M, which was utilised in hydrophobic interaction chromatography in two ways. Firstly, it allowed several non-recombinant proteins in the soluble fraction to be precipitated from the solution before the prepared protein sample was applied to the column. Secondly, it allowed the use of two purification steps in series. In the first step, a lower ammonium sulphate concentration was used to bind non-recombinant bacterial proteins to the column without RBBP6 p53BD binding. This is due to a higher concentration of ammonium sulphate being needed to cause exposure of the few hydrophobic regions in the hydrophilic RBBP6 p53BD. Therefore in the second purification step, after removing these non-recombinant bacterial proteins, a higher ammonium sulphate concentration was used to get RBBP6 p53BD to bind the column. Next, the presence of the polyhistidine tag on the recombinant protein was utilised to obtain a higher protein purity using a Nickel IMAC column. This was more efficient and resulted in higher purity than ion-exchange chromatography used for the untagged recombinant RBBP6 p53BD after the hydrophobic chromatography steps. After the three-step purification protocol, the RBBP6 p53BD was estimated to be approximately 95 % pure and could be used in downstream experiments.

As mentioned before, for both polyhistidine-tagged and RBBP6 p53BD without a tag, two prominently expressed proteins were seen when analysed by SDS-PAGE (Figure 3.2 and Figure 3.8). These proteins bound and were eluted together during purification, regardless of which chromatography technique was used. Mass spectrometry confirmed that both protein bands contained RBBP6 p53BD. A common cause of two protein bands of the same protein appearing in an SDS-PAGE is the degradation of the protein of interest. This is another common characteristic of an intrinsically disordered protein (IDP). However, when purified RBBP6 p53BD was used in Co-IP assays with endogenous p53 (Figure 3.25 and Figure 3.26), only a single band of RBBP6 p53BD appeared once it had interacted with p53. A single band of the same size of RBBP6 p53BD is also seen in the flow-through samples. This suggests that it is not a degraded protein but a protein with slightly different confirmation in the SDS-PAGE, which becomes uniform when interacting with endogenous cell proteins. A single band is also found on the clear native PAGE. This suggests that the two protein bands in SDS-PAGE are caused by different conformations potentially caused by differential SDS binding, as on clear native PAGE, the protein appears in a single protein band in the absence of SDS.

The clear native PAGE also shows that the RBBP6 p53BD appears in a single uniform form. The form is most likely monomer, as even in the presence of urea or after being heated to 90 °C, there is still

only a single protein band. This is further supported by far-UV CD monitoring of thermal unfolding, which showed unchanged unfolding transitions for the two protein concentrations investigated (Figure 3.14C, D and E). Oligomer proteins acquire increased stability with increased concentration as the protein-protein interactions must be disrupted before the structure can be unfolded (Steif *et al*., 1993; Salminen *et al*., 1996; Shriver and Edmondson, 2009). Therefore the similar unfolding transitions for the two protein concentrations suggest the presence of a single species of monomeric protein.

To confirm that the sequences predicted by Simons and colleagues and Gao and Scott contained the p53 binding domain of RBBP6 and that the recombinant RBBP6 p53BD was folded and functional, co-immunoprecipitation assays were performed (Simons *et al.,* 1997; Gao and Scott, 2003). Recombinant RBBP6 p53BD and p53 were present in the immuno-complexes isolated when either p53 or polyhistidine antibodies were used as the probes. The results show that the recombinant RBBP6 p53BD is functional and binds endogenous p53 (Figure 3.25). Furthermore, this confirms that the bacterial expression system produced a correctly folded and functional RBBP6 p53BD. This is significant as bacterial expression systems are often easier and more economical than other systems such as mammalian, insect or yeast cells when producing recombinant proteins. Additionally, it also confirms that the presence of the polyhistidine tag has not affected the recombinant domain's folding or ability to function.

4.3 Physiochemical characterisation of recombinant RBBP6 p53BD further supports that it is largely intrinsically disordered

Computational predictions of the recombinant RBBP6 p53BD's structure, using its amino acid sequence and far-UV CD spectrum, further support that the domain contains a large amount of intrinsic disorder. Model 2, predicted by I-TASSER, is the most likely model for the structure of RBBP6-p53BD despite model 1 being the highest-rated model by I-TASSER. Model 2 showed a high percentage of disordered structure and a mixture of alpha-helices and beta-strands. This is consistent with the prediction made by DichroWeb using the far-UV CD spectrum produced by recombinant RBBP6 p53BD. Both showed higher alpha-helical structure than beta-strand structure in RBBP6 p53BD. However, I-TASSER predicted a lower percentage of overall structure than the predictions made from the far-UV CD spectrum using DichroWeb. It must be noted that recent developments *in silico* predication of protein structure and structural changes have improved to include programs such as AlphaFold. Therefore, further *in silico* analysis of the RBBP6 p53BD could help to further predict and understand the structure of RBBP6 p53BD.

Assessing the stability of a protein is important for evaluating the feasibility of a protein to undergo additional testing such as drug interaction studies and further structural characterisation. Different unfolding methods can result in different unfolding states due to individual methods impacting intermolecular forces differently. The stability of the recombinant RBBP6 p53BD was evaluated using far-UV CD, whereby the protein was independently subjected to higher temperatures and denaturants. Proteins usually unfold in response to increased temperature due to the increased heat energy disrupting the stabilising interactions within the protein molecules (Baldwin, 1986; Bryngelson *et al*., 1995). The far-UV CD spectrum produced by RBBP6 p53BD, when heated to 90 °C (Figure 3.14), suggests that RBBP6 p53BD's secondary structure becomes more compact in regions. In other words, there is a temperature-induced formation of ordered secondary structures. With thermal unfolding, some proteins have been found to gain secondary structure as some native and non-native hydrophobic interactions can be maintained or even strengthened with the increase in temperature, especially in hydrophilic proteins (Baldwin, 1986; Bryngelson *et al*., 1995).

Intrinsically disordered proteins are commonly found to have high resilience to denaturing conditions such as a change in temperature and exposure to extreme changes in pH. It has even been seen that some intrinsically disordered proteins appear to gain structure upon exposure to a denaturant, particularly an increase in temperature. This is because intrinsically disordered proteins are often highly hydrophilic. Therefore, when exposed to increasing temperatures, there is an increase in hydrophobic attraction, which is a key force in protein folding (Uversky, 2017). As indicated before, the RBBP6 p53BD is highly hydrophilic; therefore, this could explain why RBBP6 p53BD shows a gain of structure when exposed to increasing temperature. In addition, IDPs can rapidly return to their native state after conditions are reversed. For RBBP6 p53BD, high recovery was seen when the domain was returned to starting temperature. The clear native PAGE (Figure 3.11) further reinforces this as the heated and renatured protein migrates in the same manner as the unheated protein. This suggests similar protein conformations as migration in native PAGE is dependent on the protein's size, intrinsic charge, and shape. In addition, the presence of the isodichroic point suggests a two-state conformational equilibrium.

The stability of RBBP6 p53BD was also evaluated by studying the far-UV CD spectrum in the presence of chemical denaturants, namely urea (Figure 3.15) and guanidinium chloride (Figure 3.16). In the presence of the denaturants, the far-UV CD spectrum produced by RBBP6 p53BD showed the ellipticity becoming more positive with an increase in denaturant concentration. This is supportive that the domain is unfolding as the spectrum produced by a random coil has positive ellipticity values in the wavelengths investigated. The ellipticity was found to decrease again once

the denaturant concentration was diluted back to 0.5 M and 1 M, respectively, suggesting recovery of the native structure. In the presence of denaturants, there was remarkably more structural loss and lower recovery compared to thermal unfolding (Table 3.3, Table 3.4 and 3.5). However, there is still a significant recovery after being exposed to denaturants. It must be taken into consideration that there is still a low concentration of denaturant in the sample for the final reading. This may explain why thermal unfolding appears to have a greater percentage recovery than denaturants, as the thermal unfolding samples were returned to starting temperature. It should also be noted that some structure remained even in the presence of 8 M urea or 6 M guanidinium chloride, as the spectrum produced was not completely characteristic of a random coil. After removing the denaturants, the relatively good structural recovery is another feature consistent with an IDP/IDR. IDPs are frequently found to be resilient under harsh conditions and quickly recover when conditions are reversed.

It can also be seen that guanidinium chloride appears to have a more significant unfolding effect on RBBP6 p53BD than urea, with more structural loss and less recovery seen for guanidinium chloride compared to urea (Table 3.4 and 3.5). This is not the first time that one denaturant is more effective at causing a protein to unfold than another. It may be due to the different mechanisms of action causing a protein to unfold in the presence of guanidinium chloride and urea. It is important to note that the precise molecular mechanism of guanidinium chloride or urea is still unknown. A significant deviation seen is that urea appears to destabilize beta-strand structures first, whereas guanidinium chloride appears to destabilize alpha-helical structures first (Camilloni *et al*., 2008). It has been found that a protein's primary sequence, as well as the secondary and tertiary structure, can influence the ability of guanidinium chloride to be more or less efficient at unfolding it. Due to guanidinium chloride's ionic nature, electrostatic interactions seem more susceptible to destabilization. Electrostatic interactions play an important role in alpha-helical stability (Greene and Pace, 1974; Monera *et al*., 1994; Dempsey *et al*., 2005). This is significant as the secondary structure prediction using the far-UV CD spectrum by DichroWeb (Miles *et al*., 2021) estimated over double the alpha-helical content than beta-strand content. The fact that guanidinium chloride caused greater structural loss and lower percentage recovery than urea suggests that the alpha-helical structures found within RBBP6 p53BD, and particularly the electrostatic forces, may play an important role in maintaining the stability of RBBP6 p53BD.

The p53 binding domain of RBBP6 may not be a good candidate for X-ray protein crystallography due to its high level of intrinsic disorder. Few IDPs have been successfully determined using this technique. Despite being largely disorganised in its native state, the stability seen for RBBP6 p53BD

suggests it might be a viable protein domain for crystallography. However, further investigations would need to be undertaken to decide if its structure could be determined using this technique. Additional experiments to characterise this domain include NMR spectrometry, EPR spectrometry, small-angle X-ray scattering and single-molecule fluorescence resonance energy transfer (Na *et al*., 2018).

4.4 Endogenous RBBP6 and p53 colocalise and can form a complex together with MDM2

In a mouse model, RBBP6 was shown to act as a scaffold protein facilitating the interaction between p53 and MDM2 (Li *et al*., 2007). The basic structural organisation of p53, RBBP6 and MDM2 is shown in Figure 4.1A. It is believed that the core DNA binding domain of p53 interacts with the c-terminal p53 binding domain of RBBP6 (Simons *et al*., 1997). It has also been suggested that the RING finger domains of RBBP6 and MDM2 can interact (Li *et al.*, 2007). Lastly, the transactivation domain of p53 has been shown to bind with the N-terminal p53 binding domain on MDM2 (Poyurovsky *et al*., 2010). These interactions are depicted in Figure 4.1B. To further investigate these interactions in humans, it first needed to be determined whether p53 and RBBP6 are in similar subcellular locations within normal and cancer cell lines. Secondly, to determine whether endogenous p53, RBBP6 and MDM2 could interact.

Subcellular localisation studies were undertaken in HEK293 T (normal), MCF7 (breast adenocarcinoma), A549 (Epithelial lung adenocarcinoma) and MDA-MB-231 (breast adenocarcinoma, with mutated p53) cell lines (Figures 3.17, 3.18, 3.19 and 3.20). It was found that p53 localises within the cytoplasm and the nucleus in all investigated cell lines, with higher levels in the nucleus of cancer cell lines. On the other hand, localisation of RBBP6 occurred predominately within the nucleus of the normal cell line, particularly in nuclear speckles. While in the cancer cell lines, in addition to high nuclear localisation, the localisation of RBBP6 in the cytoplasm increased remarkably. This is consistent with previous studies that have found higher localisation of RBBP6 in the cytoplasm of cancer cells compared to normal cells using immunohistochemistry, including the cancer types investigated in this study, namely, lung and breast (Dlamini *et al*., 2019; Motadi *et al*., 2011; Motadi *et al*., 2018).

RBBP6 contains a nuclear localisation signal on its C-terminal, and in normal cells, it has been found to be present predominantly in the nucleus, particularly in nuclear speckles, supporting its involvement in pre-mRNA splicing (Simons *et al*., 1997). Both p53 and MDM2 have been reported to be present in the nucleus and the cytoplasm and possess internal nuclear localisation and export signals (Shaulsky *et al*., 1990; Roth *et al*., 1998; Stommel *et al*., 1999).

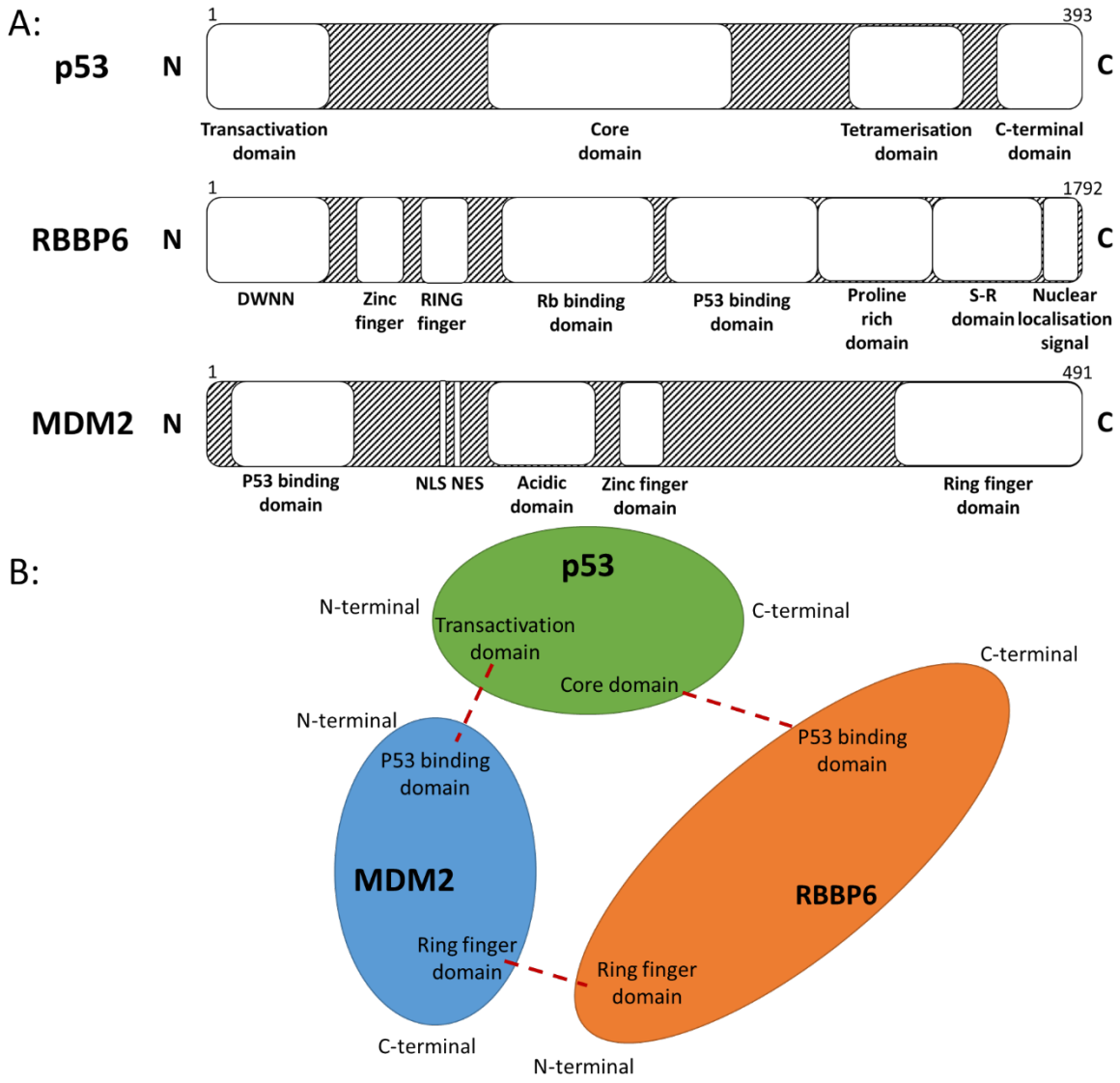

Figure 4.1. The p53-RBBP6-MDM2 interaction.

(A) *Basic structural organisation for p53, RBBP6 and MDM2 showing main domains. C and N terminals are indicated, and residue numbers are shown above each protein.* ***(B)*** *Potential interactions between p53, RBBP6 and MDM2. Interaction/binding sites are indicated with red dashes.*

p53 is primarily known for its involvement in apoptotic pathways, mainly as a transcription factor in the nucleus. In addition, it has been found that p53 has a nucleus-independent role in apoptosis within the cytoplasm. More specifically, p53's interaction with mitochondria in the cytoplasm results in the release of pro-apoptotic factors from the mitochondria's intermembrane area (Moll *et al*., 2006). This is consistent with its localisation in both compartments. It has now also been

established that p53 is not fully reliant on MDM2 and can mediate its own transport from the nucleus to the cytoplasm. In addition, p53 ubiquitination and degradation by MDM2 and MDMX was found to be possible in the cytoplasm and the nucleus, disputing previous beliefs that ubiquitination occurred solely in the nucleus and degradation solely in the cytoplasm (Stommel *et al*., 1999; Yu *et al*., 2000; O'Keefe *et al*., 2003; Shadfan *et al*., 2012).

The regulation of p53 in normal cells is a complicated process that is still not fully understood. Similarly, its dysregulation in cancer cells is complex as many negative regulators mediate it (Leng *et al*., 2003; Stommel and Wahl, 2005; Lee and Lozano, 2006; Levine *et al*., 2006; Ntwasa, 2015; Chen, 2016; Aubrey *et al*., 2018; Feroz and Sheikh, 2020; Hernández Borrero and El-Deiry, 2021). Increased RBBP6 localisation in the cytoplasm of several cancer cell lines may be biologically relevant and important to the dysregulation of p53 control in cancer cells and ultimately the suppression of apoptosis and the resultant aberrant proliferation. It appears that under normal physiological conditions, RBBP6's primary role is in the nucleus, but its role shifts to include cytoplasmic functions under abnormal physiological conditions. Therefore RBBP6's presence in the cytoplasm of cancer cell lines could be a contributing factor to the increased p53 degradation seen. It may also be needed to inhibit p53 initiating the apoptosis pathway through the mitochondria in the cytoplasm in addition to the apoptotic pathways within the nucleus. It would also be interesting to investigate if the nuclear export signals of MDM2 and p53 are involved in the localisation of RBBP6 to the cytoplasm in cancer cell lines, as RBBP6 only has an internal nuclear import signal.

RBBP6's biological relevance in the cytoplasm, as well as the nucleus, is further supported in this study as it was found that RBBP6 colocalises with p53 throughout the whole cell, not only in the nucleus in MCF7 (breast cancer) and A549 (lung cancer) cells (Figure 3.21 and Figure 3.22). Both Manders and Pearson's coefficients showed significant colocalisation; however, the Manders coefficient predicted higher colocalisation in the cells than Pearson's coefficient (Table 3.6). The Manders coefficient may be a more accurate estimation for this investigation. This is because Pearson's coefficient does not consider pixel intensity and is, therefore, not as accurate at predicting colocalisation when proteins are present in varying proportions in different compartments of a cell, which has occurred here for p53 and RBBP6. Nevertheless, these studies provided supporting evidence that RBBP6 and p53 are frequently localised in similar subcellular locations and could potentially interact within a cell.

It must be noted that colocalisation alone is not enough for the conformation of protein interactions, as a microscope's resolution is not enough to discern the exact location of two distinct molecules (Dunn *et al*., 2011). Therefore further analysis on protein interactions was needed, and

Co-IP assays were performed using p53, RBBP6 and MDM2 antibodies as probes in normal and cancer cell lines. Western blot analysis of samples collected during Co-IP showed that MDM2, p53 and RBBP6 can interact to form a protein complex, as they were pulled down together regardless of the probing antibody (Figure 3.23 and Figure 3.24). Therefore p53, RBBP6 and MDM2 are able to interact and form a complex in normal and cancer cell lines. Further studies using recombinant proteins could help understand the exact mechanism of interaction within the p53-RBBP6-MDM2 complex. They could also help determine whether the interactions depicted in Figure 4.1B result in the formation of a stable complex between all three proteins or whether MDM2's presence in the immuno-complexes isolated is from a strong interaction with p53 alone. The interaction between the RING finger domains of RBBP6 and MDM2 may only be temporary as the E3 ligase activity of the RING finger domain is required for p53 ubiquitination.

4.5 Drugability of the RBBP6-p53 interaction

RBBP6's ability to interact with p53 and the resultant degradation of p53 as well as RBBP6's overexpression in several cancers makes it a potential drug target in cancer therapy. The possible interactions between RBBP6-p53-MDM2 are depicted in Figure 4.1B**.** MDM2 has been shown to bind with the transactivation domain of p53, which is the domain that interacts with the cellular transcription machinery (Poyurovsky *et al*., 2010). On the other hand, RBBP6 has been shown to interact with the core DNA binding domain of p53, which is responsible for sequence-specific DNA binding and is involved in p53's ability to initiate the cell cycle arrest and apoptosis pathways (el-Deiry *et al*., 1992; Simons *et al*., 1997). This suggests that targeting p53 directly to prevent the interaction of RBBP6 or MDM2 is not a viable option, as a drug binding to the transactivation or core DNA binding domains of p53 could prevent p53 from functioning correctly. Therefore viable drug target pathways could include (1) inhibiting the p53 binding domain on RBBP6 (Figure 4.2A), (2) inhibiting the p53 binding domain on MDM2 (Figure 4.2B), (3) inhibiting the RING finger domain of RBBP6 (Figure 4.2C) and (4) inhibiting the RING finger domain of MDM2 (Figure 4.2D). These pathways would still interfere with MDM2 and RBBP6's interaction with p53 without blocking vital domains on the p53 molecule itself.

The p53-MDM2 interaction (Figure 4.2B) has already been targeted for cancer therapy, and currently, several small molecules that target this interaction are in human clinical trials (predominantly clinical stage I and II). Additional molecules have been reported and are in earlier stages of development (Zhao *et al*., 2015; Wang and Chen, 2022). Four main pathways to affect the p53-MDM2 interaction with small molecules are (1) inhibiting the p53-MDM2 interaction, (2) inhibiting MDM2 expression, (3) affecting MDM2 post-translational modification and (4) inhibiting MDM2 E3 Ubiquitin ligase activity (by inhibiting the RING finger domain as shown in Figure 4.2D)

(Nag *et al*., 2014). Most of these pathways result in a decrease in the degradation of p53 and, therefore, activation of p53-initiated cell cycle arrest and apoptosis pathways. Similarly, if wanting to target RBBP6 and its interaction with p53, inhibiting the RBBP6-p53 interaction by targeting the p53 binding domain of RBBP6 (Figure 4.2A) is a viable pathway. In addition, affecting RBBP6's expression or post-translational modifications are viable strategies.

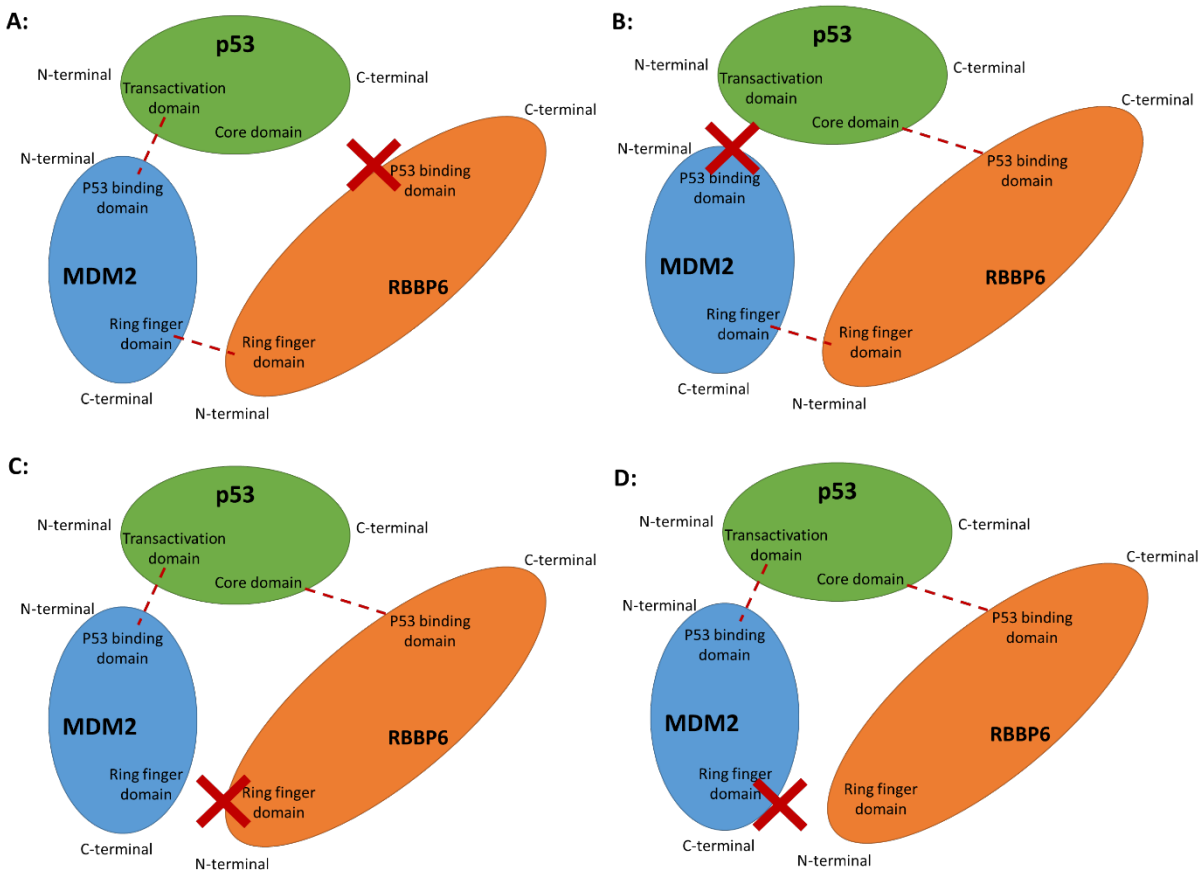

Figure 4.2. Potential drug target sites exploiting the p53-MDM2-RBBP6 complex.

*Drug target sites **(A)** to block the p53 binding domain of RBBP6 from binding p53 core DNA binding domain, **(B)** to block the p53 binding domain of MDM2 to prevent MDM2 binding to the transactivation domain of p53, **(C)** to block the RING finger domain of RBBP6 interacting with RING finger domain MDM2 and **(D)** to block the RING finger domain of MDM2 interacting with RING finger domain of RBBP6. Interaction/binding sites are indicated with red dashes. Red crosses indicate the blocking of the interaction/binding domain, preventing the interaction with the corresponding domain.*

Many proteins are regulated through post-translational modifications, including a protein's expression, stability, subcellular localisation and activity. Therefore affecting a protein's post-

translational modifications can be used to target the protein in drug therapy (Meng *et al*., 2021). More studies need to be conducted to understand the post-translational modifications of RBBP6, and potentially how they could be exploited. Studies have shown that silencing RBBP6 in cancer cells has increased apoptosis and even increased response to cancer treatments, further supporting these drug pathways as possible cancer therapies (Motadi *et al*., 2018; Moela *et al*., 2014; Xiao *et al*., 2018a).

This study provides evidence that the p53 binding domain of RBBP6 has a large amount of intrinsic disorder. Intrinsically disordered proteins have become desirable targets in drug therapy. This is due to their roles in cell regulation and cell signalling, as well as their abnormal expression resulting in many diseases. IDPs are particularly appealing in drug therapeutics as they usually bind, with modest affinity, to concave grooves on the surface of their target molecules and usually through hydrophobic interactions. IDPs present new drug design and development challenges due to the lack of a well-defined structure, making traditional drug design impossible (Chong *et al*., 2018).

Drug targeting of IDPs is still in its infancy. Current drug design strategies focus on either targeting the disordered or ordered sections within the IDP directly or indirectly targeting the molecules that bind endogenously to the IDP or affect a post-translational modification pathway. Current protocols include extensive computational analysis of the IDP and predictions of binding sites and drug targets. In addition to this, screening experiments have been performed for some IDPs. Current successful approaches have mainly been the development of small molecules or peptide inhibitors (Ambadipudi and Zweckstetter, 2016). Determining the drugability of an IDP is a complex process and cannot follow the same pathways as a highly structured protein. The drugability of a molecule is generally based on its surface cavities' size, shape, and physicochemical properties. Typically, IDPs contain more binding cavities, mainly due to a larger surface area being available. Targeting the p53-MDM2 interaction (Figure 4.2B) is an example of targeting an IDP with small molecules as the transactivation domain of p53, which interacts with MDM2, is largely intrinsically disordered.

Initial screening of the structure of the p53 binding domain of RBBP6 predicted by Twala identified NADH as a potential binding partner for RBBP6 p53BD. However, in this study, the interaction between recombinant RBBP6 p53BD and endogenous p53 was not conclusively interrupted by NADH (Figure 2.26), as was computationally predicted (Twala, 2017). This could be due to only a small portion of the domain investigated in this study being used by Twala for predictions (Twala, 2017). Therefore, further studies will be needed to evaluate the effectiveness of NADH in targeting the RBBP6 p53BD in drug therapy. From this study, the RBBP6 p53BD being in monomeric form and

the lack of aggregation upon heating or exposure to denaturants, as well as the presence of ordered secondary structure within RBBP6 p53BD suggest that the domain may be an excellent drug target. However, further structural and computational analysis is needed to predict potential drug binding sites and drug targets accurately. It is also important to investigate the domain's structure when bound to p53, not just when it is on its own, in case there is a conformational change upon binding that can be exploited.

5. Conclusion

This study presents data that demonstrates that p53 and RBBP6 are localised in similar areas of the cells, particularly in cancer cell lines and, therefore, could potentially interact *in vivo*. The increased localisation of RBBP6 in the cytoplasm of the cancer cell lines investigated may be biologically relevant to the dysregulation of p53 levels in cancer cells. The *in vitro* data presented suggests that p53, MDM2 and RBBP6 interact and form a complex in both normal and cancer cell lines. Therefore, supporting the theory that RBBP6 could act as a facilitator for the p53-MDM2 interaction and ultimately p53 degradation. This further supports RBBP6 as a prospective cancer therapy target.

In this study, a stable and functional p53 binding domain of RBBP6 has been successfully expressed and, for the first time, its secondary structure characterised using spectrometry. This study has demonstrated that the recombinant domain can interact with and bind endogenous p53. A functional domain is essential for downstream experiments to determine the mechanism of action of p53 and RBBP6. It has also been demonstrated in this study that the recombinant domain has relatively high stability in the presence of increasing temperature and known denaturants and good recovery when returned to starting conditions. High protein stability is important for downstream structural characterisation and drug binding studies. Evidence is presented here that suggests that the RBBP6 p53BD may be intrinsically disordered. However, intrinsically disordered proteins (IUPs) are increasingly becoming attractive targets of therapeutic intervention, particularly by small drug-like molecules. The knowledge produced in this study is significant as RBBP6 is a potential cancer drug therapy target, and the p53 binding domain itself is potentially drugable. Therefore, the recombinant domain is vital for drug discovery and development, targeting the interaction between RBBP6 and p53.

Future studies would include further structural characterisation of the recombinant domain to predict and investigate potential drug targets and interactions. This can hopefully be expanded to include high throughputs studies, proteomics and genomics (such as RNASeq and bioinformatics analysis). Including the overexpression and silencing of the RBBP6 p53BD. These studies could help reveal pathways that could be therapeutic targets or even confirm biomarker discovery.

6. References

Adams, B and Holmes, E. 1935. Adsorptive properties of synthetic resins. *J Soc Chem Ind*. **54**: 1-6.

Ambadipudi, S and Zweckstetter, M. 2016. Targeting intrinsically disordered proteins in rational drug discovery. *Expert Opin Drug Discov*. **11**(1): 65-77.

Aubrey, B, Kelly, G, Janic, A, Herold, M and Strasser, A. 2018. How does p53 induce apoptosis and how does this relate to p53-mediated tumour suppression? *Cell Death Differ*. **25**(1): 104-113.

Baldwin, R. 1986. Temperature dependence of the hydrophobic interaction in protein folding. *Proc Natl Acad Sci U S A*. **83**(21): 8069-72.

Banker, G and Cotman, C. 1972. Measurement of free electrophoretic mobility and retardation coefficient of protein-sodium dodecyl sulfate complexes by gel electrophoresis. A method to validate molecular weight estimates. *J Biol Chem*. **247**(18): 5856-61.

Barak, Y, Juven, T, Haffner, R and Oren, M. 1993. MDM2 expression is induced by wild type p53 activity. *EMBO J*. **12**: 461-68.

Bolte, S and Cordelières, F. 2006. A guided tour into subcellular colocalisation analysis in light microscopy. *J Microsc*. **224**(3): 213-32.

Bornhorst, J and Falke, J. 2000. Purification of Proteins Using Polyhistidine Affinity Tags. *Methods Enzymol.* **326**: 245-54.

Boveri, T. 1914. *Zur Trage der entstehung maligner Tumoren*. Germany. Jena Gustav Fisher.

Brooks, C and Gu, W. 2006. p53 ubiquitination: Mdm2 and beyond. *Mol cell*. **21**(3): 307-15.

Bruce, W, Meeker, B and Valeriote, F. 1966. Comparison of the sensitivity of normal hematopoietic and transplanted lymphoma colony-forming cells to chemotherapeutic agents administered in vivo. *J Nat Cancer Inst*. **37**: 233-45.

Brylinski, M and Lingam, D. 2012. eThread: A Highly Optimized Machine Learning-Based Approach to Meta-Threading and the Modelling of Protein Tertiary Structures. *PLoS ONE*. **7**(11): e50200.

Bryngelson, J, Onuchic, J, Socci, N and Wolynes, P. 1995. Funnels, pathways, and the energy landscape of protein folding: a synthesis. *Proteins*. **21**(3): 167-95.

Cahilly-Snyder, L, Yang-Feng, T, Francke, U and George, D. 1987. Molecular analysis and chromosomal mapping of amplified genes isolated from a transformed mouse 3T3 cell line. *Somat Cell Mol Genet.* **13**: 235-44.

Camilloni, C, Guerini Rocco, A, Eberini, I, Gianazza, E, Broglia, R and Tiana, G. 2008. Urea and Guanidinium Chloride Denature Protein L in Different Ways in Molecular Dynamics Simulations. *Biophys J*. **94**(12): 4654-61.

Chehab, N, Malikzay, A, Appel, M and Halazonetis, T. 2000. Chk2/hCds1 functions as a DNA damage checkpoint in G(1) by stabilizing p53. *Genes Dev*. **14**(3): 278-88.

Chen, J, Tang, H and Wu, Z. 2013. Overexpression of RBBP6, alone or combined with mutant TP53, is predictive of poor prognosis in colon cancer. *PLoS ONE*. **8**: e66524.

Chen, J. 2016. The Cell-Cycle Arrest and Apoptotic Functions of p53 in Tumor Initiation and Progression. *Cold Spring Harb Perspect Med*. **6**(3): a026104.

Chong, B, Li, M, Li, T, Yu, M, Zhang, Y and Liu, Z. 2018. Conservation of Potentially Druggable Cavities in Intrinsically Disordered Proteins. *ACS Omega*. **3**(11): 15643-52.

Costes, S, Daelemans, D, Cho, E, Dobbin, Z, Pavlakis, G and Lockett, S. 2004. Automatic and quantitative measurement of protein-protein colocalization in live cells. *Biophys J*. **86**(6): 3993-4003.

Crawford, L, Pim, D, Gurney, E, Goodfellow, P and Taylor-Papadimitriou, J. 1981. Detection of a common feature in several human tumor cell lines-a 53,000-dalton protein. *Proc Natl Acad Sci U S A*. **78**(1): 41-45.

Dempsey, C, Piggott, T and Mason, P. 2005. Dissecting contributions to the denaturant sensitivities of proteins. *Biochem*. **44**(2): 775-81.

Di Giammartino, D, Li, W, Ogami, K, Yashinskie, J, Hoque, M, Tian, B and Manley, J. 2014. RBBP6 isoforms regulate the human polyadenylation machinery and modulate expression of mRNAs with AU-rich 3' UTRs. *Genes dev*. **28**(20): 2248-60.

Dlamini, Z, Ledwaba, T, Hull, R, Naicker, S and Mbita, Z. 2019. RBBP6 Is Abundantly Expressed in Human Cervical Carcinoma and May Be Implicated in Its Malignant Progression. *Biomark Cancer*. **11**: 1-10.

Dlamini, Z, Mbita, Z, Rupnarain, C, Ledwaba, T and Motadi, R. 2005. RBBP6 gene expression in cancers. *Proc Amer Assoc Cancer Res*. **65**(9): 1289.

Donehower, L, Harvey, M, Slagle, B, McArthur, M, Montgomery, C Jr, Butel, J and Bradley, A. 1992. Mice deficient for p53 are developmentally normal but susceptible to spontaneous tumours. *Nature*. **356**(6366): 215-21.

Dubreuil, B, Matalon, O and Levy, E. 2019. Protein Abundance Biases the Amino Acid Composition of Disordered Regions to Minimize Non-functional Interactions. *J Mol Biol.* **431**(24): 4978-92.

Dunker, A, Lawson, J, Brown, C, Williams, R, Romero, P, Oh, J, Oldfield, C, Campen, A, Ratliff, C, Hipps, K, Ausio, J, Nissen, M, Reeves, R, Kang, C, Kissinger, C, Bailey, R, Griswold, M, Chiu, W, Garner, E and Obradovic, Z. 2001. Intrinsically disordered protein. *J Mol Graph Model.* **19**: 26-59.

Dunn, K, Kamocka, M and McDonald, J. 2011. A practical guide to evaluating colocalisation in biological microscopy. *Am J Physiol Physiol*. **300**(4): C723-C742.

Dyson, H and Wright, P. 2005. Intrinsically unstructured proteins and their functions. *Nat Rev Mol Cell Biol.* **6**: 197-208.

el-Deiry, W, Kern, E, Pietenpol, J, Kinzler, K and Vogelstein, B. 1992. Definition of a consensus binding site for p53. *Nat Genet*. **1**(1): 45-9.

Fang, S, Jensen, J, Ludwig, R, Vousden, K and Weissman, A. 2000. Mdm2 is a RING finger-dependent ubiquitin protein ligase for itself and p53. *J Biol Chem*. **275**: 8945-51.

Faro, A. 2011. *Investigation of the interactions of Retinoblastoma Binding Protein-6 with transcription factors p53 and Y-Box Binding Protein-1*. PhD. University of the Western Cape.

Ferlay, J, Colombet, M, Soerjomataram, I, Parkin, D, Piñeros, M, Znaor, A and Bray, F. 2021. Cancer statistics for the year 2020: An overview. *Int J Cancer*. **149**(4): 778-89.

Feroz, W and Sheikh, A. 2020. Exploring the multiple roles of guardian of the genome: P53. *Egypt J Med Hum Genet.* **21** (49).

Finlay, C. 1993. The mdm-2 oncogene can overcome wild-type p53 suppression of transformed cell growth. *Mol Cell Biol*. **13**: 301-306.

Finlay, C, Hinds, P and Levine, A. 1989. The p53 proto-oncogene can act as a suppressor of transformation. *Cell*. **57**(7): 1083-93.

Fong, J, Shoemaker, B, Garbuzynskiy, S, Lobanov, M, Galzitskaya, O and Panchenko, A. 2009. Intrinsic disorder in protein interactions: insights from a comprehensive structural analysis. *PLoS Comput Biol*. **5**(3): e1000316.

Gao, S and Scott, R. 2002. P2P-R protein overexpression restricts mitotic progression at prometaphase and promotes mitotic apoptosis. *J Cell Physiol*. **193**: 199-207.

Gao, S and Scott, R. 2003. Stable Overexpression of Specific Segments of the P2P-R Protein in Human MCF-7 Cells Promotes Camptothecin-Induced Apoptosis. *J Cell Physiol* **197**(3): 445-52.

Gao, S, Witte, M and Scott, R. 2002. P2P-R protein localizes to the nucleolus of interphase cells and the periphery of chromosomes in mitotic cells which show maximum P2P-R immunoreactivity. *J Cell Physiol.* **191**: 145-54.

Gasteiger, E, Hoogland, C, Gattiker, A, Duvaud, S, Wilkins, M, Appel, R and Bairoch, A. 2005. Protein Identification and Analysis Tools on the ExPASy Server. In Walker, J. (Ed). *The Proteomics Protocols Handbook*. Humana Press: 571-607.

Ghosh, M, Huang, K and Berberich, S. 2003. Overexpression of Mdm2 and MdmX fusion proteins alters p53 mediated transactivation, ubiquitination, and degradation. *Biochem*. **42**(8): 2291-99.

Greene, R and Pace, C. 1974. Urea and guanidine hydrochloride denaturation of ribonuclease, lysozyme, a-chymotrypsin, and 0-lactoglobulin. *J Biol Chem***. 249**(17): 5388-93.

Gu, W and Roeder, R. 1997. Activation of p53 sequence-specific DNA binding by acetylation of the p53 C-terminal domain. *Cell*. **90**(4): 595-606.

Hahn, W, Bader, J, Braun, T, Califano, A, Clemons, P, Druker, B, Ewald, A, Fu, H, Jagu, S, Kemp, C, Kim, W, Kuo, C, McManus, M, Mills, G, Mo, X, Sahni, N, Schreiber, S, Talamas, J, Tamayo, P, Tyner, J, Wagner, B, Weiss, W and Gerhard, D. 2021. Cancer Target Discovery and Development Network. An expanded universe of cancer targets. *Cell*. **184**(5): 1142-55.

Hanahan, D and Weinberg, R. 2011. Hallmarks of cancer: the next generation. *Cell*. **55**(144): 646-74.

Hartwell, L and Weinert, T. 1989. Checkpoints: controls that ensure the order of cell cycle events. *Science*. **246**(4920): 629-34.

Haupt, Y, Maya, R, Kazaz, A and Oren, M. 1997. Mdm2 promotes the rapid degradation of p53. *Nature* **387**: 296-99.

Hernández Borrero, L and El-Deiry, W. 2021. Tumor suppressor p53: Biology, signaling pathways, and therapeutic targeting. *Biochim Biophys Acta Rev Cancer*. **1876**(1): 188556.

Hollstein, M, Sidransky, D, Vogelstein, B and Harris, C. 1991. p53 mutations in human cancers. *Science.* **253**: 49-53.

Honda, R, Tanaka, H and Yasuda, H. 1997. Oncoprotein MDM2 is an ubiquitin ligase E3 for tumor suppressor p53. *FEBS Lett*. **420**(1): 25-27.

Hosoya, Y and Ohkanda, J. 2021. Intrinsically Disordered Proteins as Regulators of Transient Biological Processes and as Untapped Drug Targets. *Molecules*. **26**(8): 2118.

Hutchens, T and Yip, T. 1990. Differential interaction of peptides and protein surface structures with free metal ions and surface-immobilized metal ions. *J Chromatogr*. **500**: 531-42.

Iakoucheva, L, Brown, C, Lawson, J, Obradović, Z and Dunker, A. 2002. Intrinsic disorder in cell-signaling and cancer-associated proteins. *J Mol Biol*. **323**(3): 573-84.

Ikai, A. 1980. Thermostability and aliphatic index of globular proteins. *J Biochem*. **88**: 1895-98.

Jeffrey, P, Gorina, S and Pavletich, N. 1995. Crystal structure of the tetramerization domain of the p53 tumor suppressor at 1.7 angstroms. *Science*. **267**(5203): 1498-502.

Joerger, A and Fersht, A. 2008. Structural biology of the tumor suppressor p53. *Annu Rev Biochem*. **77**: 557-82.

Jones, S, Roe, A, Donehower, L and Bradley, A. 1995. Rescue of embryonic lethality in Mdm2-deficient mice by absence of p53. *Nature*. **378**(6553): 206-8.

Kappo, M, Ab, E, Hassem, F, Atkinson, R, Faro, A, Muleya, V, Mulaudzi, T, Poole, J, McKenzie, J, Chibi, M, Moolman-Smook, J, Rees, D and Pugh, D. 2012. Solution structure of RING finger-like domain of retinoblastoma-binding protein-6 (RBBP6) suggests it functions as a U-box. *J Biol Chem*. **287**(10): 7146-58.

Karlsson, E, Ryden, L and Brewer, J. 1998. Ion exchange chromatography. In Janson, J and Ryden, L. (Eds). *Protein purification. Principles, High Resolution Methods, and Applications. Ion exchange chromatography*. (2nd Ed). New York. Wiley: 145-206.

Kelly, S and Price, N. 2000. The use of circular dichroism in the investigation of protein structure and function. *Curr Prot Pept Sci*. **1**(4): 349-84.

Kerr, J, Wyllie, A and Currie, A. 1972. Apoptosis: a basic biological phenomenon with wide ranging implications in tissue kinetics. *Br J Cancer*. **26**(4): 239-57.

Klose, D, Wallace, B and Janes, R. 2010. 2Struc: the secondary structure server. *Bioinformatics*. **26**(20): 2624-25.

Kroemer, G, Bravo-San Pedro, J and Galluzzi, L. 2015. Novel function of cytoplasmic p53 at the interface between mitochondria and the endoplasmic reticulum. *Cell Death Dis*. **6**(3): e1698.

Laemmli, U. 1970. Cleavage of structural proteins during the assembly of the head of bacteriophage T4. *Nature*. **227**(5259): 680-85.

Lakowicz, J. 1999. *Principles of fluorescence spectroscopy*. (2nd Ed). USA. Plenum Press: 445-65.

Lampson, G and Tytell, A. 1965. A simple method for estimating isoelectric points. *Anal Biochem*. **11**(2): 374-77.

Lane, D. 1992. Cancer. p53, guardian of the genome. *Nature*. **358**: 15-16.

Lane, D and Verma, C. 2012. Mdm2 in Evolution. *Genes Cancer*. **3**(3-4): 320-24.

Lee, M and Lozano, G. 2006. Regulation of the p53-MDM2 pathway by 14-3-3sigma and other proteins. *Semin Cancer Biol*. **16**(3): 225-34.

Leng, R, Lin, Y, Ma, W, Wu, H, Lemmers, B, Chung, S, Parant, J, Lozano, G, Hakem, R and Benchimol, S. 2003. Pirh2, a p53-induced ubiquitin-protein ligase, promotes p53 degradation. *Cell*. **112**(6): 779-91.

Levine, A. 1997. p53, the Cellular Gatekeeper for Growth and Division. *Cell*. **88**(3): 323-31.

Levine, A, Hu, W and Feng, Z. 2006. The P53 pathway: what questions remain to be explored? *Cell Death Differ*. **13**(6): 1027-36.

Li, L, Deng, B, Xing, G, Teng, Y, Tian, C, Cheng, X, Yin, X, Yang, J, Gao, X, Zhu, Y, Sun, Q, Zhang, L, Yang, X and He, F. 2007. PACT is a negative regulator of p53 an essential for cell growth and embryonic development. *Proc Natl Acad Sci USA*. **104**(19): 7951-6.

Lim, S, Shin, J, Kim, Y and Baek, K. 2004. Identification and characterization of murine mHAUSP encoding a deubiquitinating enzyme that regulates the status of p53 ubiquitination. *Int J Oncol*. **24**(2): 357-64.

Lobstein, J, Emrich, C, Jeans, C, Faulkner, M, Riggs, P and Berkmen, M. 2012. SHuffle, a novel *Escherichia coli* protein expression strain capable of correctly folding disulfide bonded proteins in its cytoplasm. *Microb Cell Fact*. **11**(56): 1-16.

Malakar, P and Venkatesh, K. 2012. Effect of substrate and IPTG concentrations on the burden to growth of Escherichia coli on glycerol due to the expression of Lac proteins. *Appl Microbiol Biotechnol*. **93**: 2543-49.

Manavalan, P and Johnson, W Jr. 1987. Variable selection method improves the prediction of protein secondary structure from circular dichroism spectra. *Anal Biochem*. **167**: 76-85.

Mancini, F, Di Conza, G, Pellegrino, M, Rinaldo, C, Prodosmo, A, Giglio, S, D'Agnano, I, Florenzano, F, Felicioni, L, Buttitta, F, Marchetti, A, Sacchi, A, Pontecorvi, A, Soddu, S and Moretti, F. 2009. MDM4 (MDMX) localizes at the mitochondria and facilitates the p53-mediated intrinsic-apoptotic pathway. *EMBO J*. **28**(13): 1926-39.

Manders, E, Stap, J, Brakenho, G, Van Driel, R and Aten, J. 1992. Dynamics of three dimensional replication patterns during the s-phase, analysed by double labelling of dna and confocal microscopy. *J Cell Sci*. **103**(3): 857-62.

Manders, E, Verbeek, F and Aten, J. 1993. Measurement of co-localisation of objects in dualcolour confocal. *J Microsc*. **169**(3): 375-82.

Martinez, J, Georgoff, I and Levine, A. 1991. Cellular localization and cell cycle regulation by a temperature-sensitive p53 protein. *Genes Dev*. **5**: 151-9.

Mather, A, Rakgotho, M and Ntwasa, M. 2005. SNAMA, a novel protein with a DWNN domain and a RING finger-like motif: A possible role in apoptosis. *Biochim Biophys Acta BBA-Gene Struct Expr.* **1727**: 169-76.

Mbita, Z, Hull, R, Mbele, M, Makhafola, T and Dlamini, Z. 2019. Expression Analysis of RbBP6 in human cancers: a Prospective biomarker. *Anticancer Drugs*. **30**(8): 767-73.

Mbita, Z, Meyer, M, Skepu, A, Hosie, M, Rees, J and Dlamini, Z. 2012. De-regulation of the RBBP6 isoform 3/DWNN in human cancers. *Mol Cell Biochem*. **362**(1-2): 249-62.

McDonald, J and Dunn, K. 2013. Statistical tests for measures of colocalisation in biological microscopy. *J. Microsc.* **252**(3): 295-302.

McLellan, T. 1982. Electrophoresis buffers for polyacrylamide gels at various pH. *Anal Biochem*. **126**(1): 94-9.

Mendoza, M, Mandani, G and Momand, J. 2014. The MDM2 gene family. *Biomol Concepts*. **5**(1): 9-19.

Meng, F, Liang, Z, Zhao, K and Luo, C. 2021. Drug design targeting active posttranslational modification protein isoforms. *Med Res Rev*. **41**: 1701-50.

Miles, A, Ramalli, S and Wallace, B. 2021. DichroWeb, a website for calculating protein secondary structure from circular dichroism spectroscopic data. *Protein Sci*. **31**: 37-46.

Moela, P, Choene, M and Motadi, L. 2014. Silencing RBBP6 (Retinoblastoma Binding Protein 6) sensitises breast cancer cells MCF7 to staurosporine and camptothecin-induced cell death. *Immunobiology*. **219**(8): 593-601.

Moela, P and Motadi, L. 2016. RBBP6: a potential biomarker of apoptosis induction in human cervical cancer cell lines. *Onco Targets Ther*. **9**: 4721-35.

Moll, U, Marchenko, N and Zhang, X. 2006. p53 and Nur77/TR3-transcription factors that directly target mitochondria for cell death induction. *Oncogene.* **25**: 4725-43.

Moll, U and Petrenko, O. 2003. The MDM2-p53 interaction. *Mol Cancer Res*. **1**(14): 1001-8.

Momand, J, Zambetti, G, Olson, D, George, D and Levine, A. 1992. The mdm-2 oncogene product forms complex with the p53 protein and inhibits p53-mediated transactivation. *Cell*. **69**: 1237-45.

Monera, O, Kay, C and Hodges, R. 1994. Protein denaturation with guanidine hydrochloride or urea provides a different estimate of stability depending on the contributions of electrostatic interactions. *Protein Sci*. **3**(11): 1984-91.

Montes de Oca Luna, R, Wagner, D and Lozano, G. 1995. Rescue of early embryonic lethality in mdm2-deficient mice by deletion of p53. *Nature*. **378**(6553): 203-6.

Motadi, L, Bhoola, K and Dlamini, Z. 2011. Expression and function of retinoblastoma binding protein 6 (RBBP6) in human lung cancer. *Immunobiology*. **216**(10): 1065-73.

Motadi, L, Lekganyane, M and Moela, P. 2018. RBBP6 expressional effects on cell proliferation and apoptosis in breast cancer cell lines with distinct p53 statuses. *Cancer Manag Res*. **10**: 3357-69.

Na, J, Lee, W and Yu, Y. 2018. How Do We Study the Dynamic Structure of Unstructured Proteins: A Case Study on Nopp140 as an Example of a Large, Intrinsically Disordered Protein. *Int J Mol Sci*. **19**(2): 381.

Nag, S, Qin, J, Srivenugopal, K, Wang, M and Zang, R. 2013. The MDM2-p53 pathway revisited. *J Biomed Sci Res*. **27**(4):254-71.

Nag, S, Zhang, X, Srivenugopal, K, Wang, M, Wang, W and Zhang, R. 2014. Targeting MDM2-p53 interaction for cancer therapy: are we there yet? *Curr Med Chem*. **21**(5): 553-74.

Ndabambi, N. 2004. *Recombinant expression of the pRb- and p53-interacting domains from the human RBBP6 protein for in vitro binding studies.* MSc. University of the Western Cape.

Newhauser, W, Berrington de Gonzalez, A, Schulte, R and Lee, C. 2016. A Review of Radiotherapy-Induced Late Effects Research after Advanced Technology Treatments. *Front Oncol*. **6**: 13.

Nigro, J, Baker, S, Preisinger, A, Jessup, M, Hosteller, R, Cleary, K, Signer, S, Davidson, N, Baylin, S, Devilee, P, Glover, T, Collins, F, Weslon, A, Modali, R, Harris, C and Vogelstein, B. 1989. Mutations in the p53 gene occur in diverse human tumour types. *Nature.* **342**: 705-08.

Nozaki, Y. 1972.The preparation of guanidine hydrochloride. Methods *Enzymol.* **26**: 43-50.

Ntwasa, M. 2015. Cancer Drugs Targeting the p53 Regulatory Machinery. In Rahman, A. (Ed). *Frontiers in Anti-Cancer Drug Discovery.* (Vol.5). Bentham Science Publishers: 190-230. DOI: 10.2174/97816810805811150501.

Ntwasa, M, Nweke, E and Cajee, U. 2018. The Retinoblastoma Binding Protein 6 Family is Essential for Embryonic Development and Carcinogenesis. *J Cancer Res Forcast*. **1**(1): 1002.

Ochoa, J. 1978. Hydrophobic (interaction) chromatography. *Biochimie*. **60**(1): 1-15.

O'Keefe, K, Li, H and Zhang, Y. 2003. Nucleocytoplasmic shuttling of p53 is essential for MDM2-mediated cytoplasmic degradation but not ubiquitination. *Mol Cell Biol*. **23**(18): 6396-405.

Oliner, J, Pietenpol, J, Thiagalingam, S, Gyuris, J, Kinzler, K and Vogelstein, B. 1993. Oncoprotein MDM2 conceals the activation domain of tumour suppressor p53. *Nature*. **362**: 857-60.

Pace, C. 1986. Determination and analysis of urea and guanidine hydrochloride denaturation curves. *Methods Enzymol*. **131**: 266-80.

Parant, J, Chavez-Reyes, A, Little, N, Yan, W, Reinke, V, Jochemsen, A and Lozano, G. 2001. Rescue of embryonic lethality in Mdm4-null mice by loss of Trp53 suggests a nonoverlapping pathway with MDM2 to regulate p53. *Nat Genet*. **29**(1): 92-5.

Pardee, A. 1989. G1 events and regulation of cell proliferation *Science*. **246**(4930): 603-08.

Pearson, K. 1896. Mathematical Contributions to the Theory of Evolution. On a Form of Spurious Correlation Which May Arise When Indices Are Used in the Measurement of Organs. *Proc R Soc Lond*. **60**(1): 489-98.

Perkins, S. 1986. Protein volumes and hydration effects. *Eur J Biochem*. **157**(1): 169-80.

Poyurovsky, M, Katz, C, Laptenko, O, Beckerman, R, Lokshin, M, Ahn, J, Byeon, I, Gabizon, R, Mattia, M, Zupnick, A, Brown, L, Friedler, A and Prives, C. 2010. The C terminus of p53 binds the N-terminal domain of MDM2. *Nat Struct Mol Biol*. **17**(8): 982-89.

Pugh, D, Eiso, A, Faro, A, Lutya, P, Hoffmann, E and Rees, D. 2006. DWNN, a novel ubiquitin-like domain, implicates RBBP6 in mRNA processing and ubiquitin-like pathways. *BMC Struct Biol*. **6**: 1-12.

Queiroz, J, Tomaz, C and Cabral, J. 2001. Hydrophobic interaction chromatography of proteins. *J Biotechnol*. **87**(2): 143-59.

Ranjbar, B and Gill, P. 2009. Circular Dichroism Techniques: Biomolecular and Nanostructural Analyses-A Review. *Chem Biol Drug Des*. **74**(2): 101-20.

Rath, A, Cunningham, F and Deber, C. 2013. Acrylamide concentration determines the direction and magnitude of helical membrane protein gel shifts. *Proc Natl Acad Sci U S A*. **110**(39): 15668-73.

Riley, T, Sontag, E, Chen, P and Levine, A. 2008. Transcriptional control of human p53-regulated genes. *Nat Rev Mol Cell Biol*. **9**: 402-12.

Robichon, C, Luo, J, Causey, T, Benner, J and Samuelson, J. 2011. Engineering Escherichia coli BL21(DE3) Derivative Strains To Minimize E. coli Protein Contamination after Purification by Immobilized Metal Affinity Chromatography. *Appl Environ Microbiol*. **77**(13): 4634-46.

Rosso, M, Okoro, D and Bargonetti, J. 2014. Splice variants of MDM2 in oncogenesis. *Subcell Biochem*. **85**: 247-61.

Roth, J, Dobbelstein, M, Freedman, D, Shenk, T and Levine, A. 1998. Nucleo-cytoplasmic shuttling of the hdm2 oncoprotein regulates the levels of the p53 protein via a pathway used by the human immunodeficiency virus rev protein. *EMBO J*. **17**(2): 554-64.

Saadatzadeh, M, Elmi, A, Pandya, P, Bijangi-Vishehsaraei, K, Ding, J, Stamatkin, C, Cohen-Gadol, A and Pollok, K. 2017. The Role of MDM2 in Promoting Genome Stability versus Instability. *Int J Mol Sci*. **18**(10): 2216.

Saijo, M, Sakai, Y, Kishino, T, Niikawa, N, Matsuura, Y, Morino, K, Tamai, K and Taya, Y. 1995. Molecular Cloning of a Human Protein That Binds to the Retinoblastoma Protein and Chromosomal Mapping. *Genomics.* **27**(3): 511-19.

Sakai, Y, Saijo, M, Coelho, K, Kishino, T, Niikawa, N and Taya, Y. 1995. cDNA sequence and chromosomal localisation of a novel human protein, RBQ-1 (RBBP6), that binds to the retinoblastoma gene product. *Genomics.* **30**: 98-101.

Salminen, T, Teplyakov, A, Kankare, J, Cooperman, B, Lahti, R and Goldman, A. 1996. An unusual route to thermostability disclosed by the comparison of Thermus thermophilus and Escherichia m coli inorganic pyrophosphatase. *Protein Sci*. **5**(6): 1014-25.

Schmid, F. 2001. Biological macromolecules: UV-visible spectrophotometry. In Robinson, S and Ayres, E. (Eds). *Encyclopedia of Life Sciences*. London. Macmillan: 1-4.

Schneider, C, Rasband, W and Eliceiri, K. 2012. NIH Image to ImageJ: 25 years of image analysis. *Nature Methods.* **9**: 671-75.

Scott, R, Giannakouros, T, Gao, S and Peidis, P. 2003. Functional potential of P2P-R: a role in the cell cycle and cell differentiation related to its interactions with proteins that bind to matrix associated regions of DNA? *J Cell Biochem*. **90**: 6-12.

Shadfan, M, Lopez-Pajares, V and Yuan, Z. 2012. MDM2 and MDMX: Alone and together in regulation of p53. *Transl Cancer Res*. **1**(2): 88-89.

Shaulsky, G, Ben-Ze'ev, A and Rotter, V. 1990. Subcellular distribution of the p53 protein during the cell cycle of Balb/c 3T3 cells. *Oncogene*. **5**(11): 1707-11.

Shi, Y, Di Giammartino, D, Taylor, D, Sarkeshik, A, Rice, W, Yates, J, Frank, J and Manley, J. 2009. Molecular architecture of the human premRNA 3' processing complex. *Mol Cell*. **33**(3): 365-76.

Shoae, M, Safarpour, H and Khorashadizadeh, M. 2021. Recombinant Production of Bovine Enteropeptidase Light Chain in SHuffle® T7 Express and Optimization of Induction Parameters. *Protein J*. **40**: 907-16.

Shriver, J and Edmondson, S. 2009. Defining the Stability of Multimeric Proteins. *Methods Mol Biol*. **490**: 57-82.

Sigalas, I, Calvert, A, Anderson, J, Neal, D and Lunec, J. 1996. Alternatively spliced mdm2 transcripts with loss of p53 binding domain sequences: transforming ability and frequent detection in human cancer. *Nat Med.* **2**(8): 912-17.

Simons, A, Melamed-Bessudo, C, Wolkowicz, R, Sperling, J, Sperling, R, Eisenbach, L and Rotter, V. 1997. PACT: cloning and characterization of a cellular p53 binding protein that interacts with Rb. *Oncogene*. **14**: 145-55.

Smallcombe, A. 2001. Multicolor Imaging: The Important Question of Colocalisation. *Biotechniques*. **30**(6): 1-5.

Sørenson, H and Mortensen, K. 2005. Advanced genetic strategies for recombinant protein expression in Escherichia coli. *J Biotechnol*. **115**(2): 113-28.

Sreerema, N, Venyaminov, S and Woody, R. 1999. Estimation of the number of helical and strand segments in proteins using CD spectroscopy. *Protein Sci*. **8**: 370-80.

Steif, C, Weber, P, Hinz, H, Flossdorf, J, Cesareni, G and Kokkinidis, M. 1993. Subunit interactions provide a significant contribution to the stability of the dimeric four-alpha-helical-bundle protein ROP. *Biochem*. **32**(15): 3867-76.

Stewart, B and Wild, C. (Eds). 2014. *World cancer report 2014*. France. International Agency for Research on Cancer.

Stewart, C, Soria, A and Hamel, P. 2001. Integration of the pRB and p53 cell cycle control pathways. *J Neurooncol*. **51**(3): 183-204.

Stommel, J, Marchenko, N, Jimenez, G, Moll, U, Hope, T and Wahl, G. 1999. A leucine-rich nuclear export signal in the p53 tetramerization domain: regulation of subcellular localization and p53 activity by NES masking. *The EMBO journal*. **18**(6): 1660-72.

Stommel, J and Wahl, G. 2005. A new twist in the feedback loop: stress activated MDM2 destabilization is required for p53 activation. *Cell cycle*. **4**(3): 411-17.

Studier, F and Moffatt, B. 1986. Use of bacteriophage T7 RNA polymerase to direct selective high-level expression of cloned genes. *J Mol Biol*. **189**(1): 113-30.

Sun, B, Zhao, X, Ming, J, Liu, X, Liu, D and Jiang, C. 2019. Stepwise detection and evaluation reveal miR-10b and miR-222 as a remarkable prognostic pair for glioblastoma. *Oncogene*. **38**(33): 6142-57.

Tabata, N, Sakuma, Y, Honda, Y, Doi, N, Takashima, H, Miyamoto-Sato, E and Yanagawa, H. 2009. Rapid antibody selection by mRNA display on a microfluidic chip. *Nucleic Acids Res*. **37**(8): e64.

Tanaka, T, Utsunomiya, T, Utsunomiya, H and Umesaki, N. 2008. Irinotecan HCL, an anticancer topoisomerase I inhibitor, frequently induces ovarian failure in premenopausal and perimenopausal women. *Oncology rep*. **19**: 1123-33.

Tompa, P. 2003. Intrinsically unstructured proteins evolve by repeat expansion. *Bioessays*. **25**(9): 847-55.

Twala, C. 2017. *Drugs targeting the retinoblastoma binding protein 6 (RBBP6).* Msc. University of the Witwatersrand.

Uversky, V. 2010. The mysterious unfoldome: structureless, underappreciated, yet vital part of any given proteome*. J Biomed Biotechnol*. **2010**: 568068.

Uversky, V. 2017. Paradoxes and wonders of intrinsic disorder: Stability of instability. *Intrinsically disordered proteins*. **5**(1): e1327757.

Van Stokkum, I, Spoelder, H, Bloemendal, M, Van Grondelle, R and Groen, F. 1990. Estimation of protein secondary structure and error analysis from CD spectra. *Anal Biochem*. **191**: 110-18.

Vaux, D, Cory, S and Adams, J. 1988. Bcl-2 gene promotes haemopoietic cell survival and cooperates with c-myc to immortalize pre-B cells. *Nature*. **335**: 440-42.

Vo, L, Minet, M, Schmitter, J, Lacroute, F and Wyers, F. 2001. Mpe1, a zinc knuckle protein, is an essential component of yeast cleavage and polyadenylation factor required for the cleavage and polyadenylation of mRNA. *Mol Cell Biol*. **21**: 8346-56.

Vogelstein, B, Lane, D and Levine, A. 2000. Surfing the p53 network. *Nature*. **408**: 307-10.

Wang, P, Reed, M, Wang, Y, Mayr, G, Stenger, J, Anderson, M, Schwedes, J and Tegtmeyer, P. 1994. p53 domains: structure, oligomerization, and transformation. *Mol Cell Biol*. **14**(8): 5182-91.

Wang, Q, Wei, S and Xiao, H. 2020. RBBP6 induces non-small cell lung cancer cell proliferation and high expression is associated with poor prognosis. *Oncol Lett*. **19**(4): 2895-901.

Wang, S and Chen, F. 2022. Small-molecule MDM2 inhibitors in clinical trials for cancer therapy. *Eur J Med Chem*. **236**: 114334.

Wang, X, Yeh, H, Schaeffer, L, Roy, R, Moncollin, V, Egly, J, Wang, Z, Freidberg, E, Evans, M, Taffe, B, Bohr, V, Weeda, G, Hoeijmakers, J, Forrester, K and Harris, C. 1995. p53 modulation of TFIIH-associated nucleotide excision repair activity. *Nat Genet*. **10**: 188-95.

Wang, Z, Wu, X and Friedberg, E. 1991. Nucleotide excision repair of DNA by human cell extracts is suppressed in reconstituted nucleosomes. *J Biol Chem*. **266**: 22472-478.

Witte, M and Scott, R. 1997. The proliferation potential protein-related (P2P-R) gene with domains encoding heterogeneous nuclear ribonucleoprotein association and Rb1 binding shows repressed expression during terminal differentiation. *Proc Natl Acad Sci USA*. **94**: 1212-17.

Woods, D and Vousden, K. 2001. Regulation of p53 function. *Exp Cell Res*. **264**(1): 56-66.

Woody, R. 1995. Circular Dichroism. *Methods Enzymol.* **246**: 34-71.

World Health Organization, 2015. Cancer Fact sheet [WWW Document]. URL http://www.who.int/mediacentre/factsheets/fs297/en/.

Wright, P and Dyson, H. 2015. Intrinsically disordered proteins in cellular signalling and regulation. *Nat Rev Mol Cell Biol*. **16**(1):18-29.

Wu, J, Jin, Z, Zheng, H and Yan, L. 2016. Sources and implications of NADH/NAD(+) redox imbalance in diabetes and its complications. *Diabetes Metab Syndr Obes*. **9**:145-53.

Wu, S and Zhang, Y. 2007. LOMETS: A local meta-threading-server for protein structure prediction. *Nucl Acids Res*. **35**: 3375-82.

Xiao, C, Wang, Y, Zheng, M, Chen, J, Song, G, Zhou, Z, Zhou, C, Sun, X, Zhong, L, Ding, E, Zhang, Y, Yang, L, Wu, G, Xu, S, Zhang, H and Wang, X. 2018a. RBBP6 increases radioresistance and serves as a therapeutic target for preoperative radiotherapy in colorectal cancer. *Cancer sci*. **109**(4): 1075-87.

Xiao, C, Wu, G, Zhou, Z, Zhang, X, Wang, Y, Song, G, Ding, E, Sun, X, Zhong, L and Li, S. 2019. RBBP6, a RING finger-domain E3 ubiquitin ligase, induces epithelialmesenchymal transition and promotes metastasis of colorectal cancer. *Cell Death Dis*. **10**: 1-17.

Xiao, W, Wang, R, Handy, D and Loscalzo, J. 2018b. NAD(H) and NADP(H) Redox Couples and Cellular Energy Metabolism. *Antioxid Redox Signal*. **28**(3): 251-72.

Xirodimas, D, Saville, M, Bourdon, J, Hay, R and Lane, D. 2004. Mdm2- mediated NEDD8 conjugation of p53 inhibits its transcriptional activity. *Cell*. **118**(1): 83-97.

Xu, J and Zhang, Y. 2010. How significant is a protein structure similarity with TM-score =0.5? *Bioinformatics*. **26**: 889-95.

Yang, J, Yan, R, Roy, A, Xu, D, Poisson, J and Zhang, Y. 2015. The I-TASSER Suite: Protein structure and function prediction. *Nature Methods*. **12**: 7-8.

Yang, J and Zhang, Y. 2015. I-TASSER server: new development for protein structure and function predictions. *Nucleic Acids Res*. **43**(W1): W174-W181.

Yarawsky, A, English, L, Whitten, S and Herr, A. 2017. The Proline/Glycine-Rich Region of the Biofilm Adhesion Protein Aap Forms an Extended Stalk that Resists Compaction. *J Mol Biol*. **429**(2): 261-279.

Yip, T, Nakagawa, Y and Porath, J. 1989. Evaluation of the interaction of peptides with Cu(II), Ni(II), and Zn(II) by high-performance immobilized metal ion affinity chromatography. *Anal Biochem*. **183**(1): 159-71.

Yoshitake, Y, Nakatsura, T, Monji, M, Senju, S, Matsuyoshi, H, Tsukamoto, H, Hosaka, S, Komori, H, Fukuma, D, Ikuta, Y, Katagiri, T, Furukawa, Y, Ito, H, Shinohara, M, Nakamura, Y and Nishimura, Y. 2004. Proliferation potential-related protein, an ideal esophageal cancer antigen for imunotherapy, identified using complimentary DNA microarray analysis. *Clin Cancer Res*. **10**: 6437-48.

Yu, Z, Geyer, R and Maki, C. 2000. MDM2-dependent ubiquitination of nuclear and cytoplasmic P53. *Oncogene*. **19**(51): 5892-97.

Zhang, Y and Xiong, Y. 2001. A p53 Amino terminal nuclear export signal inhibited by DNA damage-induced phosphorylation. *Science.* **292**: 1910.

Zhao, Y, Aguilar, A, Bernard, D and Wang, S. 2015. Small-molecule inhibitors of the MDM2-p53 protein-protein interaction (MDM2 Inhibitors) in clinical trials for cancer treatment. *J Med Chem*. **58**(3): 1038-52.

Zheng, T, Wang, J, Zhao, Y, Zhang, C, Lin, M, Wang, X, Yu, H, Liu, L, Feng, Z and Hu, W. 2013. Spliced MDM2 isoforms promote mutant p53 accumulation and gain-of-function in tumorigenesis. *Nat Commun*. **4**: 2996.

Zinchuk, V, Zinchuk, O and Okada, T. 2007. Quantitative colocalisation analysis of multicolour confocal immunofluorescence microscopy images: pushing pixels to explore biological phenomena. *Acta histochemica et cytochemica*. **40**(4): 101-11.

7. Appendix

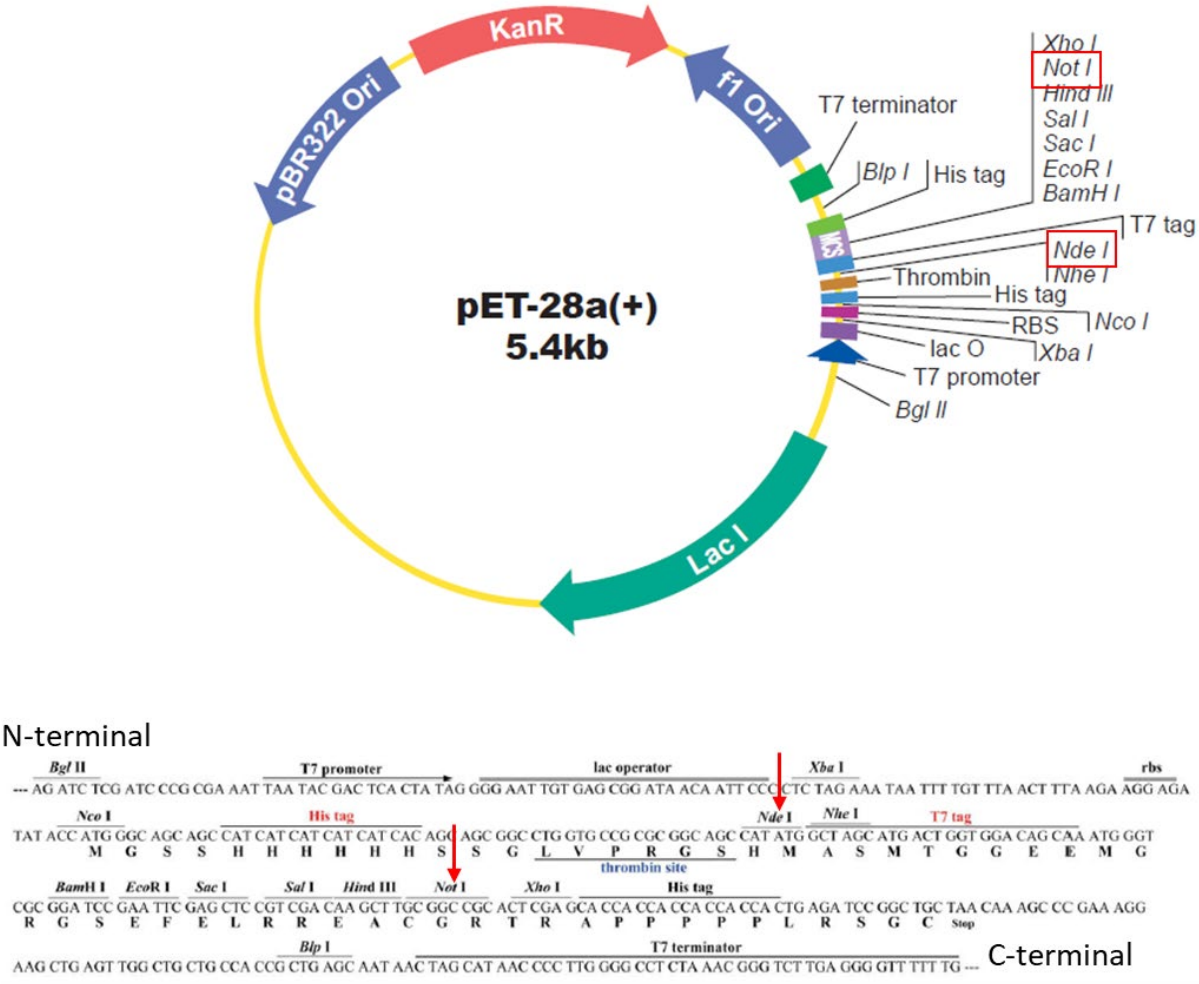

Figure A1. Vector map for pET28a+ with the construct for RBBP6 p53BD with a polyhistidine tag. *The red boxes and arrows show the position of the insert encoding RBBP6 p53BD. Nde I was used for the inclusion of the N-terminal histag. A stop codon was used to remove the C-terminal histag. N and C terminals are indicated. Image adapted from GenScript Vector Map pET28a+ (New Jersey, USA).*

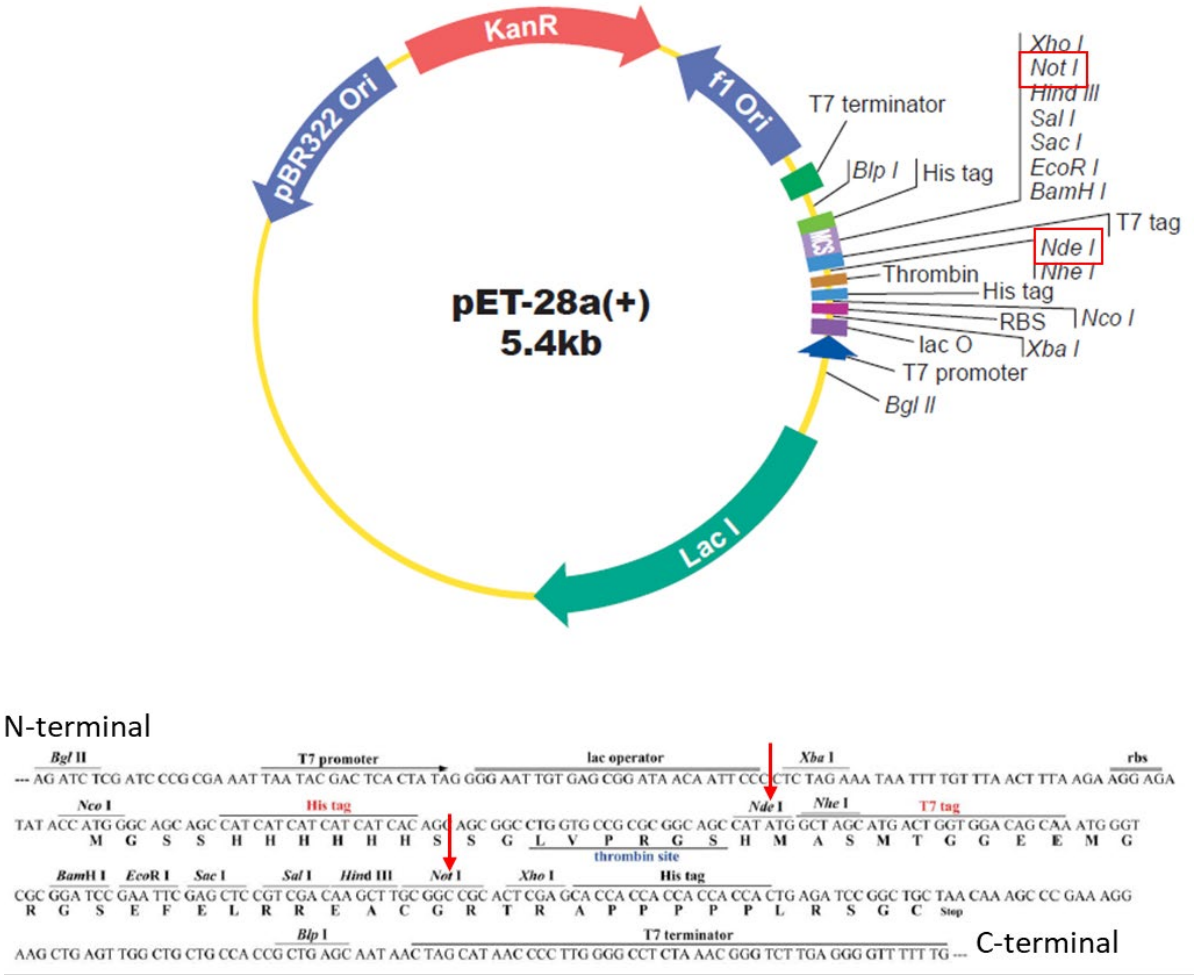

Figure A2. Vector map for pET28a+ with the construct for RBBP6 p53BD without the inclusion of a tag.

The red boxes and arrows show the position of the insert encoding RBBP6 p53BD. Nco I was used to exclude the N-terminal histag. A stop codon was used to remove the C-terminal histag. N and C terminals are indicated. Image adapted from GenScript Vector Map pET28a+ (New Jersey, USA).

```
        10         20         30         40         50         60
VSHEIIQHEV KSSKNSASSE KGKTKDRDYS VLEKENPEKR KNSTQPEKES NLDRLNEQGN

        70         80         90        100        110        120
FKSLSQSSKE ARTSDKHDST RASSNKDFTP NRDKKTDYDT REYSSSKRRD EKNELTRRKD

       130        140        150        160        170        180
SPSRNKDSAS GQKNKPREER DLPKKGTGDS KKSNSSPSRD RKPHDHKATY DTKRPNEETK

       190        200        210        220        230        240
SVDKNPCKDR EKHVLEARNN KESSGNKLLY ILNPPETQVE KEQITGQIDK STVKPKPQLS

       250        260        270        280        290        300
HSSRLSSDLT RETDEAAFEP DYNESDSESN VSVKEEESSG NISKDLKDKI VEKAKESLDT

       310        320        330        340
AAVVQVGISR NQSHSSPSVS PSRSHSPSGS QTRSHSSSAS SAESQDS
```

Total number of negatively charged residues (Asp + Glu): 62
Total number of positively charged residues (Arg + Lys): 68

Atomic composition:

Carbon	C	1615
Hydrogen	H	2646
Nitrogen	N	518
Oxygen	O	597
Sulfur	S	1

Number of amino acids: 347

Molecular weight: 38903.95

Theoretical pI: 9.00

Formula: $C_{1615}H_{2646}N_{518}O_{597}S_1$
Total number of atoms: 5377

Extinction coefficients:

This protein does not contain any Trp residues. Experience shows that this could result in more than 10% error in the computed extinction coefficient.

Extinction coefficients are in units of M^{-1} cm^{-1}, at 280 nm measured in water.

Ext. coefficient 8940
Abs 0.1% (=1 g/l) 0.230, assuming all pairs of Cys residues form cystines

Ext. coefficient 8940
Abs 0.1% (=1 g/l) 0.230, assuming all Cys residues are reduced

Estimated half-life:

The N-terminal of the sequence considered is V (Val).

The estimated half-life is: 100 hours (mammalian reticulocytes, in vitro).
>20 hours (yeast, in vivo).
>10 hours (Escherichia coli, in vivo).

Instability index:

The instability index (II) is computed to be 58.83
This classifies the protein as unstable.

Aliphatic index: 41.30

Grand average of hydropathicity (GRAVY): -1.645

Figure A3. ExPASy results for RBBP6 p53BD sequence.

Results produced by ExPASy (Gasteiger et al., 2005) using the RBBP6 p53BD amino acid sequence investigated in this study. Including the amino acid sequence submitted, theoretical pI, the extinction coefficient, instability index, aliphatic index and GRAVY scores.

Table A1: Amino acid composition of RBBP6 p53BD.

The absolute number and frequency expressed as percentages are indicated for every amino acid. Amino acid residues considered order promoting are Trp, Met, Cys, Phe, Ile, Tyr, Val, Leu and Asn. On the other hand, amino acid residues considered disorder promoting include Gln, Ser, Pro, Glu, Lys, Gly, Ala and Arg.

Amino acid	Number of residues	Percentage of composition (%)
Alanine (Ala)	13	3.7
Arginine (Arg)	24	6.9
Asparagine (Asn)	22	6.3
Aspartic acid (Asp)	28	8.1
Cysteine (Cys)	1	0.3
Glutamine (Gln)	13	3.7
Glutamic acid (Glu)	34	9.8
Glycine (Gly)	10	2.9
Histidine (His)	10	2.9
Isoleucine (Ile)	8	2.3
Leucine (Leu)	15	4.3
Lysine (Lys)	44	12.7
Methionine (Met)	0	0.0
Phenylalanine (Phe)	3	0.9
Proline (Pro)	18	5.2
Serine (Ser)	65	18.7
Threonine (Thr)	19	5.5
Tryptophan (Trp)	0	0
Tyrosine(Tyr)	6	1.7
Valine (Val)	14	4.0